DOCTORAL THESIS

Effect of Different Sweep Gases on Sulfur Behavior during Pyrolysis of Kukersite Oil Shale

Sepehr Mozaffari

TALLINNA TEHNIKAÜLIKOOL
TALLINN UNIVERSITY OF TECHNOLOGY
TALLINN 2022

TALLINN UNIVERSITY OF TECHNOLOGY
DOCTORAL THESIS
60/2022

Effect of Different Sweep Gases on Sulfur Behavior during Pyrolysis of Kukersite Oil Shale

SEPEHR MOZAFFARI

TAL TECH PRESS

TALLINN UNIVERSITY OF TECHNOLOGY
School of Engineering
Department of Energy Technology
This dissertation was accepted for the defence of the degree 23/09/2022

Supervisor: Senior Researcher Oliver Järvik
School of Engineering
Tallinn University of Technology
Tallinn, Estonia

Co-supervisor: Researcher Zachariah Steven Baird
School of Engineering
Tallinn University of Technology
Tallinn, Estonia

Opponents: Prof Omar S. Al-Ayed
Vice Dean of Scientific Research & Innovation
Department of Chemical Engineering
Faculty of Engineering Technology
Al-Balqa Applied University
Amman, Jordan

Dr Indrek Aarna
Head of Development Department
Viru Keemia Grupp
Kohtla Järve, Estonia

Defence of the thesis: 25/10/2022, Tallinn
Declaration:
Hereby I declare that this doctoral thesis, my original investigation and achievement, submitted for the doctoral degree at Tallinn University of Technology has not been submitted for doctoral or equivalent academic degree.

Sepehr Mozaffari

---
signature

European Union
European Regional
Development Fund

Investing
in your future

ISSN 2585-6898 (publication)
ISBN 978-9949-83-907-0 (publication)
ISSN 2585-6901 (PDF)
ISBN 978-9949-83-908-7 (PDF)
Printed by Koopia Niini & Rauam

TALLINNA TEHNIKAÜLIKOOL
DOKTORITÖÖ
60/2022

Pürolüüsikeskkonna mõju väävli käitumisele kukersiitse põlevkivi pürolüüsil

SEPEHR MOZAFFARI

TAL TECH
KIRJASTUS

Contents

List of Publications 7
Author's Contribution to the Publications 8
Introduction 9
Abbreviations 10
Terms 11
1 Literature review 12
1.1 Oil shale 12
1.2 Pyrolysis 13
1.2.1 Kerogen to thermobitumen 14
1.2.2 Thermobitumen to pyrolysates 16
1.3 Oil shale processing in Estonia 16
1.4 Sulfur 17
1.5 Objectives 18
2 Experimental 19
2.1 Oil shale 19
2.2 Oil shale thermobitumen formation studies 20
2.3 Fischer Assay (FA) 20
2.4 Analytical methods 21
2.4.1 Elemental analysis 21
2.4.2 Fourier-Transform Infrared Spectroscopy (FTIR) 21
2.4.3 Differential Scanning Calorimetry (DSC) 21
2.4.4 Thermogravimetric Analysis – Mass Spectrometry (TGA-MS) 21
2.4.5 Density measurement 22
2.4.6 Refractive Index (RI) measurement 22
2.4.7 Molecular Weight (MW) measurement 22
2.4.8 Gas Chromatography (GC) 22
2.4.9 Gas Chromatography – Mass Spectrometry (GC-MS) 23
3 Results and discussion 24
3.1 The effect of sweep gas on pyrolysis yields 24
3.1.1 TGA 24
3.1.2 DSC 27
3.2 The effect of sweep gas on shale oil 27
3.2.1 Composition and properties 27
3.3 The effect of sweep gas on pyrolysis gas composition 31
3.3.1 Sulfurous gases 35
3.4 Analysis of sulfur in semi-coke 38
4 Conclusion 39
List of Figures 41
List of Tables 42
References 43
Acknowledgements 49
Abstract 50

Lühikokkuvõte 51
Appendix 53
Curriculum vitae 123
Elulookirjeldus 124

List of Publications

The thesis has been prepared based on the following publications:

I **S. Mozaffari**, O. Järvik, and Z. S. Baird, "Effect of N_2 and CO_2 on shale oil from pyrolysis of Estonian oil shale" *Int. J. Coal Prep. Util.*, 2021, doi: 10.1080/19392699.2021.1914025.

II **S. Mozaffari**, O. Järvik, and Z. S. Baird, "Composition of gas from pyrolysis of Estonian oil shale with various sweep gases" *Oil Shale*, vol. 38, no. 3, pp. 215–227, 2021, doi: 10.3176/oil.2021.3.03.

III H. Astra, T. Albert, **S. Mozaffari**, O. Järvik, A. Yanchilin, S. Kamenev, S. Karagöz, V. Oja, "Yields and the selected physicochemical properties of thermobitumen as an intermediate product of the pyrolysis of Kukersite oil shale" vol. 38, no. 4, pp. 295–316, 2021, doi: 10.3176/oil.2021.4.02.

IV **S. Mozaffari**, Z. S. Baird, and O. Järvik, "Sulfur in kukersite shale oil: its distribution in shale oil fractions and the effect of gaseous environment" J. Therm. Anal. Calorim., 2022, doi: 10.1007/s10973-022-11359-8.

Author's Contribution to the Publications

Contribution to the papers in this thesis are:

I Performing the experiments, analyzing the data processed, carrying out the majority of measurements, and writing the article.

II Conducting the experimental work, performing data processing, analyzing the samples obtained, and writing the article

III Being partly involved in experimental work and performing measurements on the selected properties of the produced samples.

IV Carrying out the experiment, processing the data and analyzing the results together with other co-authors.

Introduction

The global energy demand is increasing. Fossil fuels are still considered as important energy sources [1]. Among fossil fuels, oil shale has gained lots of interest as substantial deposits are available in the world [2]. Moreover, oil shale reserves in Estonia is estimated to have the equivalent of 2.5 billion tons of shale oil [3,4].

Oil shale is a sedimentary rock containing organic matter (kerogen) [5]. Several countries, such as Estonia, have been using oil shale as their primary source of energy to meet their domestic power and heat demand [6] as well as for power export. Oil shale in Estonia has been also extensively applied to produce shale oil [3], which has been and still is an important export commodity used mostly as marine fuel. Shale oil is produced by means of the pyrolysis process, which takes place at around 500 °C under an inert environment. As a result of thermal decomposition of kerogen, oil vapors and combustible gas are formed [7,8]. In Estonia, the solid heat carrier (SHC) method is mainly used where hot shale ash, which is produced by the combustion of semi-coke (the solid residue left after pyrolysis), is used as the heat carrier. It is mixed with dried oil shale so that shale oil and gas are produced [9]. A greater rate of production, fewer environmental problems, and the possibility of using a low-quality oil shale in pyrolysis have made this technology preferable over others [10]. The aggravation of environmental problems is one of the aspects that has affected and continues to affect the shale oil industry. A burning issue is the relatively high sulfur content of shale oil. The sulfur content of fuels has always been an important aspect of the fuel industry because its presence leads to environmental issues and problems for upgrading processes as well [11]. Also, according to the regulation set by the International Maritime Organization (IMO), since 2015 the sulfur content of marine fuels has to be lower than 0.1% by mass in SOx Emission Control Areas [12].

Studying sulfur chemistry has been of great interest from academia to industry. The biggest motivator to study sulfur is environmental-related matters. The properties of oil shale depend on numerous factors, such as geographical location, pyrolysis process and so on. As a result, the sulfur in kerogens differ from each other, as well [13]. In addition, sulfur chemistry has an impact on the rate of kerogen decomposition, and thus, formation of oil and gas [14]. Consequently, the sulfur content of kerogen plays a key role in determining the sulfur content of the resulting shale oil [15]. Additionally, the extent of the release of sulfur from oil shale is dependent on many factors, such as the reactive medium, retorting temperature, type of pyrolysis process, etc. [16–20].

Information on the impact of different sweep gases (also called purge gas or carrier gas), such as CO_2 and steam, on the pyrolysis of Estonian kukersite oil shale is scarce. In addition, there is little information available on the effect of various atmospheres on the release of sulfur, both as sulfurous gases as well as sulfur compounds in the shale oil. Therefore, this study was carried out to understand how CO_2 and steam plays a role in transformation of sulfur during pyrolysis. Subsequently, a comparative analysis with the conventional method – which is the use of a nitrogen atmosphere – was performed so that a deeper understanding of the impact of CO_2 and steam can be acquired. The results presented in this thesis are beneficial for obtaining a comprehensive understanding of the different aspects influencing oil shale pyrolysis and shale oil composition.

Abbreviations

SHC	Solid Heat Carrier
IMO	International Maritime Organization
GHC	Gas Heat Carrier
TB	Thermobitumen
THF	Tetrahydrofuran
FA	Fischer Assay
FTIR	Fourier-Transform Infrared Spectroscopy
ASTM	American Society for Testing and Materials
TGA-MS	Thermogravimetric Analyzer – Mass Spectrometer
DSC	Differential Scanning Calorimetry
MW	Molecular Weight
RI	Refractive Index
GC	Gas Chromatography
GC-MS	Gas Chromatography – Mass Spectrometry
FPD	Flame Photometric Detector
HC	Hydrocarbon

Terms

H/C	Hydrogen to Carbon ratio
O/C	Oxygen to Carbon ratio
SOx	Sulfur oxides
NOx	Nitrogen oxides
Al_2O_3	Aluminum oxide
Pt/Rh	Platinum-Rhodium
wt	Weight
U	Expanded uncertainty
FeS_2	Pyrite
FeS_x	Pyrrhotite

1 Literature review

1.1 Oil shale

Due to the large quantity of oil shale deposits in the world, oil shale has been considered a potential alternative to petroleum. Oil shale is a complex mixture of kerogen, minerals and water [21]. Oil shale reserves comprise about 35% of the total fossil fuel reserves in the world [22]. This fossil fuel can be used to produce electricity, various chemical products and oil [3].

Because of the increase in the use of petroleum resources, as well as the uncertainty in the price of crude oil and its derivative products, interest has arisen in the development of oil shale retorting processes as an alternative resource. Such resources can be of use for energy production in the future although, despite its promise, the oil shale industry face environmental and economic challenges as well. For instance, production of petroleum crude oil is less costly than oil production from oil shale. In addition, operational issues appearing in pulverized oil shale combustion system, such as corrosion and fouling, as well as serious environmental pollution difficulties arising from the development of oil shale industry are some of the major problems caused by oil shale industry [21,23,24]. In addition, a low viscosity, low asphalt content and similar properties to crude oil have made shale oil an attractive fossil fuel source in the long run [25]. Furthermore, about 25% of oil shale production in the world is used to make shale oil and combustible gas, which undergo upgrading processes to produce jet fuel, gasoline, light fuel oil, bitumen, coke, phenols, liquefied shale gas, wax, lubricating oil and other products [26].

For these reasons, countries such as Estonia, China, and Brazil have been investigating ways to economically and environmentally valorize oil shale [21]. Speaking of the role of oil shale in Estonia, 60% of primary energy consumption as well as much of the electricity production in the country is supplied by oil shale exploitation [3]. Moreover, several shale oil plants have been built in Estonia in recent years [27]. At the same time, the need to develop more efficient and sustainable methods for oil shale utilization is of high significance in order to improve the performance of the pyrolysis process. It is, therefore, important to analyze and study the pyrolysis of oil shale and its products: oil, gas and solid residue. The two types of oil shale in Estonia are Dictyonema argillite and kukersite. However, due to the higher organic matter and lower sulfur content of kukersite, it is the oil shale used in the country [28]. Kukersite oil shale, in general, has low H/C (1.26) and high O/C (0.09) molar ratios, and therefore, it can be classified as Type II oil shale, as shown using the van Krevelen diagram in Figure 1.

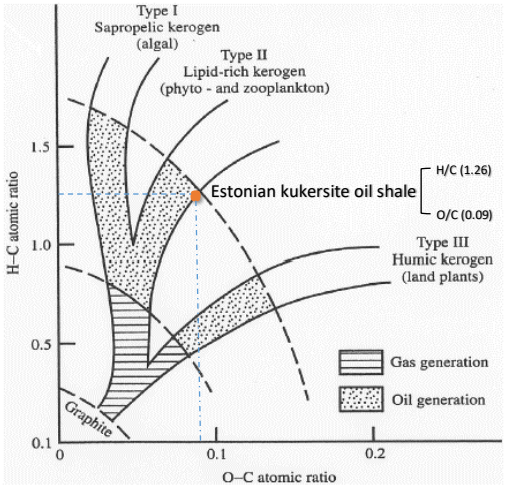

Figure 1. Kerogen classification according to The van Krevelen diagram [29]

The classification of kerogen type evaluates the kerogen maturity in regard to burial depth through thermal evolution using elemental hydrogen to carbon (H/C) and oxygen to carbon (O/C) ratios [30,31]. Type I and Type III kerogen are considered to have the highest and the lowest level of thermal maturity, respectively [32]. In addition, some literature had added a type IV kerogen with H/C ratio of below 0.5 in the graph and described that the decomposed organic matter in this type of kerogen is mainly the form of polycyclic aromatic hydrocarbons [32]. It can be inferred from the diagram that the kerogen in kukersite oil shale is from marine organic materials, ocean plankton, and exists in marine sediments. This type of kerogen produces larger amounts oil and gas than Type III, but lower than Type I. However, the sulfur content of some kerogen in Type II is higher than the other types of kerogen in general, thus more specifically categorized as type IIS. The kerogen in beginning of the Type I pathway seems to largely consists of aliphatic whereas, the kerogen at the beginning of Type III contains largely aromatic structures [29–32].

1.2 Pyrolysis

One primary difference between oil shale deposits and conventional oil and gas reservoirs is that oil shales contain substantial amounts of solid hydrocarbons; namely bitumen (soluble) and kerogen (insoluble) [14]. The pyrolysis process of kukersite oil shale can be generally divided into five steps: 1. At a temperature lower than 150 °C, occlusion of gases and water separation occur, 2. Kerogen decomposition begins at 170–180 °C, 3. At 320–340 °C, kerogen decomposition and gas formation largely take place, 4. Destruction of polymerization products leading to liquid production happens at 380–390 °C, 5. At around of 415–420 °C, endothermic reactions of coke formation occur [33]. Thus, optimization of the shale oil production process by means of pyrolysis is undoubtedly an imperative goal to achieve, and therefore, the conditions in which the conversion process is undergone have to be investigated. It is worth noting that 40–60% of oil shale organic matter can be turned into shale oil [34].

There are many parameters that affect these conditions such as the retorting technologies, pyrolysis atmosphere, temperature, heating rate, flow rate, and so on [35].

Moreover, the yield of liquid products (oil + water) is affected by the temperature and residence time. In this case, at similar temperatures, longer residence time yielded more liquid products. Likewise, a higher quantity of oil and water were produced when the pyrolysis temperature was increased. Apart from the pyrolysis conditions, the quality of pyrolysis yields such as sulfur content is reliant on the shale formation and dynamics and also on the retorting techniques used [14]. In addition, the characteristics and geological origin of oil shale and the differences in organic matter of the sample affect the properties and chemical composition of the shale oil and gas produced [36]. Overall, it can be deduced that oil shales from different deposits have different characteristics; therefore, the properties of the resulting shale oils differ from each other as well. This was also confirmed by Järvik and Oja in [37], in which some properties of the produced shale oils, such as H/C ratio, MW and density, vary from those of oils from other deposits. Moreover, it can even be perceived that oil shale from the same deposit could result in shale oils with different characteristics if different technologies are used to pyrolyze the sample. In general, shale oil has a higher H/C atomic ratio than other fossil fuels (except for petroleum; 1.9), thus enabling production of a variety of chemicals, as presented in Figure 2. Also, a low H/C ratio shale oil is not suitable for production of high quality gasoline and diesel fuels [34].

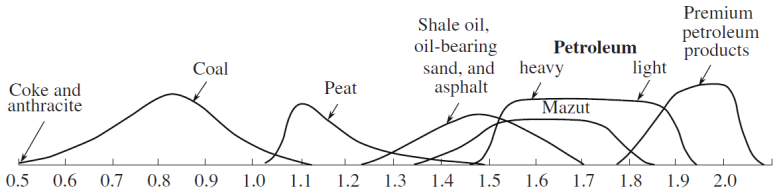

Figure 2. Comparison between the Hydrogen/Carbon atomic ratios in different hydrocarbon materials [34]

To give another example, Figures 1 and 2 in **Publication IV**, which respectively illustrate the distribution of sulfur in shale oils produced under different technologies and also shale oils from different countries (origins), show that the concentration of sulfur is also strongly affected by many parameters.

In conclusion, the properties of the shale oil produced are not only related to the technologies used, but are also strongly dependent on the oil shale derivatives and carbonaceous macromolecule as well as the kerogen and bitumen pyrolysis process [38,39].

1.2.1 Kerogen to thermobitumen

Kerogen - the organic matter fraction of oil shale – is a structure containing mainly carbon, hydrogen, oxygen, and low amounts of nitrogen and sulfur [8,21]. Kerogen is a heteropolymer with a high molecular weight that is not soluble in common organic solvents [40]. A proposed model of Estonian kukersite kerogen, which is known to be a marine kerogen, is shown in Figure 3 [41].

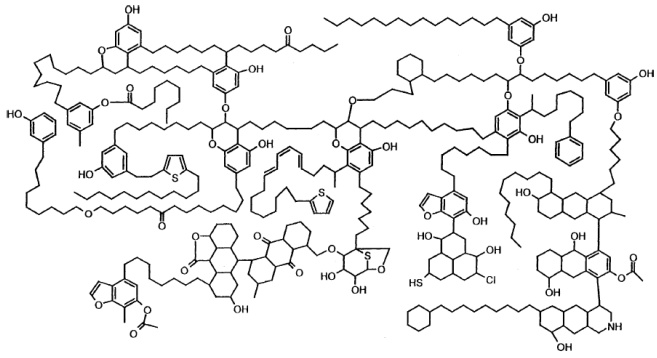

Figure 3. A model of the proposed structure of Estonian kukersite kerogen [41]

For the kerogen to decompose, it must be exposed to heat. Therefore, to produce shale oil, oil shale has to be thermally pyrolyzed in the absence of oxygen. Moreover, the generation of oil and gas begins when the pyrolysis temperature of kerogen is reached [42]. When oil shale is heated, kerogen is first converted to bitumen – a soluble intermediate that has a somewhat similar composition and chemical structure to kerogen – and the formed bitumen is then turned into oil, gas and carbonaceous residues, as well as pyrolytic water. CH_4, H_2, CO, CO_2, H_2S, and $<C_5$ are the primary gaseous products of kerogen decomposition released from the shale sample [21,25]. Therefore, pyrolysis is not a single-step process, and several chemical reactions take place through various steps for oil shale to convert into shale oil and gas. Based on the proposed mechanism for the thermal decomposition of kerogen, as presented in Figure 4, in the first step, the macromolecular organic structure of kerogen and thermally unstable heterocyclic compounds undergo depolymerization and decomposition to form bitumen and gas. The kerogen macromolecule is mostly comprised of aliphatic structures [33]. However, during the formation of bitumen, the aliphatic carbons in kerogen tend to crack into oil and gas, due to the poor thermal stability of the aromatic structures and their aromatization. [25,43–45].

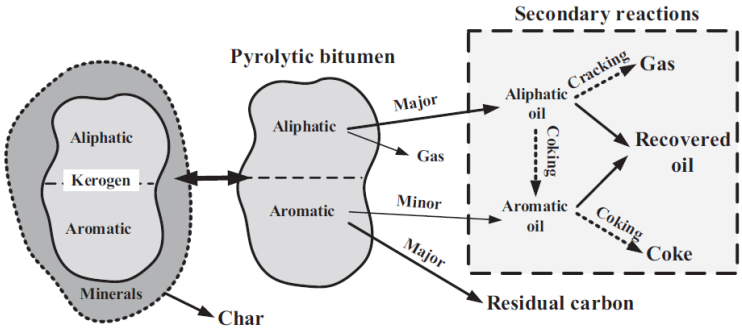

Figure 4. Proposed mechanism model of carbon transformation in kerogen pyrolysis [43]

1.2.2 Thermobitumen to pyrolysates

In the next step, the formed bitumen, undergoes decomposition at elevated temperatures and subsequently, oil, gas and semi-coke are produced. Analysis of the carbon residue showed that a large amount of condensed aromatic ring structure is present in the residue. Hence, it can be derived that a great amount of aromatic carbon is concentrated in the carbon residue, which is due to the occurrence of polymerization and condensation reactions. This takes place as the results of volatilization of lighter compounds during the pyrolysis of kerogen, and conversion of aliphatic hydrocarbons into aromatic structure by means of secondary reactions. Therefore, volatile compounds which are formed in pyrolysis process as a result of kerogen cracking end up in shale oil. However, on the other hand, the aliphatic carbon can be further cracked into liquid and gas, as can be inferred from the figure above. This indicates that the oil composition is highly dependent on the chemical structure of kerogen. By contrast, aromatic carbon in kerogen mostly remains unchanged [25,43–45]. In addition, although the composition of shale oil could be affected by the secondary reactions, it is the structure of kerogen that mainly shapes the composition of shale oil. Therefore, the structures in kukersite shale oil are mostly aromatic due to the structure of kukersite oil shale [46]. Besides, another parameter that has effect on the compounds of shale oil, gas and solid residue is thermal decomposition process. Furthermore, at every stage of kerogen decomposition, the kerogen solid residue has a tendency toward its most stable form resulting in reduction of the H/C ratio over pyrolysis time. It means that there is a tendency for compounds with higher H/C ratio to escape from oil shale under pyrolysis conditions followed by their subsequent condensation at lower temperatures. Consequently, the H/C ratio for the solid residue is the lowest and this value for the gas is the highest.

1.3 Oil shale processing in Estonia

It is about a century that shale oil has been produced in Estonia using 5 main technologies: Kiviter process (vertical retort), Galoter process (solid heat carrier), tunnel ovens, Davidson rotating retorts, chamber ovens and in which excerpt for the first two processes, the rest is not currently used [27,47]. Thus, the oil shale industry in Estonia has had major development historically and plays a key role in supplying the domestic energy of the country [25]. As stated previously, the type of technologies used for processing would have effect on the pyrolysis process, and consequently, the properties of the shale oils products are different, as shown for the sulfur content of the oil produced under various processing technologies in **Publication IV**. The two types of oil shale in Estonia are Dictyonema argillite and kukersite. However, due to the higher organic matter and lower sulfur content of kukersite it is the main oil shale utilized in the country [28]. Estonian kukersite shale oil contains a considerable amount of oxygen compounds, mainly phenols. Also, its specific properties such as low viscosity and low sulfur content make it favorable for the use as a marine fuel [48].

In order for energy and chemicals production, thermochemical conversion technology is considered to be the most suitable method for processing the oil shale [25]. As explained in above, oil shale mostly contains long-chain aliphatic structure while the aromatics are present in small amount therefore, a low-temperature pyrolysis is a suitable to process the oil shale [25]. In low-temperature thermal processing – currently used – oil shale is heated up to 500 °C as opposed to a high-temperature processing method in which the temperature is raised up to 1200 °C (coking) in order for production of city gas [48,49].

In terms of retorting technologies, Kiviter and Galoter retorting processes are used nowadays in Estonia. Kiviter process is based on internal combustion technology using recycled gas and air whereas in Galoter, the presence of ash plays a role in transferring heat to the oil shale particles, however it can also increase the possibility of occurrence of secondary reactions resulting in less oil yield [48,50]. It is worth mentioning that nowadays, modified Galoter technologies, called Petroter, Enefit, and TSK-500, are used. These technologies are different from each other in terms of sizing, technical solutions and layouts [49]. Secondary reactions take place as a result of contact between the oil and a hot carrier (gas or solid) [50]. That being said, there is a need to find a balance between the quality and quantity of the produced shale oil when a processing method is selected.

1.4 Sulfur

As described previously, oil shale has a complex nature with much heteroatom compounds, therefore, the produced liquid product from oil shale degradation is thermodynamically unstable and contain large amount of sulfur-, oxygen- and nitrogen-containing compounds. Therefore, shale oils have to be processed in order to be used as a liquid hydrocarbon fuel [34]. Investigating the composition and structure of these compounds in shale oil is crucial and the acquired analysis would be very beneficial in its upgrading process [51].

In general, sulfur compounds in oil shale can be classified as organic and inorganic sulfur, elemental sulfur [52], in which are released at different temperatures [53]. Sulfur compounds are present in 3 forms: sulfide, sulfate and organic sulfur [13]. Pyrite and sulfate are the forms of inorganic sulfur compounds [52]. These compounds are present as both aromatic rings or aliphatic-structured functional groups [13]. Thiophenic, sulfoxidic, sulfone, and acidic sulfate fractions comprise the organic sulfur content of Estonian kukersite oil shale kerogen [25]. In addition, benzothiophenes, dibenzothiophenes, thioesters and thiols and also, possibly some disulfides are present in the produced shale oil [54].

The sulfur content in Estonian kukersite oil shale is about 2%, and this value for the crude shale oil is about 1% [55]. It is worth noting that some shale oils have higher sulfur content. A major difference between shale oil and crude oil is the quantity of heteroatoms that they contain. For shale oil, the amount of these compounds is much higher than that in crude oil. More specifically, most heteroatomic compounds in shale oil samples are nitrogen and oxygen compounds, while sulfur compounds make up the majority for the petroleum [54].

During the pyrolysis of oil shale, sulfur is distributed in the products and can be detected in the oil, gas and semi-coke [56]. In the process, sulfur reacts with minerals and organic matter resulting in the release of sulfur-containing gases such as H_2S, COS, SO_2 [57]. It is reported that after pyrolysis of Estonian oil shale, majority of sulfur remains in solid residue (50%), while shale gas and oil contain about 35% and 8% of raw oil shale total sulfur, respectively [58]. The presence of such compounds is a big drawback as they act as air pollutants by emitting nitrogen oxides (NOx) and sulfur oxides (SOx) when combusted [2]. In addition, sulfur also plays a role in corrosion of refining equipment as well as poisoning of catalysts. According to [59], the price of oil is largely affected by its sulfur content as well as gravity. For these reasons, their high concentration in the shale oil lowers the quality of the oil and further upgrading processes for refining are required [11].

As mentioned, kukersite shale oil can be used as a component in marine fuels. However, the presence of sulfur is problematic to the environment. For this reason,

based on the strict regulations set by the International Maritime Organization (IMO), the concentration of sulfur in marine fuels in SOx Emission Control Areas has to be limited to 0.1% by mass since 2015. In addition, starting from 2020, the global sulfur limit was also decreased to 0.5% [12]. Therefore, it would be very beneficial to investigate the liberation of sulfur during the utilization of oil shale and identify the compounds for economic and environmental considerations. This would lead to achieving suitable conditions for obtaining high-quality oil with lower sulfur emission.

In conclusion, even though heteroatoms (sulfur, nitrogen and oxygen) comprise about 15% of Estonian oil shale kerogen [25], they have a large effect on properties of oil and gas products, and therefore, their behavior in the retorting process must not be neglected. For instance, in pyrolysis, the sulfur containing groups are transformed into different compounds and distributed in shale oil, gas and solid residue. Thus, utilization of these products causes harm to the environment and also industrial equipment [60]. In addition, the pyrolysis of oil shale is very complex in nature and numerous reactions take place simultaneously. For these reasons, investigating the release of sulfur and its distribution through the pyrolysis products is beneficial for better understanding the pyrolysis mechanism. As a result, the adverse effects on sulfur compounds on applicability of pyrolysis products can be mitigated.

1.5 Objectives

The exploitation of fossil fuels has always been associated with environmental risks. Consequently, the reduction of emissions of CO_2 and hazardous pollutants has been an important objective of research. Therefore, reducing the emissions of CO_2 is one of the goals of future fossil fuels utilization to meet the strict climate requirements. Developing new technologies as well as new methods in the oil shale sector is closely connected to its environmental footprints. Therefore, seeking a more sustainable way for oil shale valorization to produce shale oil and gas has been of great interest.

As known, N_2 is used as carrier gas in the oil shale industry and CO_2 is one of the main by-products released as pyrolysis gas. The focus of this study is the effect of CO_2 on pyrolysis products if used as a sweep gas in place of N_2. This analysis is done to study the impact of CO_2 on the release of sulfur from oil shale and its distribution in the pyrolysis oil and gas. In addition, the effect of humidity by introducing steam to the CO_2 and N_2 atmospheres has also been investigated so that a more comprehensive conclusion, in regard to the effect of various carrier gases, is reached. Therefore, the aim of this study was to investigate the effect of CO_2 N_2, CO_2/steam and N_2/steam sweep gases on the shale oil and gas, and also to learn about the behavior of sulfur during the pyrolysis of Estonian kukersite oil shale. Therefore, the objectives are:

- to study the effect of CO_2, CO_2/steam, N_2, and N_2/steam on the kukersite oil shale sample during the pyrolysis process,
- to investigate the effect of these sweep gases on the yields and properties of the pyrolysates,
- to perform comparative analysis on the produced shale oil samples,
- to analyze the impacts of the carrier gases on generation of pyrolysis gas, and
- to study the effect of the gaseous atmospheres used in pyrolysis on shale oil sulfur compounds and also the release of sulfurous gases during the pyrolysis process.

The analysis conducted in this work can be useful for taking into consideration the environmental aspects of oil shale utilization processes, such as sulfur related issues and the use of CO_2 in pyrolysis.

2 Experimental

In the experimental part of the thesis, the step-by-step experimental work, measurements techniques as well as the calculation methods used have been discussed. Information on the kukersite oil shale sample used for pyrolysis experiments as well as its preparation for thermobitumen experiments and also information on the shale oil fractions can be found in **Publications I and III**. This section initially describes the experiment procedure to produce the desired oil and gas samples. Subsequently, all the equipment used to conduct analyses have been given a detailed description of so that this study can be repeated by any researcher. A schematic diagram of the oil shale pyrolysis experiment, and analysis carried out in this study is depicted in Figure 5.

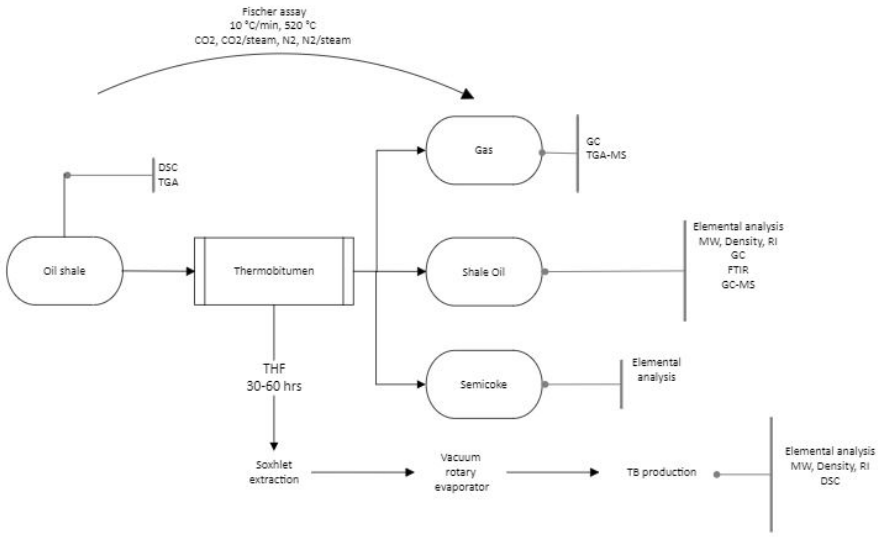

Figure 5. Schematic diagram of the analysis carried out in the study

2.1 Oil shale

The Kukersite oil shale from this study was taken from the Ojamaa mine. Table 1 (Table 1 in **Publication I**) shows the ultimate and proximate analysis performed on the sample. Furthermore, more comprehensive information about the sample can be found in [58]. From the table, it can be figured that the organic matter of the sample is 28.8%. Also, total organic carbon as well as total inorganic carbon are 19.71%, and 5.83%, respectively. In addition, the H/C (1.26) and high O/C (0.09) molar ratio of the sample shows that the kukersite oil shale is of Type II kerogen classification.

*Table 1. Ultimate and proximate analysis for the kukersite oil shale sample (from **Publication I**)*

Ultimate analysis		
	Dry basis, wt %	Organic matter, wt %
C	25.54	69.1
H	2.38	8.3
N	0.06	0.2
S	1.73	2.1
Cl	0.15	0.5
O	18.69	19.8
Proximate analysis		
Volatile matter	31.36%	
Moisture content	0.44%	
Ash content at 950°C	51.59%	
Fixed carbon	16.61%	
Lower heating value	8.89 MJ/kg	

2.2 Oil shale thermobitumen formation studies

A U-shaped reactor with a volume capacity of 30 ml was built from a stainless-steel pipe (9.4 × 2.3 mm) to pyrolyze the oil shale sample isothermally. The reactor was placed in a preheated convection oven at temperatures of 340 °C, 380 °C, and 420 °C at the rate of 20–25 °C/min. The pyrolysis was done under a flow of N_2 at about 100 ml/min. The pyrolysis took between 15 minutes to 16 hours. Afterward, the weight of liquid products and the solid residue were noted. Additionally, the separation of oil and water was done by means of centrifugal force. After pyrolysis, a Soxhlet extraction with solvent tetrahydrofuran (THF, boiling point 66 °C) was used to extract the TB from the solid residue. The extraction process took until the solvent which passed through the solid residue became colorless (36 and 60 hours). Then, in order to remove the solvent from the TB solution, a vacuum rotary evaporator at a pressure of about 4 mmHg (in a water bath at 95 °C) was employed.

2.3 Fischer Assay (FA)

A particle size of 500–710 µm was sieved from the 50g of the grounded kukersite oil shale sample in order to be used for the experiments in a modified Fischer assay retort. Fischer assay is a standard laboratory method so that yield of an oil shale sample can be estimated. In this method (GOST standard; GOST 3168-66) the temperature programs used to heat up the sample in the retort is as follows: 1) from room temperature to 500 °C at 10 °C/min, 2) rising the temperature from 500 °C to 520 °C in 20 minutes (1 °C/min), 3) holding at final temperature (520°C) for 20 minutes. After the test, the weight of the liquid products and solid residue can be obtained weighing and the amount of the produced gas can calculated by difference using the material balance.

Four different sweep gases were introduced into the retort: CO_2, CO_2/steam, N_2, and N_2/steam using a tube with the connection on the retort lid. The flow rate in dry CO_2 and

N_2 environments was 21 ml/min and for the test with the water vapor, the water flow and N_2/CO_2 flow rates were set at 10 ml/min and 0.1 ml/min, respectively. Also, the water was heated up to 150 °C prior to entering the retort. In addition, the retort was flushed with N_2 or CO_2 an hour before the start of the experiment to make sure the system is under the desired environment. Moreover, to take the possible water loss into account and for the calculation accuracy, three blank runs were made separately with only water.

2.4 Analytical methods

2.4.1 Elemental analysis

For the oil and TB samples, the elemental analysis was carried out by an Exeter Analytical model CE440 elemental analyzer (Exeter Analytical, Coventry, United Kingdom) to mainly obtain the H/C ratio. Also, a Vario MACRO CHNS Cube system (Elementar Analysensysteme GmbH, Langenselbold, Germany) was used in this study to conduct the elemental analysis on the produced shale oil sample as well the semi-cokes. The expanded relative uncertainty is 1.11%, for carbon, 16.56% for nitrogen, 2.56% for hydrogen, and 5.7% for sulfur element. The sulfur content of FA oil was determined using the above apparatus. However, a Lab-X 3500 Benchtop XRF Analyser (Oxford Instruments, Abingdon, United Kingdom) was employed to determine the concentration of sulfur in shale oil fractions using the ASTM D 4294 method. For the sulfur measurements, the standard uncertainty was estimated to be 0.0024 wt% (expanded uncertainty of 0.0043 wt% at the 95% confidence interval level).

2.4.2 Fourier-Transform Infrared Spectroscopy (FTIR)

The IR spectra of the shale oil samples was measured using an Interspec 301-X spectrometer provided with an ATR accessory. The spectra analysis of each sample was conducted spectra were analyzed in the wavenumber range of 600–4000 cm^{-1} at a resolution of 1 cm^{-1}. To make sure that the effect of noise is reduced, for all the samples, an average of 10 scans was used. In this way the repeatability of the measured spectra can be ensured as well. The estimated standard uncertainty and estimated expanded uncertainty (95% level) are 0.00053 and 0.0012 absorbance units (on average), respectively.

2.4.3 Differential Scanning Calorimetry (DSC)

A NETZSCH 204HP Phoenix DSC was used to perform the DSC tests on the oil shale sample in N_2 and CO_2 atmospheres with similar conditions as FA. Approximately 10 mg of the sample was used to fill the open Al-crucibles. Each test was repeated three times to ensure reproducibility. In addition, this instrument was used to measure the heat capacity of the TBs as well. The test was carried out with 20 mg of TB sample under a N_2 flow (40 ml/min) using a sealed Al crucible. More details on temperature program used to perform the test and the equation is given in **Publication I**.

2.4.4 Thermogravimetric Analysis – Mass Spectrometry (TGA-MS)

The TGA-MS tests on the oil shale samples was carried out by a NETZSCH STA 449 F3 Jupiter® TG-DSC coupled with a NETZSCH QMS Aëolos® mass spectrometer under similar conditions as a FA; test atmospheres (CO_2, CO_2/steam, N_2 and N_2/steam) and temperature profile. In these tests, Pt/Rh alloy crucibles with removable thin-walled Al_2O_3 liners were filled with about 8 mg of the shale sample. The coupled mass spectrometer was used to

detect and analyze the release trend of the of H_2S and SO_2 gases through the process of pyrolysis. A detailed explanation of how they were analyzed is available in **Publication IV**. The value for the normalized intensity of these measurements was calculated to be 0.02. To ensure repeatability, the tests for each atmosphere were done at least three times.

2.4.5 Density measurement

To measure the density of TB samples which are solid at room temperature, they were first dissolved in tetralin (anhydrous 99% pure, Sigma-Aldrich); 20–30 wt%. To ensure that the solution was well mixed, it was kept at 60 °C for a couple of hours in a closed vial and then, an ultrasonic bath was used for 20 minutes to assist the dissolution process. The mixing rule equation used to calculate the density can be found in **Publication III**. Also, the density of the FA oil samples was measured at temperatures of 15 and 20 °C. The standard uncertainty as well as the expanded uncertainty (95% level) of the oil samples measurements were estimated to be 0.00015 g/cm^3 and 0.0003 g/cm^3, respectively.

2.4.6 Refractive Index (RI) measurement

Similar to density measurement for the TB samples, the prepared solution was used to calculate the RI value as well. Correspondingly, the equation used is shown in **Publication I**. An Abbemat HT refractometer (Anton Paar GmbH) was used to measure the refractive index of the oil sample at a temperature of 20 °C and a wavelength of 589.592 nm. In this refractometer, the estimated standard uncertainty and expanded uncertainty (95% level) are to be 0.0011 and 0.0021.

2.4.7 Molecular Weight (MW) measurement

To measure the molecular weight of the oil samples, a Knauer K-7000 vapor pressure osmometer (Wissenschaftliche Gerätebau Dr Ing Herbert KNAUER GmbH, Germany) was used. The standard uncertainty and the expanded uncertainty (95% level) for this device are estimated to be 7 g/mol and 14 g/mol, respectively. However, for the TB samples, an Osmomat 070 (Gonotec GmbH, Germany) was also used to obtain the MW value. To prepare a TB solution, a pyridine solvent (99% pure, Sigma-Aldrich) was used. More detailed information regarding the MW measurement can be acquired from **Publication I**.

2.4.8 Gas Chromatography (GC)

For the compositional analysis of the produced gas samples, two different gas chromatographs were used. Detailed explanation of how the calibration and analysis was done with the GCs are present in **Publication II**. To calculate the composition of O_2, N_2, CO, and CO_2, a Shimadzu GC-2014 gas chromatograph (GC1) equipped with a thermal conductivity detector (GC-TCD) and a valve system was used. The quantity of oxygen, nitrogen and carbon monoxide gases were computed using a 3 m packed column with a 5 Å molecular sieve (OD 1/8”, ID 2 mm, 80/100 mesh), and the quantity of CO_2 was obtained using a 9 m 25% DC-200/Shimalite packed column (60/80 mesh, OD 1/8”, ID 2 mm). The column temperature program is as follows: the program began at a temperature of 35 °C which was kept for 3 minutes isothermally, then increased up to 85 °C at 5 °C/min (kept isothermally as well for 3 minutes), and was lastly heated at 10 °C/min to a temperature of 125 °C. The total program time was 20 min. The injection temperature was 250 °C and the split ratio was 10:1. The second GC used was a Gazohrom-3101 gas chromatograph (GC2) which was equipped with a thermal

conductivity detector used to quantify the composition of H_2, CO and CH_4. In the GC2, air was used as the carrier gas (at 65 mL/min). It should be noted that the GC1 was also used to determine the amounts of C2 and C3 hydrocarbons. The precise description of how these compounds were analyzed quantitatively is present in **Publication II**. The relative standard deviation for parallel measurements for the GC1 and GC2 did not exceed 10% and 5%, respectively.

2.4.9 Gas Chromatography – Mass Spectrometry (GC-MS)

To analyze the sulfur-containing compounds present in the FA oil, an Agilent 7890B gas chromatograph wich was connected to an Agilent 5975C Inert MSD mass spectrometer and Agilent Flame Photometric Detector (FPD) Plus was used. Helium at 0.9 mL/min with a purity of 99.9999% was introduced as the carrier gas. The injection of the samples was done by a CTC Combi/GC-PAL 80 autosampler as follows: the injection amount was 1 µl at 10:1 split ratio, in which the temperature of an injector was set at 260 °C. The initial oven temperature was determined to be 40 °C kept for 5 min. Subsequently, the temperature was rised up to 160 °C at a rate 3 °C/min. Lastly, the temperature of oven was heated up from 160 °C to 280 °C at a rate of 20 °C/min. The duration of the run was 51 minutes. The FPD temperature of the was determined at 300 °C and the flow rates of detector were set at 60 mL/min for hydrogen and air (1:1). In addition, the column was a DB Petro with dimensions of 100 m x 250 µm x 0.5 µm. Also, the dimensions of the capillary to the MS and to the FPD+ were 1 m x 250 µm x 0 µm and 5 m x 200 µm x 0 µm, respectively. The column was a DB Petro (100 m x 250 µm x 0.5 µm). To detect the sulfur compounds, three shale oils produced under each FA atmosphere was analyzed. The estimated expanded uncertainty (95% level) for each of detected sulfur compound was presented separately.

3 Results and discussion

3.1 The effect of sweep gas on pyrolysis yields

The yields from Fischer assay experiments are presented in Table 2 (Table 2 in **Publication I**). Since only a small amount of liquid product was produced, providing precise quantitative analysis of oil and water was not possible. Therefore, only a summation of them as a total liquid product was reported. It is worth mentioning that the calculated uncertainty for the liquid and gas is 7% and 13%, respectively.

*Table 2. Yields of Fischer assay products on the dry oil shale basis (wt%) in different experiment atmospheres (from **Publication I**)*

Pyrolysis products	*N_2*	*N_2/steam*	*CO_2*	*CO_2/steam*
Oil + Water	15.9	17.2	16.1	17.4
Gas	6.7	7.8	6.8	7.6
Semicoke	77.3	75.0	77.1	75.0

**The estimated expanded uncertainty (95% level) value for the FA tests is 1.1 g.*

The results show that injection of steam increased the yield of liquid and gas products. According to Ekinci [61], the higher liquid product yield is mainly because of the prevention of char-forming reactions such as dehydrogenation of alkanes to alkenes and cyclization. As a result, it can be deduced that the weight of the solid residue under steam tests is lower. This could be due to the lower formation of coke and higher production of oil vapor under a steam environment [62]. Steam breaks down the bonds of low molecular weight components attached to the macromolecular part by means of vaporization, desorption, and diffusion processes, and thus, these components are released as volatiles [63].

3.1.1 TGA

Thermal analysis of the oil shale sample was carried out to better perceive the behavior of kerogen decomposition in different sweep gases. For more accurate analysis, atmospheres, and a temperature profile similar to a Fischer assay were used. The mass loss curve from TGA consists of three stages: 1. From ambient temperature to a temperature of 200 °C, in which the mass loss is due to the presence of moisture/water in interlayers as well as clay minerals, and also nahcolite ($NaHCO_3$) decomposition. In this stage, kerogen conversion to bitumen begins, resulting in physical changes, such as softening, and molecular rearrangement. However, the liberation of gas may also take place. In the temperature range of 200–550 °C in which the weight loss is attributed to the hydrocarbon material. In this stage, the mass loss occurs as a result of the decomposition of kerogen and bitumen to produce volatile hydrocarbons. The second stage is the cause of the biggest mass loss in the sample. 3. In stage three, which is above 600 °C, the thermal decomposition of carbonates and clay minerals is the reason for sample mass loss. Moreover, the release of CO because of the reaction of CO_2 with char is also responsible for the additional weight loss in the sample [64,65].

Figure 6 (Figure 1 in **Publication I)** compares the mass loss of the oil shale sample in CO_2 and N_2 as a function of temperature. From the figure, it can be observed that below

200 °C no major mass loss occurred, apart from moisture evaporation. Also, up to about 350 °C the change in the sample mass is similar. However, above 350 °C the decomposition of organic matter takes place to a significant extent and continues until about 520 °C. The sharp slope of mass loss started approximately at 380 °C. This could be due to the decomposition of TB to oil and gas, as discussed in **Publication I**. The findings show that at around this temperature the formation of TB is maximized. Above this temperature, much of the hydrocarbons are released from the sample. Additionally, a small difference can be seen in that the sample under CO_2 experienced a higher mass loss. Even though this occurrence could also be a result of the heterogeneity of the samples, but it was suggested that higher reactivity of CO_2 than N_2 is due to the role of alkali metals in CO_2 and H_2O reactions with carbon [66].

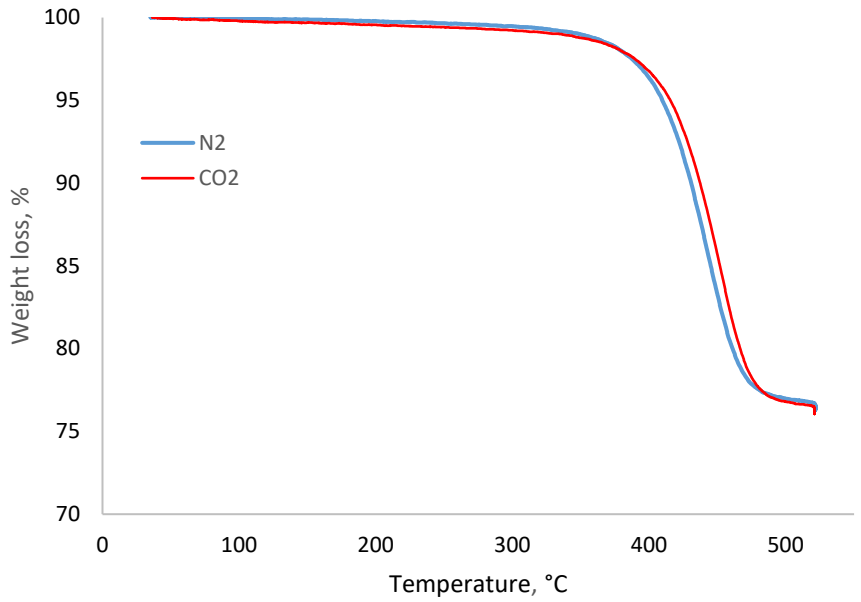

*Figure 6. TGA curves of the oil shale sample in N_2 and CO_2 (from **Publication I**)*

Moreover, Figure 7 and Figure 8 (Figures 2 and 3 in **Publication I**) analyze the effect of adding steam. As these figures illustrate, steam significantly increased weight loss in both environments. Furthermore, it should be noted that steam also reduces the temperature of pyrolysis. These points were similarly observed in both N_2 and CO_2 environments.

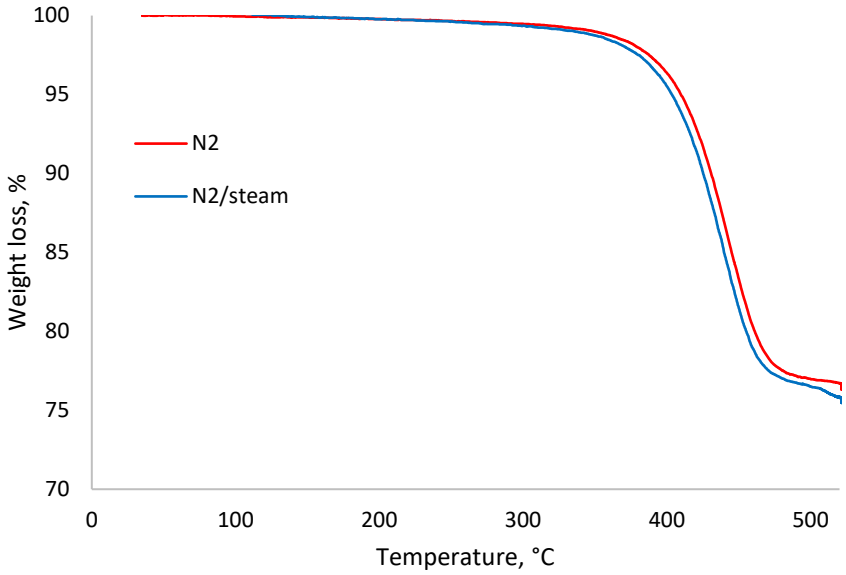

*Figure 7. TGA curves of oil shale pyrolysis in N_2 and N_2/steam (from **Publication I**)*

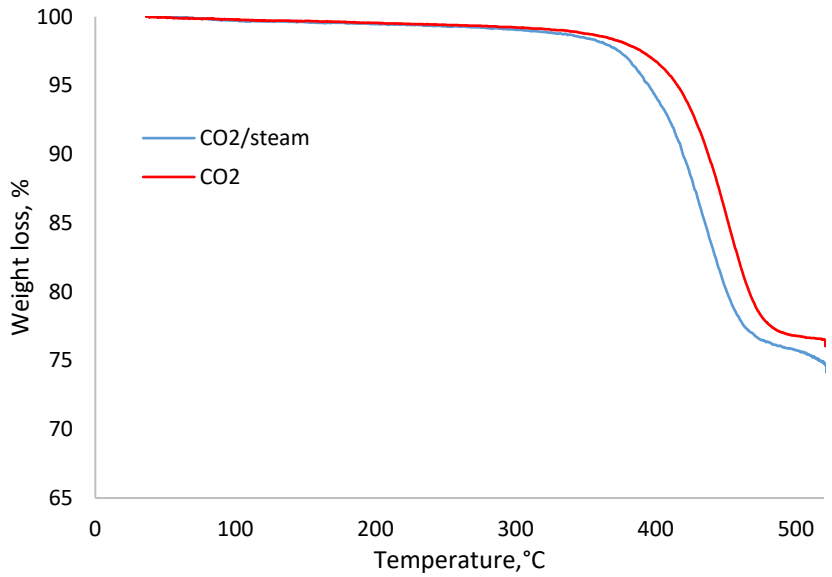

*Figure 8. TGA curves of oil shale pyrolysis in CO_2 and CO_2/steam (from **Publication I**)*

3.1.2 DSC

The DSC graph obtained for oil shale under CO_2 and N_2 atmosphere is presented and compared in Figure 9 (Figure 4 in **Publication I**). As can be seen, the endothermic peak appearing at 150 °C is mainly due to the evaporation of water particles from clay minerals [65].

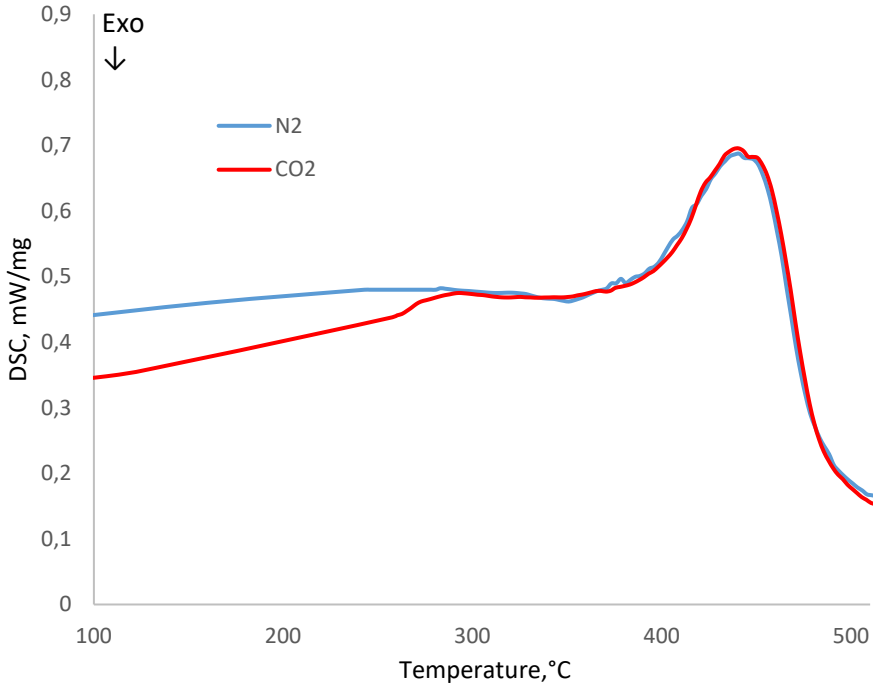

*Figure 9. DSC graph for the oil shale under CO_2 and N_2 atmosphere (from **Publication I**)*

At around 200 °C however, a sharper peak shows up as kerogen begins to convert into bitumen. This happens as the kerogen molecular structure softens and changes resulting in depolymerization of kerogen. This can be explained by the cracking process of thermally unstable heterocyclic compounds followed by the release of gases and light hydrocarbons [66,67]. The downtrend peak after completion of pyrolysis is observed and the heat requirement is lowered. It can be inferred from the CO_2 and N_2 DSC trends that the curves behave similarly and the type of gas did not have a noticeable effect on the thermal behavior during pyrolysis.

3.2 The effect of sweep gas on shale oil

3.2.1 Composition and properties

The ultimate analysis of the produced shale oil under Fischer assay are presented in Table 3 in **Publication I**. Oils produced in N_2, and CO_2 do not vary much; however, for the oils produced under steam, a higher H/C ratio is obtained. This means that more aliphatic compounds are present in the oils produced in the steam environment [68]. Additionally, looking at the shale oil compositions, it can be understood that N_2 and CO_2 gases did not have a big impact on the amount of nitrogen in the oils, whereas steam reduced the

amount of nitrogen in the oil (up to 0.05%). Different explanations have been brought for this. The reduction of nitrogen could be since nitrogen is largely present in aromatic molecules, which are more stable thermodynamically in thermal cracking processes [69,70]. As explained previously (as presented in **Publication I**), shale oils produced under steam are aliphatic-richer compared to dry N_2 and CO_2 atmospheres. Therefore, steam oil contains lower amounts of aromatics, and thus, a lower nitrogen content. Additionally, very light fractions produced in a steam environment contain low amounts of nitrogen [71]. Furthermore, according to Nazzal [72], this could occur as steam partly reacts with organic nitrogen and reduces the nitrogen of the derived oil. In addition, some physical properties of the oils, such as molecular weight, density, and refractive index, have been measured and are shown in Table 4 in **Publication I**.

Combining the analysis of data in Tables 3 and 4 in **Publication I**, it can be concluded that the use of CO_2 or N_2 had some impacts on the yield of pyrolysis products as well as the composition of the corresponding oils produced. However, the introduction of steam into a pyrolysis atmosphere not only enhanced the oil and gas production but also produced an oil with lower nitrogen content. This is in accordance with the literature that by adding steam, an increase in the ratio of H/C was observed, Therefore, a higher amount of gaseous products was produced, and also the quantity of solid residue was smaller [73]. Additionally, it can be inferred from Table 4 in **Publication I** that the density of the oils produced under steam atmosphere increased while the MW decreased. This explains that the MWs of the produced oils in steam environments do not greatly vary from the other oils and therefore, their difference falls within the reported expanded uncertainty.

Since the presence of sulfur is of high importance, and also the aim was to compare the effect of different atmospheres on concertation of several common sulfur compounds, therefore, presence of some of these compounds were identified and analyzed quantitatively using GC-MS-FPD. Subsequently, the results of the analysis are presented in Table 1 in **Publication IV**. The expanded uncertainty for each compound is calculated and presented in the last column.

The identified peaks detected in the oil chromatograms included were mostly the largest peaks present. Therefore, it can be deduced that the majority of the sulfur compounds in the shale oil samples are thiophene derivatives. Their thermal stability is the main reason that they comprise most of the sulfur compounds in the oil [51]. It should also be noted that the structure of the original kerogen plays a part as well. Moreover, it can be noticed that the concentration of some compounds in CO_2 is higher than that of in N_2. Although, for other compounds the slight difference seems to be too small to be significant. This implies that the concentration of sulfur compounds in the shale oil could possibly be increased when CO_2 is used as a sweep gas. Furthermore, the effect of steam on the concentration of these compounds is presented as well. The analysis of the data shows that introduction of steam greatly increases the concentration of sulfur compounds in the oil samples. Therefore, it can be deduced that reactive gases enhance the transformation of sulfur compounds from the oil shale sample to shale oil and gas (the sulfurous gas is discussed later). In addition to the compounds above, the content of H_2S and SO_2 were analyzed as well. The results show that an abundant amount of these compounds was dissolved in the oil. The release of these gases was studied in **Publication IV**. Consequently, it can be found that at lower temperatures most of oil shale sulfur is turned into dissolved gases (mainly H_2S), different forms of thiophene and other thermostable heterocyclic compounds [74].

3.2.1.1 FTIR

Similar to TGA analysis, a comparative analysis of the FTIR spectra for oil samples from all atmospheres has been done as well. Detailed information on assignments for each absorbance peak in spectra can be found in **Publication I** and in the literature [75,76]. Figure 10 (Figure 5 in **Publication I**) illustrates the FTIR spectra for the oils produced in CO_2 and N_2.

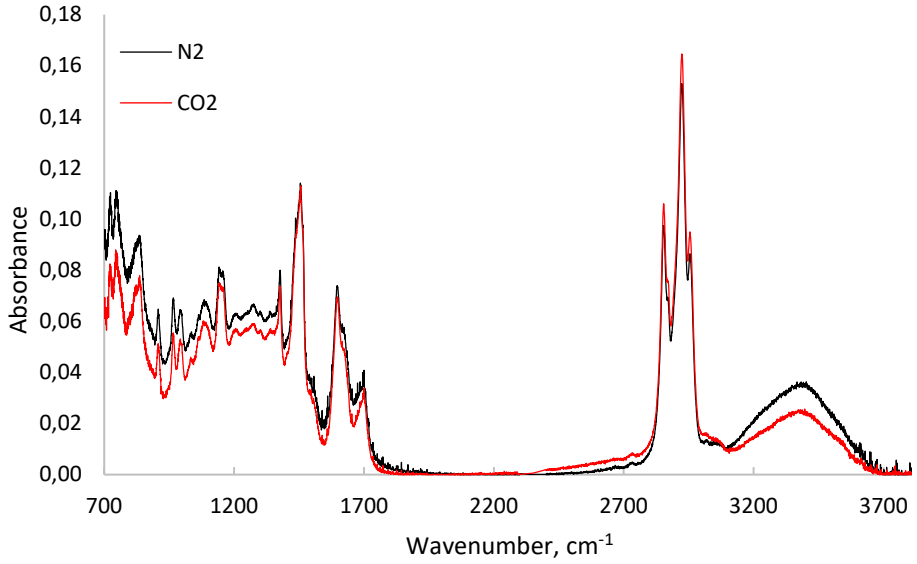

*Figure 10. FTIR spectra of CO_2 and N_2 shale oils (from **Publication I**)*

As can be seen from the figure, the peaks for the CO_2 sample in the range of 700–1000 cm^{-1} are lower than those of the N_2 sample. Likewise, the CO_2 curve in the region 3200-3600 cm^{-1} is smaller. These indicate that fewer hydroxyl groups were present in the oil produced in CO_2 atmosphere. Furthermore, in pyrolysis oil produced under CO_2, the intensity of the aliphatic peaks at 2750–3000 cm^{-1} is larger than that of the N_2 sample. This suggests that the use of CO_2 as a sweep gas produced oil which is richer in aliphatic compounds. On the other hand, the oil from N_2 pyrolysis has greater peak in aromatic regions (700–1200 cm^{-1}, 1600–1650 cm^{-1}), thus a more aromatic oil was produced. This agrees with our earlier result when the H/C of the shale oil under N_2 was lower, indicative of more aromatic oil. This could be due to the increase in the concentration of existing aromatics, and also aromatization of aliphatic compounds in the shale oil [50].

Figure 11 and Figure 12 (Figures 6 and 7 in **Publication I)** illustrate the FTIR spectra of the oils produced under steam when injected along with the N_2 and CO_2. Comparing the effect of steam in both, it can be perceived that steam did not have a big impact on the hydroxyl group content of the oil. Moreover, when steam was added to N_2, the intensity of aliphatic peak slightly increased, whereas the corresponding peak in CO_2/steam shows a slightly lower peak than that of the CO_2 sample, however, the H/C ratio was obtained to be higher. This could be as a result of uncertainty in measurement. Furthermore, at the band region 700–1700 cm^{-1}, steam has an adverse effect on the intensity of the

alkene and aromatic C–H bonds peaks when injected along with the N_2, whereas introduction of steam to CO_2 does not cause a great change in these chemical structures of the oil, as compared to dry CO_2.

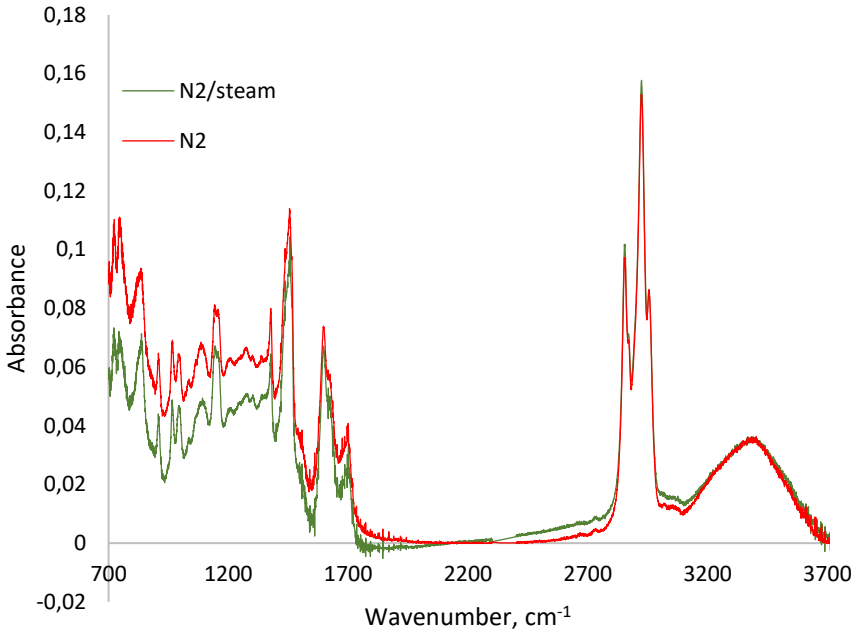

*Figure 11. FTIR spectra of N_2 and N_2/steam oils (from **Publication I**)*

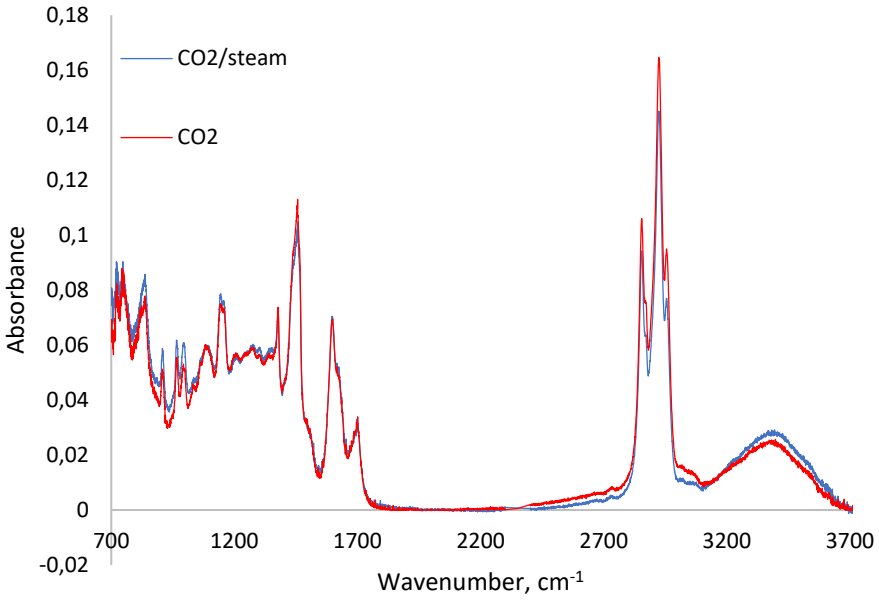

*Figure 12. FTIR spectra of CO_2 and CO_2/steam oil (from **Publication I**)*

3.3 The effect of sweep gas on pyrolysis gas composition

Studying the release of gaseous products and their evolution during the pyrolysis of oil shale is beneficial for better understanding their behavior throughout the process and their dependency on the temperature. This could be helpful to find out more about the mechanism of oil shale decomposition. Table 1 and Table 2 in **Publication II** show the compositional analysis of gas samples taken at different temperatures during oil shale pyrolysis. Moreover, analyzing them provide important information about the evolution of hydrocarbon gases. In addition, a detailed analysis of the effect of steam on production of gases can also be gained. As can be seen, small amounts of non-condensable gases were produced before 400 °C, however, most of the gas was produced after this temperature. According to Campbell et al. [77], in the conversion process of kerogen to bitumen, not much oil and gas are produced, and hydrocarbon production mainly occurs after TB is produced. This result was obtained in this study as well.

Looking at the tables above, additional information such as the alkenes/alkanes ratio is provided. The alkenes to alkanes ratio can be helpful to determine reaction mechanisms and indicates pyrolysis conditions [78,79]. It has been stated by researchers that occurrences of secondary cracking reactions are the reason that the alkenes/alkanes ratio is increased [78–80] and coking reactions are the cause of a smaller ratio [81]. The results show that the ratio initially increased and then decreased through the pyrolysis process. Also, steam generally increased the ratio when present in the pyrolysis atmosphere. The increase in composition of C_2 and C_3 hydrocarbons is mainly because of the oil vapor cracking during kerogen decomposition at higher temperatures resulting in breakage of C–C bond cleavage [50]. According to Williams and Nazzal [82], the occurrence of vapor phase cracking reactions is enhanced under steam. Therefore, higher oil production is due to the role of steam in increasing the secondary vapor phase cracking reactions and also, decreasing the secondary coking reaction.

Also, to easily analyze the evolution of such gases in different environments, the data in the table were drawn as a bar chart. Figures 13–15 (Figures 1–3 in **Publication II**) display the evolution of HC gases, alkane gases and alkene gases, respectively.

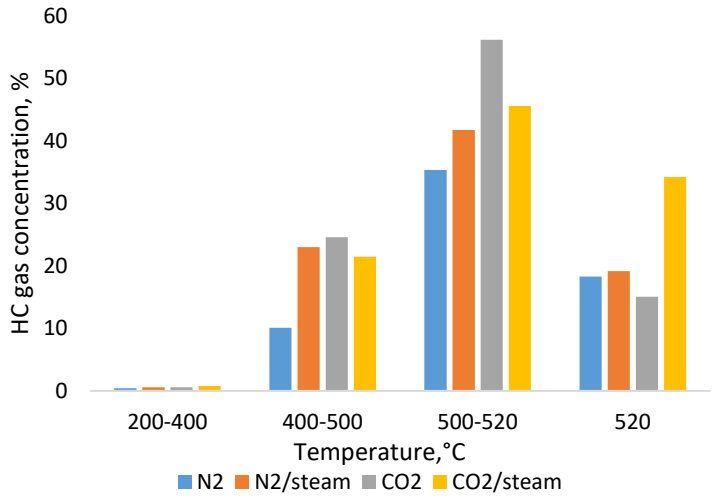

*Figure 13. Evolution of HC gases during the pyrolysis in all test atmospheres (from **Publication II**)*

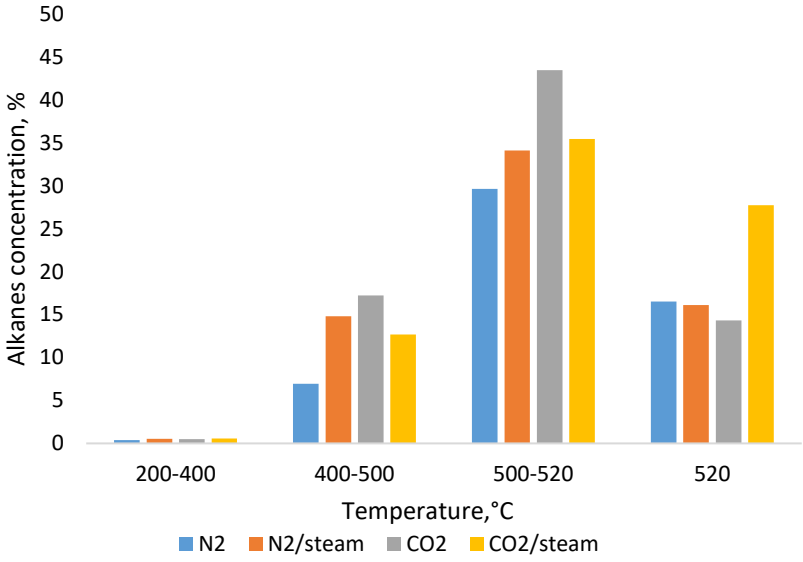

*Figure 14 Evolution of alkanes (from **Publication II**)*

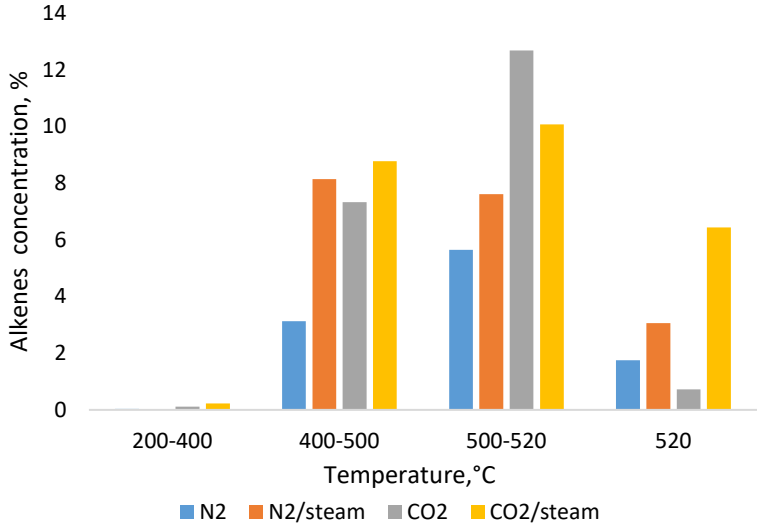

*Figure 15. Evolution of alkenes (from **Publication II**)*

Figure 16, 17 and 18 (modified Figures 5–7 in **Publication II**) present the trends for the yields of CO, H_2 and CH_4 during the pyrolysis process of oil shale. The sampling of the gas was carried out offline and the gas samples were taken only when the retort temperature reached the target temperature, as shown in changes of gas compositions during the pyrolysis process in **Publication II**.

Formation of gases in the pyrolysis process consists of three stages: initially and in the temperature range of up to 340 °C, breaking of weak chemical bonds like C−O and −OH as well as decomposition of oxygenated chemical compounds takes place, mainly resulting

in the production of pyrolysis water, CO_2 and CO gases. Furthermore, at higher temperatures, C−C and C−H chains bonds are broken down. Also, the generation of H_2 and C_1−C_5 organic gases occurs, and the production of water, CO_2, and CO reduce. Eventually, the generation of gases is mostly maximized in a temperature range of 450–500 °C [25].

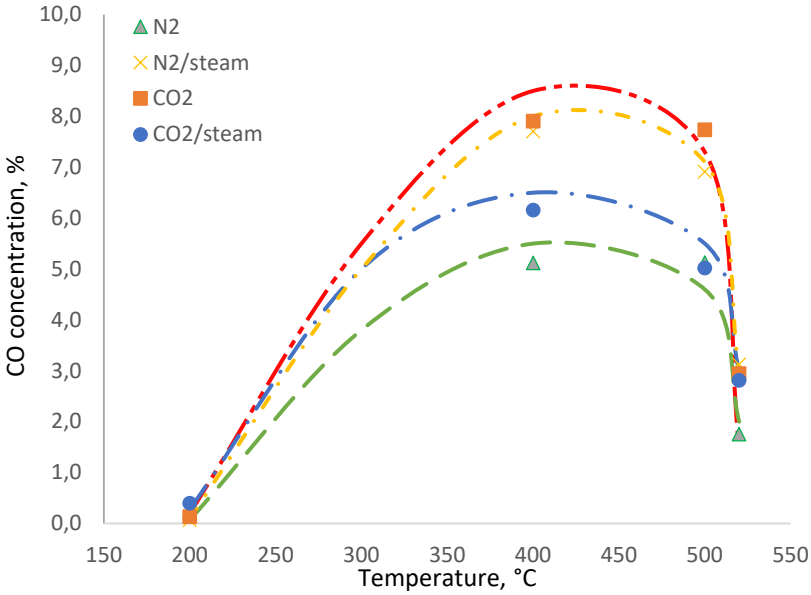

*Figure 16. Expected evolution trend for CO during pyrolysis (from **Publication II**)*

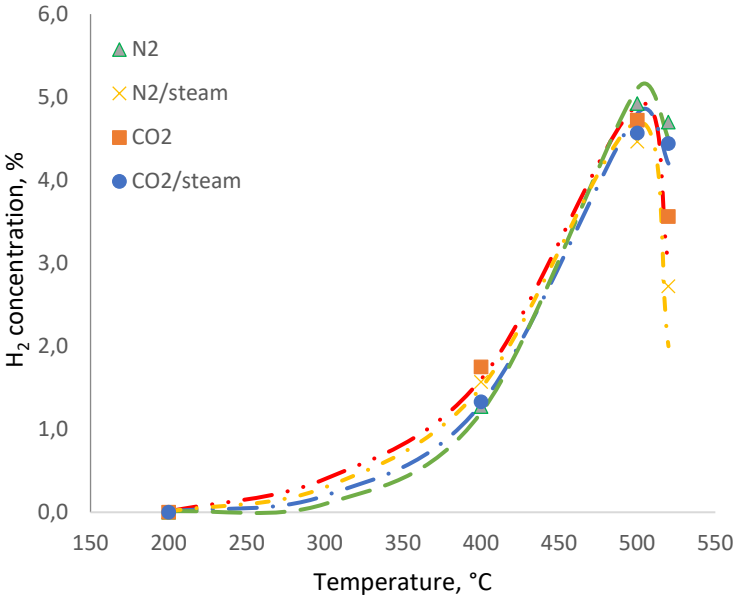

*Figure 17. Expected evolution trend for H_2 during pyrolysis (from **Publication II**)*

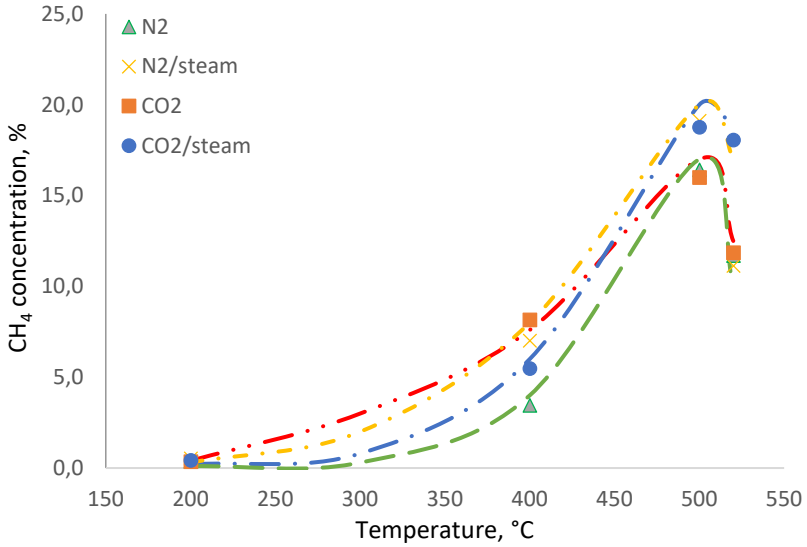

*Figure 18. Expected evolution trend for CH_4 during pyrolysis (from **Publication II**)*

As the results of Table 2 in **Publication III** indicate, at temperatures less than 340 °C, since the pyrolysis temperature is low, not much kerogen was yet converted to TB, and therefore, only small amounts of oil and gas were produced. However, as temperature increased, more TB was formed due to a more complete conversion path of kerogen-TB. The result show that the maximum amount of TB was formed at 380 °C (47% of organic matter). It can be deduced that the production of oil and gas just begins once TB production is initiated and increases at higher temperatures. The sharp slope of gas curves starting at around 400 °C is primarily because of maximum kerogen decomposition to TB, which occurs along with the oil generation. Therefore, the formation of TB and its decomposition to produce oil and gas take place simultaneously [25]. By increasing the temperature and looking at the finding of TB formation at 420 °C, it can be derived that most of the organic matter (56–59% of organic matter) was converted into oil and water. This then can be compared with the oil production in pyrolysis of kukersite oil shale in a Fischer assay retort which yielded about 60% of organic matter (discussed in **Publication III**).

From the figures and tables in **Publication II**, some important information from the peak of gas evolution can be obtained. It appears that the majority of the gas produced at oil evolution temperatures (400–450 °C) in N_2 and N_2/steam atmospheres is CO_2. However, at higher temperature, more CH_4 was produced in N_2/steam. In CO_2 and CO_2/steam atmospheres, alkanes (mainly CH_4) greatly evolved prior to the beginning oil evolution up to the temperature of 500 °C. It can also be noted that before oil evolution (kerogen to TB formation) – small amount of H_2 was produced and main generation of H_2 gas when TB decomposition begins. Moreover, it seems that the yield of H_2 production was independent of the presence of steam in the environment.

Furthermore, the figures show that the CO, H_2 and CH_4 evolution peaks approximately appears at 400–450 °C, 480–510 °C and 500 °C, respectively. Although, the precise value could not be reported due to the offline gas sampling, the obtained values are consistent with literature data to a great extent [83]. The higher yield of CH_4

in steam can be primarily due to the reaction of steam and hydrocarbon gases to form oxygen and methane. As opposed to H_2 and CH_4, in which their production increased at higher temperatures, it was observed that the amount of CO started to decrease before reaching 500 °C. Moreover, the peak of CO production is almost at its highest when oil generation takes place. Having compared the effect of CO_2 and N_2 environments, it can be seen that the yields of CO, H_2 and CH_4 markedly increased under a CO_2 environment (except for CH_4 at about 500 °C). The reaction between the produced water as well as the added steam with the char which results in generation of H_2 and CO gases can affect the amount of the yielded CO. Besides, the reaction of steam and CO produce H_2 and CO_2 in the water gas shift reaction. It can also be noticed that in general, addition of steam to N_2 increased the production amount of CO, H_2 and CH_4, whereas CO_2/steam reduced the concentration of these gases as compared to dry CO_2. According to [42,72,80,83,84], the following reactions are suggested to indicate the effect of steam in the pyrolysis process:

1) $C + H_2O \rightarrow H_2 + CO$ (water or char steam reaction)
2) $CO + H_2O \leftrightarrow CO_2 + H_2$ (water shift reaction)
3) $CO_2 + C \leftrightarrow 2CO$ (producer gas reaction)
4) $MCO_3 \rightarrow MO + CO_2$ (mineral carbonate decomposition)
5) $HC + H_2O \rightarrow CO_2 + CH_4$ (hydrocarbon-steam reaction)
6) $2HC + H_2O \rightarrow O_2 + CH_4$

In an N_2 environment, reaction (1) may occur as pyrolyzed water is produced during pyrolysis 450–500 °C. Therefore, reaction (2) may take place simultaneously along with reaction (1) in the retort. Through these reactions, the pyrolyzed water could produce molecular hydrogen. At higher temperatures, since more pyrolyzed water is produced, and due to the decomposition of mineral carbonates, the equilibrium of reactions (2), (4), and (5,6) would shift to the right. In N_2/steam atmosphere, due to the presence of steam and its reaction with the carbonaceous residue, CO_2 is produced by means of reactions (2), (4), and (5,6). However, Dung [85] suggests that steam gasification of hydrocarbon (water gas-shift reaction + steam reforming of hydrocarbon reaction) is also responsible for the quantity of CO and H_2 during the pyrolysis process:

7) $2H_2O + CH_x \rightarrow \left(2 + \frac{x}{2}\right) H_2 + CO_2$

The decrease in the trends of all curve during last phase of the test at 520 °C is because the shale sample was spent, and therefore, less hydrocarbons were produced.

3.3.1 Sulfurous gases

The intensity of the release trend for H_2S and SO_2 gases during the pyrolysis process has also been investigated to analyze how different atmospheres affect the release of sulfur in the process. This type of analysis can be used for the optimization of sulfur removal processes. The forms of sulfur in the kukersite oil shale sample used by wt% are as following: S_{total} : 1.72, S_{pyrite}: 1.1, $S_{sulfate}$:0.13, $S_{organic}$:0.49 [58]. Figure 19 and 20 (Figures 3 and 4 in **Publication IV)** show the trend for the release of H_2S and SO_2 gases when pyrolysis was done in different environments. The intensity of the curves was normalized per sample mass used. The detailed information on how curves were drawn, and also the normalization was done can be found in **Publication IV**. By comparing both graphs, it can be observed that the relative intensity of H_2S is much higher than SO_2 intensity. This means that at lower temperatures, H_2S generation is greater thus, accounting for the release of most of the sulfurous gas during pyrolysis [86].

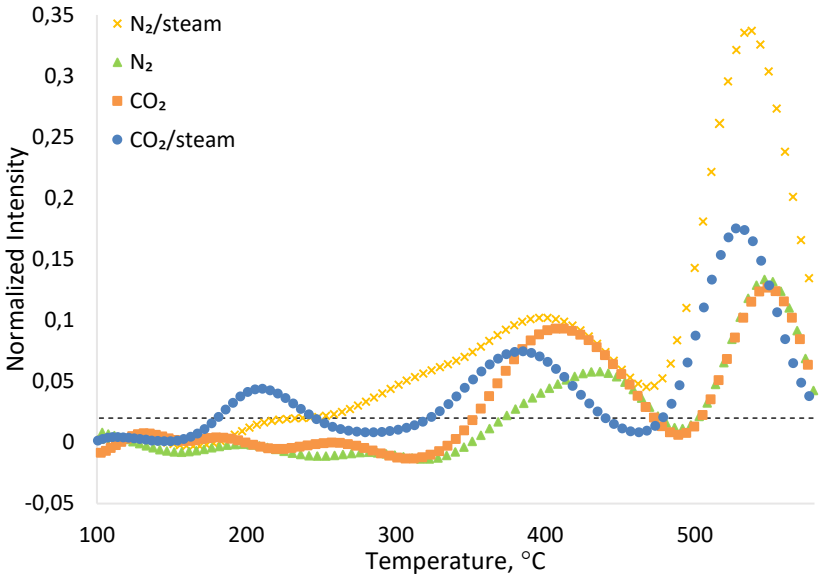

*Figure 19. Evolution trend of H_2S gas during the pyrolysis process (the measurement uncertainty was displayed dotted line, meaning that below this line the results can possibly be noise) (from **Publication IV**)*

The formation of H_2S in Figure 19 the effect of employing a reactive gas in the pyrolysis environment as compared to an inert gas. Having compared the release of H_2S in CO_2 and N_2, it can be noticed that the release of sulfur is greater when a CO_2 atmosphere is used. An increase in H_2S intensity could mainly be a result of higher reactivity of CO_2 during the pyrolysis process [87]. Additionally, looking at the trends obtained from the steam atmospheres indicates that the presence of steam enhances the formation of H_2S. This is due to the occurrence of reactions between steam and pyrite based on the following suggested reactions [16,18] as also given in **Publication IV**:

8) $3FeS_2 + 2H_2O \rightarrow 3FeS + 2H_2S + SO_2$
9) $FeS_2 + 2H_2O + C \rightarrow FeS + H_2S + CO$
10) $FeS_2 + 2H_2O \rightarrow 3FeS + 2H_2 + SO_2$
11) $FeS + H_2O \rightarrow FeO + H_2S$
12) $Fe_3O_4 + 4H_2O \rightarrow Fe_3O_4 + 4H_2S$
13) $Fe_3O_4 + 3H_2O \rightarrow Fe_2O_3 + 3H_2S$
14) $FeS_x + H_2O \rightarrow Fe_3O_4 + H_2S + SO_2$
15) $FeS_2 + H_2 \rightarrow FeS + H_2S$
16) $1/2S_2 + H_2 \rightarrow H_2S$
17) $FeS_2 \rightarrow Fe_yS_x + \left(y + \frac{1}{2}x\right)S_2$

Reactions 8–14 and 15–16 take place as a result of sulfur reacting with steam and H_2, respectively. Therefore, more H_2S gas is formed. Reaction 17 indicates the conversion of pyrite to elemental sulfur due to the decomposition process, thus releasing more sulfur from the sample. Pyrite initially decomposes to pyrrhotite (FeS_x) as an intermediate step [88]. In addition, it can be perceived from the curves that steam increases the release of sulfur compounds from oil shale and also decreases the temperature of their release as

well. This means that the release temperature of sulfurous volatile compounds for N_2 and CO_2 occur at about 440 °C and 410 °C, respectively. While the addition of steam to the dry sweep gas lowers the peak temperature to below 400 °C. On the other hand, it seems that for the dry gases, the H_2S formation initiates slightly above 300 °C, whereas under steam, it takes place at temperatures between 200 °C and 300 °C.

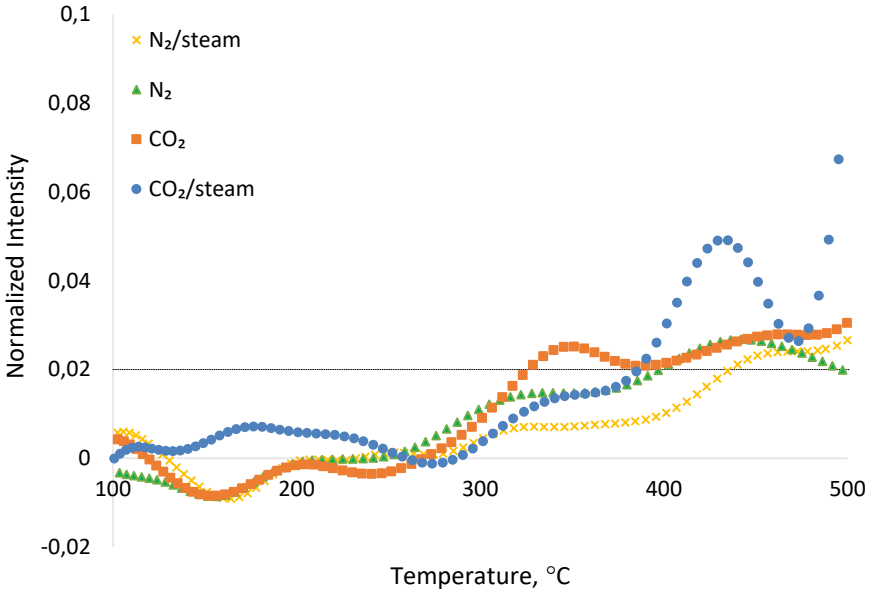

*Figure 20. Evolution trend of SO_2 gas during the pyrolysis process (the measurement uncertainty was displayed dotted line, meaning that below this line the results can possibly be noise) (from **Publication IV**)*

Figure 20 exhibits the intensity for the generation of SO_2 registered in different atmospheres. Similar to H_2S, the intensity rose by increasing the temperature. At higher temperatures, due to the higher reactivity of oxygen-bearing groups, more SO_2 was formed [89]. Also, the figure demonstrates that SO_2 formation did not vary much by changing the sweeping gases at low temperatures. This suggests that below 500 °C the effect of CO_2 as well as steam on the yield of SO_2 is not significant. Additionally, it can be deduced that SO_2 just begins to form at about 300–350 °C, meaning that the yield of SO_2 is small at temperatures below 400 °C. The analysis of SO_2 evolution at temperatures above 400 °C indicates that due to the oxidizing effect of CO_2, the abundance of SO_2 under CO_2 and CO_2/steam environments was found to be higher. The following reactions may be used to describe this phenomenon in a CO_2 atmosphere [87,88] as also included in **Publication IV**.

18) $FeS_2 \rightarrow FeS_x + S_2$

19) $FeS_x + CO_2 \rightarrow Fe_3O_4 + CO + SO_2$

20) $Fe_3O_4 + CO_2 \rightarrow Fe_2O_3 + CO$

21) $FeS_2 + 2CO_2 \rightarrow Fe_{1-x}S + 2CO + SO_2 + xFe$

In Figures 19 and 20, the bigger peaks at higher temperatures could be a result of overlapping two peaks: aliphatic and elemental sulfur species decomposition taking place at about 330 °C, which was later enhanced by decomposition of aromatic and

pyritic sulfur [53]. As mentioned before, the sample contains significant amounts of pyrite sulfur. Also, SO_2 is mainly formed when oxygen-containing compounds react with pyrite and unstable elemental sulfur. However, when hydrogen radicals are present, which are abundant in the presence of steam – they tend to react with the pyrite and elemental sulfur to generate H_2S [52]. It should also be stated that reactions 8–14 may also occur in dry atmospheres as well. However, since in CO_2 and N_2 environments, the formation of water as a by-product in pyrolysis is not as large as in steam atmospheres, therefore the effect of these reactions is smaller accordingly. In addition, in the presence of water, the sulfur gases escape the sample at a higher rate as compared to when their presence is small because the lower molar mass of H_2O causes an increase in the diffusion rate of sulfur gas [88].

3.4 Analysis of sulfur in semi-coke

In order to further understand the effect of various sweep gases, elemental analysis measurement was also conducted on the semi-coke samples. This data is presented in Table 3 (Table 3 in **Publication IV**). As can be seen, the use of reactive gases (CO_2 and steam) increased the release of sulfur from the oil shale sample. Thus, the presence of a lower amount of sulfur in the semi-coke.

*Table 3 Elemental analysis of semi-cokes in various sweep gases, wt% (from **Publication IV**)*

Pyrolysis atmosphere	*N*	*C*	*H*	*S*
N_2	0.04	13.55	0.24	1.80
CO_2	0.04	13.88	0.28	1.76
N_2/steam	0.04	13.74	0.29	1.67
CO_2/steam	0.04	13.86	0.27	1.65

**The expanded relative uncertainty (95%): Carbon (1.11%), Nitrogen (16.56%), Hydrogen (2.56%) and Sulfur (5.7%).*

Table 4 (Table 4 in **Publication IV**) provides data on how sulfur is distributed in pyrolysis products when different sweep gases were employed. The amount of sulfur in the pyrolysis gas was calculated using the mass balance equation. From the table, it can be deduced that most of the sulfur during the pyrolysis process remains in the solid residue. In addition, looking at the produced shale oil and gas, it can be seen that a large amount of liberated sulfur was released as non-condensable gases. Furthermore, a conclusion that can be drawn is that employing steam noticeably increased the release of sulfur from the oil shale sample.

*Table 4 Sulfur Distribution in pyrolysis products under various sweep gases, wt% (from **Publication IV**)*

Sulfur balance	*Semi-coke*	*Shale oil*	*Gas*
N_2	80.5	7.7	11.8
CO_2	78.4	8.2	13.4
N_2/steam	72.2	8.4	19.4
CO_2/steam	71.5	8.0	20.5

4 Conclusion

The aim of this work was to investigate the effect of N_2, CO_2, and their mixtures with steam on the produced shale oil and gas. Also, the impact of different sweep gases on the release of sulfur and its distribution in the pyrolysis products were also investigated. Performing such studies is very beneficial in achieving a suitable condition for the pyrolysis process by taking environmental problems into consideration. Optimal conditions lead to production of shale oil with a lower sulfur content, resulting in eliminating expensive sulfur removal processes and also lowering the emissions of sulfur to the environment. This is an effective way to develop new technologies and optimize new methods for shale oil and gas production plants with respect to the importance of both quality and quantity.

To the author's knowledge, previous work on Estonia kukersite oil shale was conducted in an N_2 atmosphere and the use of CO_2 or steam as a sweep gas was not investigated. For that purpose, a modified Fischer assay method was used to pyrolyze an Estonian kukersite oil shale sample under different sweep gases: CO_2, CO_2/steam, N_2 and N_2/steam so that a broad comparative analysis could be carried out to investigate their effects on the oil and gas produced. In order to do so, various apparatus and techniques were employed to analyze the samples; mainly, GC, DSC, TGA-MS, GC-MS, and FTIR. The results demonstrate that, compared to N_2, the introduction of dry CO_2 produced more liquid products. Also, analyzing the curves from TGA indicates that CO_2 could possibly enhance the weight loss in the oil shale sample as a result of oxidation, although the difference is slight. In addition, studying the effect of steam showed that the sample mass loss under steam was observed to be considerably higher, which means that more of the oil shale is converted into hydrocarbons, thus giving a higher yield of liquid and gaseous products. Moreover, the concentration of some of the sulfur compounds was increased in the shale oil sample produced in CO_2 atmosphere as compared with N_2. However, the corresponding values for the shale oils produced in the presence of steam were significantly higher in comparison with the dry sweep gases. Besides, the analysis of all shale oil samples showed that some physical properties (MW, RI and density) are similar; however, their chemical structure was somewhat influenced by the type of carrier gas employed.

Furthermore, the trends for the release of C_1–C_3 hydrocarbons, H_2, CO as well as sulfurous gases (H_2S and SO_2) were also investigated in all atmospheres. The results indicate that CO_2 enhanced the generation of CH_4, CO, alkanes and hydrocarbon gases, as compared to N_2. However, addition of steam to CO_2 and N_2 atmospheres had different impacts on the formation behavior of these gases. Even though, N_2/steam increased the concentration of the above-mentioned gases, this was not the case for the CO_2/steam atmosphere. It was also perceived that the generation of H_2 gas was independent of the type of sweep gas used in pyrolysis at low temperatures. Based on the analysis of data on H_2S and SO_2 generation, it was found that CO_2 had a major influence on the release of SO_2 due to its oxidizing effect. Additionally, it was deduced that the least amount of H_2S was released in an N_2 atmosphere while the presence of steam increased the formation of H_2S in the process.

Overall, carbon dioxide is one of the products of pyrolysis, which is released as a gas during oil shale pyrolysis. The results in this work show at temperatures up to 500 °C, the results obtained for CO_2 as a carrier gas in pyrolysis process is similar to when N_2 is used in the reactor. Therefore, the use of CO_2 in the pyrolysis process would be very helpful to

understand further the effect of a different sweep gas on pyrolysis products. Also, the use of CO_2 can help reduce the carbon footprint of oil shale industry by eliminating the cost as well as the energy spent on generating N_2 to create an inert atmosphere. Consequently, although viability and feasibility of the use of CO_2 gas in oil shale industrial processes still requires further research, preliminary results indicate that employing CO_2 as the pyrolysis atmosphere has led to promising outcomes in oil and gas generation. Also, carrying out analysis on the effect of steam in general indicated that it has a significant effect on the production of shale oil and pyrolysis gas. Additionally, the result from the analysis of the semi-cokes showed the use of reactive gases (mainly steam) in general increases the release of sulfur from the oil shale sample during pyrolysis.

In order to further understand the effect of different sweep gases on the oil shale pyrolysis process – apart from applying different parameters – it would be helpful to analyze the transformation of various compounds such as oxygen and nitrogen compounds. Also, to gain more comprehensive information on the reactivity and effect of these gases, a deep analysis on the resulting semi-cokes is also important. Such analysis would offer insight into valorizing the oil shale in a more environmentally friendly way.

List of Figures

Figure 1. Kerogen classification according to The van Krevelen diagram [29]..... 13
Figure 2. Comparison between the Hydrogen/Carbon atomic ratios in different hydrocarbon materials [34] 14
Figure 3. A model of the proposed structure of Estonian kukersite kerogen [41] 15
Figure 4. Proposed mechanism model of carbon transformation in kerogen pyrolysis [43] 15
Figure 5. Schematic diagram of the analysis carried out in the study 19
Figure 6. TGA curves of the oil shale sample in N_2 and CO_2 (from **Publication I**)..... 25
Figure 7. TGA curves of oil shale pyrolysis in N_2 and N_2/steam (from **Publication I**) 26
Figure 8. TGA curves of oil shale pyrolysis in CO_2 and CO_2/steam (from **Publication I**) . 26
Figure 9. DSC graph for the oil shale under CO_2 and N_2 atmosphere (from **Publication I**).. 27
Figure 10. FTIR spectra of CO_2 and N_2 shale oils (from **Publication I**)..... 29
Figure 11. FTIR spectra of N_2 and N_2/steam oils (from **Publication I**)..... 30
Figure 12. FTIR spectra of CO_2 and CO_2/steam oil (from **Publication I**)..... 30
Figure 13. Evolution of HC gases during the pyrolysis in all test atmospheres (from **Publication II**)..... 31
Figure 14 Evolution of alkanes (from **Publication II**) 32
Figure 15. Evolution of alkenes (from **Publication II**) 32
Figure 16. Expected evolution trend for CO during pyrolysis (from **Publication II**)..... 33
Figure 17. Expected evolution trend for H_2 during pyrolysis (from **Publication II**)..... 33
Figure 18. Expected evolution trend for CH_4 during pyrolysis (from **Publication II**)..... 34
Figure 19. Evolution trend of H_2S gas during the pyrolysis process (the measurement uncertainty was displayed dotted line, meaning that below this line the results can possibly be noise) (from **Publication IV**)..... 36
Figure 20. Evolution trend of SO_2 gas during the pyrolysis process (the measurement uncertainty was displayed dotted line, meaning that below this line the results can possibly be noise) (from **Publication IV**)..... 37

List of Tables

Table 1. Ultimate and proximate analysis for the kukersite oil shale sample (from **Publication I**)..... 20
Table 2. Yields of Fischer assay products on the dry oil shale basis (wt%) in different experiment atmospheres (from **Publication I**) 24
Table 3 Elemental analysis of semi-cokes in various sweep gases, wt% (from **Publication IV**) 38
Table 4 Sulfur Distribution in pyrolysis products under various sweep gases, wt% (from **Publication IV**) 38

References

[1] Z. Jiang, W. Zhang, C. Liang, Y. Wang, H. Liu, and X. Chen, "Basic characteristics and evaluation of shale oil reservoirs" *Pet. Res.*, vol. 1, no. 2, pp. 149–163, 2016, doi: 10.1016/S2096-2495(17)30039-X.

[2] T. Dijkmans, M. R. Djokic, K. M. Van Geem, and G. B. Marin, "Comprehensive compositional analysis of sulfur and nitrogen containing compounds in shale oil using GC x GC - FID/SCD/NCD/TOF-MS" *Fuel*, vol. 140, pp. 398–406, 2015, doi: 10.1016/j.fuel.2014.09.055.

[3] N. D. Ristic, M. R. Djokic, A. Konist, K. M. Van Geem, and G. B. Marin, "Quantitative compositional analysis of Estonian shale oil using comprehensive two dimensional gas chromatography" *Fuel Process. Technol.*, vol. 167, pp. 241–249, 2017, doi: 10.1016/j.fuproc.2017.07.008.

[4] J. Qian, J. Wang, and S. Li, "World's oil shale available retorting technologies and the forecast of shale oil production" *Proc. Int. Offshore Polar Eng. Conf.*, vol. 8, pp. 19–20, 2008.

[5] W. Wang, L.-Y. Li, S.-Y. Li, Y. Ma, C.-T. Yue, and J.-L. He, "Pyrolysis Kinetics of North-Korean Oil Shale" *Oil Shale*, vol. 31, no. 3, p. 250, 2014, doi: 10.3176/oil.2014.3.05.

[6] C. Gülamber, K. M. Ibrahim, S. Aljurf, and H. A. Rahman, "Introduction of analytical methods for oil shale resource evaluation" *IMCET 2019 - Proc. 26th Int. Min. Congr. Exhib. Turkey*, no. February 2020, pp. 1154–1168, 2019.

[7] P. Mozaffari, Z. S. Baird, M. Listak, and V. Oja, "Vapor pressures of narrow gasoline fractions of oil from industrial retorting of Kukersite oil shale" *Oil Shale*, vol. 37, no. 4, pp. 288–303, 2020, doi: 10.3176/oil.2020.4.03.

[8] P. Mozaffari, O. Järvik, and Z. S. Baird, "Vapor Pressures of Phenolic Compounds Found in Pyrolysis Oil" *J. Chem. Eng. Data*, 2020, doi: 10.1021/acs.jced.0c00675.

[9] N. Golubev, "Solid oil shale heat carrier technology for oil shale retorting" *Oil Shale*, vol. 20, no. 3, pp. 324–332, 2003.

[10] B. Maaten, L. Loo, A. Konist, T. Pihu, and A. Siirde, "Investigation of the evolution of sulphur during the thermal degradation of different oil shales" *J. Anal. Appl. Pyrolysis*, vol. 128, no. September, pp. 405–411, 2017, doi: 10.1016/j.jaap.2017.09.007.

[11] V. Chandra Srivastava, "An evaluation of desulfurization technologies for sulfur removal from liquid fuels" *RSC Adv.*, vol. 2, no. 3, pp. 759–783, 2012, doi: 10.1039/c1ra00309g.

[12] T. Chu Van, J. Ramirez, T. Rainey, Z. Ristovski, and R. J. Brown, "Global impacts of recent IMO regulations on marine fuel oil refining processes and ship emissions" *Transp. Res. Part D Transp. Environ.*, vol. 70, pp. 123–134, 2019, doi: 10.1016/j.trd.2019.04.001.

[13] B. Maaten, H. Pikkor, A. Konist, and A. Siirde, "Determination of the total sulphur content of oil shale by using different analytical methods" *Oil Shale*, vol. 35, no. 2, pp. 144–153, 2018, doi: 10.3176/oil.2018.2.04.

[14] A. E. Pomerantz *et al.*, "Sulfur speciation in kerogen and bitumen from gas and oil shales" *Org. Geochem.*, vol. 68, pp. 5–12, 2014, doi: 10.1016/j.orggeochem.2013.12.011.

[15] W. L. Orr and J. S. D. Sinninghe, “Geochemistry of Sulfur in Petroleum Systems” in *In W. L. Orr and C. M. White, Eds., Geochemistry of Sulfur in Fossil Fuels*, Washington DC: American Chemical Society, 1990, pp. 2–29.

[16] O. S. Al-Ayed and M. Matouq, “Influence of pyrolysis environment on liquid product and sulfur of oil shale” *Energy Sources, Part A Recover. Util. Environ. Eff.*, vol. 31, no. 8, pp. 679–686, 2009, doi: 10.1080/15567030701752529.

[17] X. Lan, W. Luo, Y. Song, J. Zhou, and Q. Zhang, “Effect of the Temperature on the Characteristics of Retorting Products Obtained by Yaojie Oil Shale Pyrolysis” *Energy and Fuels*, vol. 29, no. 12, pp. 7800–7806, 2015, doi: 10.1021/acs.energyfuels.5b01645.

[18] O. S. Al-Ayed and M. Matouq, “Factors affecting sulfur reactions in high sulfur oil shale pyrolysis” *J. Energy Resour. Technol. Trans. ASME*, vol. 131, no. 1, pp. 0125011–0125014, 2009, doi: 10.1115/1.3068338.

[19] Q. Zhou, H. Hu, Q. Liu, S. Zhu, and R. Zhao, “Effect of atmosphere on evolution of sulfur-containing gases during coal pyrolysis” *Energy and Fuels*, vol. 19, no. 3, pp. 892–897, 2005, doi: 10.1021/ef049773p.

[20] N. Yang, H. Guo, F. Liu, H. Zhang, Y. Hu, and R. Hu, “Effects of atmospheres on sulfur release and its transformation behavior during coal thermolysis” *Fuel*, vol. 215, no. November 2017, pp. 446–453, 2018, doi: 10.1016/j.fuel.2017.11.099.

[21] X. Han, I. Kulaots, X. Jiang, and E. M. Suuberg, “Review of oil shale semicoke and its combustion utilization” *Fuel*, vol. 126, pp. 143–161, 2014, doi: 10.1016/j.fuel.2014.02.045.

[22] Y. H. Sun *et al.*, “A Novel Energy-Efficient Pyrolysis Process: Self-pyrolysis of Oil Shale Triggered by Topochemical Heat in a Horizontal Fixed Bed” *Sci. Rep.*, vol. 5, pp. 1–8, 2015, doi: 10.1038/srep08290.

[23] Z. Kang, Y. Zhao, and D. Yang, “Review of oil shale in-situ conversion technology” *Appl. Energy*, vol. 269, no. April, p. 115121, 2020, doi: 10.1016/j.apenergy.2020.115121.

[24] J. O. Jaber and S. D. Probert, “Environmental-impact assessment for the proposed oil-shale integrated tri-generation plant” *Applied Energy*, 1999.

[25] J. Shi, Y. Ma, S. Li, J. Wu, Y. Zhu, and J. Teng, “Characteristics of Estonian Oil Shale Kerogen and Its Pyrolysates with Thermal Bitumen as a Pyrolytic Intermediate” *Energy and Fuels*, vol. 31, no. 5, pp. 4808–4816, 2017, doi: 10.1021/acs.energyfuels.7b00054.

[26] M. A. Raja, Y. Zhao, X. Zhang, C. Li, and S. Zhang, “Practices for modeling oil shale pyrolysis and kinetics” *Rev. Chem. Eng.*, vol. 34, no. 1, pp. 21–42, 2017, doi: 10.1515/revce-2016-0038.

[27] Z. S. Baird, O. Järvik, V. Oja, and R. Rannaveski, “Properties of kukersite shale oil” *Oil Shale*, vol. 38, no. 4, p. 265, 2021, doi: 10.3176/oil.2021.4.01.

[28] E. VÄLI, I. VALGMA, and E. REINSALU, “Usage of Estonian Oil Shale” *Oil Shale*, vol. 25, no. 2s, p. 101, 2008, doi: 10.3176/oil.2008.2S.02.

[29] J. Speight, *Shale oil and gas production processes*. Gulf Professional Publishing, 2019.

[30] X. Wang, X. Huang, K. Lin, and Y. Zhao, “The Constructions and Pyrolysis of 3D Kerogen Macromolecular Models: Experiments and Simulations” *Glob. Challenges*, vol. 3, no. 5, p. 1900006, 2019, doi: 10.1002/gch2.201900006.

[31] N. E. Altun, C. Hiçyilmaz, J. Y. Hwang, A. S. Bağci, and M. V. Kök, "Oil shales in the world and Turkey; reserves, current situation and future prospects: A review" *Oil Shale*, vol. 23, no. 3, pp. 211–227, 2006.

[32] A. Demirbas, "Conversion of oil shale to liquid hydrocarbons" *Energy Sources, Part A Recover. Util. Environ. Eff.*, vol. 38, no. 18, pp. 2698–2703, 2016, doi: 10.1080/15567036.2015.1115925.

[33] L. Tiikma, A. Zaidentsal, and M. Tensorer, "Formation of thermobitumen from oil shale by low-temperature pyrolysis in an autoclave" *Oil Shale*, vol. 24, no. 4, pp. 535–546, 2007.

[34] Y. A. Strizhakova and T. V. Usova, "Current trends in the pyrolysis of oil shale: A review" *Solid Fuel Chem.*, vol. 42, no. 4, pp. 197–201, 2008, doi: 10.3103/S0361521908040022.

[35] Y. Luo, H. Ben, Z. Wu, K. Nie, G. Han, and W. Jiang, "Impact of CO2 on pyrolysis products of bituminous coal and platanus sawdust" *Polymers (Basel).*, vol. 11, no. 8, pp. 1–12, 2019, doi: 10.3390/polym11081370.

[36] S. Lee, M. E. Polasky, and K. L. Fullerton, "Chemical composition of oil shale II. Dependence on the extraction process" *Fuel Sci. Technol. Int.*, vol. 9, no. 9, pp. 1151–1179, 1991, doi: 10.1080/08843759108942316.

[37] O. Järvik and V. Oja, "Molecular weight distributions and average molecular weights of pyrolysis oils from oil shales: Literature data and measurements by size exclusion chromatography (SEC) and atmospheric solids analysis probe mass spectroscopy (ASAP MS) for oils from four different deposits" *Energy and Fuels*, vol. 31, no. 1, pp. 328–339, 2017, doi: 10.1021/acs.energyfuels.6b02452.

[38] S. Pan *et al.*, "Investigation of Behavior of Sulfur in Oil Fractions during Oil Shale Pyrolysis" *Energy and Fuels*, 2019, doi: 10.1021/acs.energyfuels.9b02406.

[39] J. D. Tucker, B. Masri, and S. Lee, "Comparison of retorting and supercritical extraction techniques on El-Lajjun oil shale" *Energy Sources*, vol. 22, no. 5, pp. 453–463, 2000, doi: 10.1080/00908310050013866.

[40] B. Avid, M. Born, B. Purevsuren, N. Undrakh, and A. Tuvshinjargal, "Thermal behavior of Khoot oil shale in different conditions" *Oil Shale*, vol. 20, no. 1, pp. 47–55, 2003.

[41] Ü. Lille, I. Heinmaa, and T. Pehk, "Molecular model of Estonian kukersite kerogen evaluated by 13C MAS NMR spectra" *Fuel*, vol. 82, no. 7, pp. 799–804, 2003, doi: 10.1016/S0016-2361(02)00358-7.

[42] S. Zhao, Y. Sun, X. Lü, and Q. Li, "Kinetics and thermodynamics evaluation of carbon dioxide enhanced oil shale pyrolysis" *Sci. Rep.*, vol. 11, no. 1, pp. 1–14, 2021, doi: 10.1038/s41598-020-80205-4.

[43] D. Lai, J. H. Zhan, Y. Tian, S. Gao, and G. Xu, "Mechanism of kerogen pyrolysis in terms of chemical structure transformation" *Fuel*, vol. 199, pp. 504–511, 2017, doi: 10.1016/j.fuel.2017.03.013.

[44] A. K. Burnham and J. A. Happe, "On the mechanism of kerogen pyrolysis" *Fuel*, vol. 63, no. 10, pp. 1353–1356, 1984, doi: 10.1016/0016-2361(84)90336-3.

[45] F. Hershkowitz, W. N. Olmstead, R. P. Rhodes, and K. D. Rose, "Molecular Mechanism of Oil Shale Pyrolysis in Nitrogen and Hydrogen Atmospheres" *Am. Chem. Soc. Symp. Ser.*, vol. 230, pp. 301–316, 1983, doi: 10.1021/bk-1983-0230.ch015.

[46] Z. S. Baird, O. Järvik, and V. Oja, "The composition of kukersite shale oil Experimental" pp. 1–18.

[47] V. Oja, R. Rooleht, and Z. S. Baird, “Physical and thermodynamic properties of kukersite pyrolysis shale oil: Literature review” *Oil Shale*, vol. 33, no. 2, pp. 184–197, 2016, doi: 10.3176/oil.2016.2.06.

[48] Easac, “A study on the EU oil shale industry – viewed in the light of the Estonian experience” *Energy*, no. May, pp. 1–65, 2007.

[49] D. Neshumayev, T. Pihu, A. Siirde, O. Järvik, and A. Konist, “Solid heat carrier oil shale retorting technology with integrated CFB technology” *Oil Shale*, vol. 36, no. 2S, pp. 99–113, 2019, doi: 10.3176/oil.2019.2S.02.

[50] D. Lai *et al.*, “Secondary reactions in oil shale pyrolysis by solid heat carrier in a moving bed with internals” *Fuel*, vol. 173, pp. 138–145, 2016, doi: 10.1016/j.fuel.2016.01.052.

[51] D. Cui *et al.*, “Compositional Analysis of Heteroatom Compounds in Huadian Shale Oil Using Various Analytical Techniques” *Energy and Fuels*, vol. 33, no. 2, pp. 946–956, 2019, doi: 10.1021/acs.energyfuels.8b03889.

[52] M. Wang, Q. Du, Y. Li, J. Xu, J. Gao, and H. Wang, “Effect of steam on the transformation of sulfur during demineralized coal pyrolysis” *J. Anal. Appl. Pyrolysis*, vol. 140, no. March, pp. 161–169, 2019, doi: 10.1016/j.jaap.2019.03.011.

[53] L. Frigge, G. Elserafi, J. Ströhle, and B. Epple, “Sulfur and Chlorine Gas Species Formation during Coal Pyrolysis in Nitrogen and Carbon Dioxide Atmosphere” *Energy and Fuels*, vol. 30, no. 9, pp. 7713–7720, 2016, doi: 10.1021/acs.energyfuels.6b01080.

[54] Z. S. Baird, H. Rang, and V. Oja, “Desulfurization, denitrogenation and deoxygenation of shale oil” *Oil Shale*, vol. 38, no. 2, pp. 137–154, 2021, doi: 10.3176/oil.2021.2.03.

[55] Paul N. Kogermann, “Desulphurisation of Estonian Oil Shale” Tartu: Oil Shale Research Laboratory, 1932.

[56] F. D. Guffey, F. A. Barbour, and R. E. Cummings, “Analysis of oil shale retort production stream gases for sulfur species” *Liq. Fuels Technol.*, vol. 1, no. 4, pp. 235–257, 1983, doi: 10.1080/07377268308915324.

[57] X. Wang, H. Guo, F. Liu, R. Hu, and M. Wang, “Effects of CO2 on sulfur removal and its release behavior during coal pyrolysis” *Fuel*, vol. 165, pp. 484–489, 2016, doi: 10.1016/j.fuel.2015.10.047.

[58] B. Maaten, O. Järvik, O. Pihl, A. Konist, and A. Siirde, “Oil shale pyrolysis products and the fate of sulfur” *Oil Shale*, vol. 37, no. 1, pp. 51–69, 2020, doi: 10.3176/oil.2020.1.03.

[59] A. Demirbas, H. Alidrisi, and M. A. Balubaid, “API gravity, sulfur content, and desulfurization of crude oil” *Pet. Sci. Technol.*, vol. 33, no. 1, pp. 93–101, 2015, doi: 10.1080/10916466.2014.950383.

[60] J. Tong, X. Han, S. Wang, and X. Jiang, “Evaluation of structural characteristics of huadian oil shale kerogen using direct techniques (Solid-state 13C NMR, XPS, FT-IR, and XRD)” *Energy and Fuels*, vol. 25, no. 9, pp. 4006–4013, 2011, doi: 10.1021/ef200738p.

[61] E. Ekinci, A. E. Putun, M. Citiroglu, C. J. Lafferty, and C. E. Snape, “Effect of Steam and Hydrogen Pressure on Fixed-Bed Pyrolysis of Lignites and Oil Shales” *1991 Int. Conf. Coal Sci. Proc.*, pp. 520–523, 1991, doi: 10.1016/b978-0-7506-0387-4.50132-7.

[62] K. El Harfi, A. Mokhlisse, and M. Ben Chanâa, “Effect of water vapor on the pyrolysis of the Moroccan (Tarfaya) oil shale” *J. Anal. Appl. Pyrolysis*, vol. 48, no. 2, pp. 65–76, 1999, doi: 10.1016/S0165-2370(98)00108-9.

[63] V. Minkova, M. Razvigorova, M. Goranova, L. Ljutzkanov, and G. Angelova, “Effect of water vapour on the pyrolysis of solid fuels. 1. Effect of water vapour during the pyrolysis of solid fuels on the yield and composition of the liquid products” *Fuel*, vol. 70, no. 6, pp. 713–719, 1991, doi: 10.1016/0016-2361(91)90067-K.

[64] F. Bai *et al.*, “Kinetic investigation on partially oxidized Huadian oil shale by thermogravimetric analysis” *Oil Shale*, vol. 31, no. 4, pp. 377–393, 2014, doi: 10.3176/oil.2014.4.06.

[65] W. Qing, S. U. N. Baizhong, H. U. Aijuan, B. A. I. Jingru, and L. I. Shaohua, “Pyrolysis Charactersitics of Huadian Oil Shales” *Oil Shale*, vol. 24, no. 2, pp. 147–157, 2007.

[66] J. O. Jaber and S. D. Probert, “Non-isothermal thermogravimetry and decomposition kinetics of two Jordanian oil shales under different processing conditions” *Fuel Process. Technol.*, vol. 63, no. 1, pp. 57–70, 2000, doi: 10.1016/S0378-3820(99)00064-8.

[67] C. S. Wen and T. P. Kobylinski, “Low-temperature oil shale conversion” *Fuel*, vol. 62, no. 11, pp. 1269–1273, 1983, doi: 10.1016/S0016-2361(83)80008-8.

[68] N. Olukcu, J. Yanik, M. Saglam, and M. Yuksel, “Liquefaction of beypazari oil shale by pyrolysis” *J. Anal. Appl. Pyrolysis*, vol. 64, no. 1, pp. 29–41, 2002, doi: 10.1016/S0165-2370(01)00168-1.

[69] S. Wang, X. Jiang, X. Han, and J. Tong, “Effect of retorting temperature on product yield and characteristics of non-condensable gases and shale oil obtained by retorting Huadian oil shales” *Fuel Process. Technol.*, vol. 121, pp. 9–15, 2014, doi: 10.1016/j.fuproc.2014.01.005.

[70] S. Wang, X. Jiang, X. Han, and J. Tong, “Effect of residence time on products yield and characteristics of shale oil and gases produced by low-temperature retorting of Dachengzi oil shale” *Oil Shale*, vol. 30, no. 4, pp. 501–516, 2013, doi: 10.3176/oil.2013.4.04.

[71] S. D. Carter and D. N. Taulbee, “Fluidized bed steam retorting of kentucky oil shale” *Fuel Process. Technol.*, vol. 11, pp. 251–272, 1985.

[72] J. M. Nazzal, “The influence of grain size on the products yield and shale oil composition from the Pyrolysis of Sultani oil shale” *Energy Convers. Manag.*, vol. 49, no. 11, pp. 3278–3286, 2008, doi: 10.1016/j.enconman.2008.03.028.

[73] P. Basu, *Biomass Gasification and Pyrolysis*. Academic Press, 2010.

[74] V. Fainberg, A. Garbar, and G. Hetsroni, “Secondary pyrolysis of the products of the thermal destruction of high-sulfur oil shale” *Energy and Fuels*, vol. 11, no. 4, pp. 915–919, 1997, doi: 10.1021/ef9601733.

[75] J. Coates, “Interpretation of Infrared Spectra, A Practical Approach” *Encycl. Anal. Chem.*, pp. 1–23, 2006, doi: 10.1002/9780470027318.a5606.

[76] A. G. Borrego, J. G. Prado, E. Fuente, M. D. Guillén, and C. G. Blanco, “Pyrolytic behaviour of Spanish oil shales and their kerogens” *J. Anal. Appl. Pyrolysis*, vol. 56, no. 1, pp. 1–21, 2000, doi: 10.1016/S0165-2370(99)00092-3.

[77] J. H. Campbell, G. J. Koskinas, G. Gallegos, and M. Gregg, “Gas evolution during oil shale pyrolysis. 1. Nonisothermal rate measurements” *Fuel*, vol. 59, no. 10, pp. 718–726, 1980, doi: 10.1016/0016-2361(80)90027-7.

[78] P. T. Williams and N. Ahmad, “Influence of process conditions on the pyrolysis of Pakistani oil shales” *Fuel*, vol. 78, no. 6, pp. 653–662, 1999, doi: 10.1016/S0016-2361(98)00190-2.

[79] P. T. Williams and J. M. Nazzal, “Polycyclic aromatic compounds in oils derived from the fluidised bed pyrolysis of oil shale,” *J. Anal. Appl. Pyrolysis*, vol. 35, no. 2, pp. 181–197, 1995, doi: 10.1016/0165-2370(95)00908-9.

[80] J. M. Nazzal, “Gas evolution from the pyrolysis of Jordan oil shale in a fixed-bed reactor” *J. Therm. Anal. Calorim.*, vol. 65, no. 3, pp. 847–857, 2001, doi: 10.1023/A:1011936401407.

[81] W. Sha, J. Liu, X. Jiang, X. Han, and J. Tong, “Effect of heating rate on products yield and characteristics of non-condensable gases and shale oil obtained by retorting Dachengzi oil shale” *Oil Shale*, vol. 30, no. 1, pp. 27–47, 2013, doi: 10.3176/oil.2013.1.04.

[82] P. T. Williams and J. M. Nazzal, “Polycyclic aromatic compounds in shale oils: Influence of process conditions” *Environ. Technol. (United Kingdom)*, vol. 19, no. 8, pp. 775–787, 1998, doi: 10.1080/09593331908616734.

[83] E. B. Huss and A. K. Burnham, “Gas evolution during pyrolysis of various Colorado oil shales” *Fuel*, vol. 61, no. 12, pp. 1188–1196, 1982, doi: 10.1016/0016-2361(82)90018-7.

[84] J. M. Nazzal and P. T. Williams, “Influence of temperature and steam on the products from the flash pyrolysis of Jordan oil shale” *Int. J. Energy Res.*, vol. 26, no. 14, pp. 1207–1219, 2002, doi: 10.1002/er.845.

[85] N. V. Dung, “Yields and chemical characteristics of products from fluidized bed steam retorting of Condor and Stuart oil shales: effect of pyrolysis temperature” *Fuel*, vol. 69, no. 3, pp. 368–376, 1990, doi: 10.1016/0016-2361(90)90102-V.

[86] H. Qin, Z. Zheng, Q. Wang, B. Sun, and J. Bai, “H2S evolution during oil shale pyrolysis” *Asia-Pacific Power Energy Eng. Conf. APPEEC*, pp. 2–5, 2010, doi: 10.1109/APPEEC.2010.5448345.

[87] Y. Gu, J. Yperman, J. Vandewijngaarden, G. Reggers, and R. Carleer, “Organic and inorganic sulphur compounds releases from high-pyrite coal pyrolysis in H2, N2 and CO2: Test case Chinese LZ coal” *Fuel*, vol. 202, pp. 494–502, 2017, doi: 10.1016/j.fuel.2017.04.068.

[88] F. Huang, L. Zhang, B. Yi, Z. Xia, and C. Zheng, “Effect of H2O on pyrite transformation behavior during oxy-fuel combustion” *Fuel Process. Technol.*, vol. 131, pp. 458–465, 2015, doi: 10.1016/j.fuproc.2014.12.027.

[89] L. Li *et al.*, “Release of sulfur and nitrogen during co-pyrolysis of coal and biomass under inert atmosphere” *ACS Omega*, vol. 5, no. 46, pp. 30001–30010, 2020, doi: 10.1021/acsomega.0c04372.

Acknowledgements

First of all, I would like to express my sincere gratitude to my supervisors Mr. Oliver Järvik and Mr. Zachariah Steven Baird for their continuous support, invaluable advice and help throughout my Ph.D. study.

Besides, I am also extremely thankful to my colleagues, lab assistants and fellow researchers in the department of Energy Technology; in particular Professor Andres Siirde for all their support.

Furthermore, my special thanks go to my friends who made the Ph.D. pursuit more enjoyable for me.

Last but not the least, I would like to give my heartfelt thanks to my family; my dear parents and to my brother for their unconditional support and encouragement through all my journeys in life, whom without this would have not been possible.

The author would also like to acknowledge the financial support from Estonian Research Council from National Programme for Addressing Socio-Economic Challenges through R&D (RITA1/01-60), which is supported by the Estonian Government and European Regional Development Fund. Also, support for the study was partially provided by the National R&D program “Energy” under the Project AR10129 “Examination of the Thermodynamic Properties of Relevance to the Future of the Oil Shale Industry”.

Abstract

Effect of different sweep gases on sulfur behavior during pyrolysis of kukersite oil shale

The exploitation of oil shale, and also development and advancement of technologies in this sector have made Estonia one of the foremost oil shale utilizers in the world. Currently, the processing of oil shale in Estonia is conducted at a low temperature by heating up the oil shale to 500 °C.

Generally, pyrolysis of oil shale under nitrogen and/or steam in different process conditions has been widely studied by many researchers. However, studies on pyrolysis of oil shale in CO_2 seem to be rare. Therefore, a kukersite oil shale sample from Estonia was pyrolyzed using a Fischer assay method, and its behavior in N_2, N_2/steam, CO_2, and CO_2/steam atmospheres was investigated. For that purpose, many techniques and analytical methods, such as differential scanning calorimetry, gas chromatography, Fourier-transform infrared spectroscopy, and thermogravimetric analysis – mass spectrometry, were used to analyze the shale oil and gas generated during the pyrolysis. In this study, the effect of aforenoted sweep gases on the produced shale oil and gas were comprehensively investigated, and their impact on the release and distribution of sulfur in the pyrolysis products was also analyzed. Performing such analysis would be beneficial to achieve a deeper understanding of the decomposition process of oil shale and provide information about the changes in composition when different environments are applied.

In this study, C_1–C_3 gases, H_2, CO_2, CH_4, and CO, as the main gaseous products of pyrolysis, were quantified and their expected formation during the process was subsequently discussed. Also, the trends in the evolution of H_2S and SO_2 gases formed were presented. The results showed that the addition of steam to N_2 generated more alkanes and in general total hydrocarbon gases than dry N_2, whereas, in CO_2, the injection of steam had the converse effect and reduced the formation of these gases. Analysis of the release of sulfurous gases showed that steam promoted the generation of H_2S and SO_2 in the gas and increase their concentration in the oil as well, confirming the role of steam in enhancing the volatilization of sulfur compounds.

In addition, analysis of several sulfur compounds in the shale oil samples showed how different sweep gases could affect their concentration in the oil. In comparison with N_2, CO_2 increased the concentration of some of the sulfur compounds in shale oil. Moreover, an analysis of the produced shale oils was carried out to compare their molecular structure. It was found that in the CO_2 atmosphere the formed shale oil had a more aliphatic composition whereas the aromatic peak for oil produced in the N_2 atmosphere was higher. Moreover, the addition of steam to N_2 and CO_2 showed different behaviors. In N_2, steam decreased the intensity of the alkene and aromatic C-H bond peaks, while in CO_2, the change was slight. Additionally, the measurements carried out on several properties of the produced shale oils (Elemental analysis, MW, RI, and density) showed fairly similar results.

Combining the oil and gas analysis results, it can be perceived that introduction of reactive gases could have a significant effect on the final products. Based on the results of the current study, it can be concluded that CO_2 behaves as an inert gas in pyrolysis temperatures below 500 °C and could therefore be used in place of N_2 as a sweep gas in the pyrolysis atmosphere.

Lühikokkuvõte

Pürolüüsikeskkonna mõju väävli käitumisele kukersiitse põlevkivi pürolüüsil

Uute tehnoloogiate kasutusele võtmine ja arendamine põlevkivitööstuses on muutnud Eesti juhtivaks põlevkivi väärindavaks ja kasutavaks riigiks maailmas. Praegu on Eestis põlevkivi peamiseks väärindamise viisiks tema pürolüüs temperatuuridel ligi 500 °C.

Üldiselt on põlevkivi pürolüüsi lämmastiku ja/või auru keskkonnas erinevates protsessitingimustes paljude teadlaste poolt laialdaselt uuritud. Uuringuid põlevkivi pürolüüsi kohta CO_2 keskkonnas on aga vähe. Käesolevas töös uuriti kukersiitse põlevkivi pürolüüsi laboratoorses Fischeri retordis N_2, N_2/aur, CO_2 ja CO_2/aur atmosfäärides. Saadud pürolüüsisaaduste analüüsimiseks kasutati erinevaid tehnikaid ja analüütilisi meetodeid, nagu diferentsiaalne skaneeriv kalorimeetria, gaasikromatograafia, Fourier teisendusega infrapunaspektroskoopia, termogravimeetriline analüüs koos massispektromeetriaga jne. Põhjalikult uuriti eelnimetatud gaasikeskkondade mõju pürolüüsil saadavale põlevkiviõlile ja pürolüüsigaasile. Samuti analüüsiti gaasikeskkondade mõju väävli eraldumisele ja jaotumisele pürolüüsiproduktides. Sellise analüüsi läbiviimine on vajalik põlevkivi pürolüüsiprotsessi sügavamaks mõistmiseks, et hinnata erinevate keskkondade rakendamise mõju pürolüüsisaaduste koostisele.

Selles uuringus kvantifitseeriti C_1–C_3 süsivesinikud, H_2, CO_2, CH_4 ja CO, kui peamised pürolüüsil tekkivad gaasilised produktid ning käsitleti nende eeldatavat moodustumist protsessi käigus. Samuti käsitleti töös pürolüüsil tekkiva H_2S ja SO_2 eraldumise suundumusi. Tulemused näitavad, et auru lisamine N_2-le pürolüüsikeskkonnas soodustas võrreldes kuiva N_2 keskkonnaga süsivesinikgaaside teket, samas kui CO_2 keskkonna puhul oli auru lisamisel vastupidine mõju. Aur pürolüüsikeskkonnas soodustas H_2S ja SO_2 teket, mistõttu nii pürolüüsigaasis kui ka õlis nende kontsentratsioonid kasvasid, kinnitades veeauru olulist rolli väävliühendite lendumise suurendamisel.

Väävliühendite analüüs põlevkiviõli proovides näitab kuidas erinevad gaasikeskkonnad võivad mõjutada nende kontsentratsiooni õlis. Võrreldes N_2 keskkonnaga suurendas CO_2 osade väävliühendite kontsentratsiooni põlevkiviõlis. Põlevkiviõlis sisalduvate funktsionaalsete rühmade analüüs näitas, et CO_2 atmosfääris moodustunud põlevkiviõli koostises oli rohkem alifaatseid rühmi, samas kui N_2 atmosfääris tekkivas õlis oli aromaatsete rühmade sisaldus suurem. Auru lisamine N_2 keskkonda vähendas süsinik-süsinik kaksiksidemete ja aromaatsete süsinik-vesinik sidemete intensiivsust FTIR analüüsil võrreldes N_2 keskkonnaga. CO_2 ja CO_2/H_2O võrdluses olid muutused väikesed. Lisaks näitasid toodetud põlevkiviõlide mitmete omaduste (elemendianalüüs, MW, RI ja tihedus) mõõtmised õlide sarnasust.

Kombineerides põlevkiviõli ja pürolüüsigaasi analüüsi tulemusi, võib näha, et reaktiivsetel gaasidel pürolüüsireaktoris on oluline mõju pürolüüsisaadustele. Käesoleva uuringu tulemuste põhjal võib järeldada, et CO_2 käitub uuritud pürolüüsitemperatuuridel inertgaasina ning võib pürolüüsiatmosfääris asendada N_2.

Appendix

Publication I

S. Mozaffari, O. Järvik, and Z. S. Baird, "Effect of N_2 and CO_2 on shale oil from pyrolysis of Estonian oil shale" *Int. J. Coal Prep. Util.*, 2021, doi: 10.1080/19392699.2021.1914025.

INTERNATIONAL JOURNAL OF COAL PREPARATION AND UTILIZATION
https://doi.org/10.1080/19392699.2021.1914025

Taylor & Francis
Taylor & Francis Group

Effect of N_2 and CO_2 on shale oil from pyrolysis of Estonian oil shale

Sepehr Mozaffari, Oliver Järvik, and Zachariah Steven Baird

Department of Energy Technology, Tallinn University of Technology, Tallinn, Estonia

ABSTRACT

A kukersite oil shale sample from Estonia was pyrolyzed using a Fischer assay method under N_2, N_2/steam, CO_2 and CO_2/steam environments. The thermal behavior of the oil shale sample was also studied using TGA and DSC with similar conditions. Also, several properties of produced oils were measured and FTIR analysis was carried out to compare the molecular structure of the derived oils. The presence of steam increased the liquid and gaseous yields, and also caused a greater weight loss in the oil shale. The pyrolysis tests in both the CO_2 and N_2 atmospheres produced oils with relatively similar properties however, the molecular structure was different.

ARTICLE HISTORY
Received 23 February 2021
Accepted 5 April 2021

KEYWORDS
Oil shale; Fischer assay; pyrolysis; steam; CO_2; N_2

Introduction

Fossil fuels, such as crude oil, natural gas and coal, provide most of the energy in the world (Demirbas, Alidrisi, and Balubaid 2015). Oil shale is another widely available fossil fuel, although less used. It is a sedimentary rock that contains significant amount of organic matter called kerogen (Wang et al. 2014). Oil shale has attracted lots of interest due to the large amount of available oil shale deposits (Dijkmans et al. 2015) as well as the possibility of utilizing them as a source of energy and chemicals (Strizhakova and Usova 2008). The processing of oil shale to produce shale oil is often considered to be costly with a large environmental impact. For this reason, oil shale has not been widely utilized. However, some countries such as Estonia use oil shale extensively to supply their domestic energy (Baird et al. 2018; Mozaffari et al. 2020; Mozaffari, Järvik, and Baird 2020).

The chemical composition and physical properties of kerogen vary widely depending on the geographical locations, deposit conditions and oil shale formation conditions. Understanding the characteristics of the oil shale kerogen is essential for its beneficial utilization (Pomerantz et al. 2014). The organic matter in the oil shale is classified into two groups: soluble bitumen and insoluble kerogen (Vandenbroucke and Largeau 2007), of which about two thirds can be turned into oil by means of pyrolysis (Kann et al. 2004).

The production of shale oil via pyrolysis has been one of the main methods of oil shale valorization. Pyrolysis takes place in the absence of oxygen at around 500°C, causing oil shale kerogen to decompose into oil vapor compounds, hydrocarbon and non-hydrocarbon gases, pyrogenic water and semi coke (Gülamber et al. 2019). Among the technologies used, this low temperature pyrolysis has been of more interest for oil shales with a high oil yield

CONTACT Sepehr Mozaffari Sepehr.mozaffari@taltech.ee Department of Energy Technology, Tallinn University of Technology, Tallinn, Estonia

(Oja, Rooleht, and Baird 2016). The Fischer assay is a standard lab method used to estimate the oil yield by applying a slow heating rate. Utilizing such pyrolysis methods can be a beneficial way to analyze and associate the produced oil, gas and solid residue compositions with their corresponding test conditions, which results in improving the quality and quantity of the shale oil (Shadle, Seshadri, and Webb 1994).

Pyrolysis of oil shale under nitrogen and/or steam in different process conditions has been widely studied by many researchers. However, using CO_2 as the purge gas has relatively recently attracted attention, and therefore, the number of studies on CO_2 pyrolysis of oil shale seems to be small (David, Masri, and Lee 2000; Fang-Fang et al. 2010; Jaber and Probert 2000; Lee, Polasky, and Fullerton 1991; Polasky and Lee 1988; Tang et al. 2019). Tang et al. (Tang et al. 2019) studied the activation energy of several oil shales and found that a CO_2 atmosphere decreased the activation energy due to higher reactivity of long-chain organics under CO_2 in which lighter hydrocarbons were produced. They then concluded that using CO_2 could enhance the decomposition of oil shale. Consequently, Lee and Joshi (Lee and Joshi 1985) reported that exploiting CO_2 as the carrier gas can enhance the oil production by 7–25%, compared to N_2 under similar test conditions. However, Fang-Fang et al. (Fang-Fang et al. 2010) studied oil shale pyrolysis under N_2 and CO_2 and found that at lower temperatures (up to 500°C), both sweep gases showed almost identical behavior. Furthermore, they reported that the activation energy under CO_2 is almost the same as that of in N_2 at this temperature range; however, at higher temperatures of 600–1000°C, CO_2 increased the activation energy. In addition, they showed that CO_2 pyrolysis produced shale oil containing longer chain hydrocarbons than the oil produced under N_2. Also, in another study, Zhao et al. found that the activation energy of oil shale pyrolysis in N_2 atmosphere is higher. They explained that since the heat capacity of N_2 is higher than CO_2 therefore, the heat transfer resistance is larger as well, leading in greater dispersion of oil shale pyrolysis. (Zhao et al. 2021). These results show that different oil shales – due to their complex structures and different properties – show different behaviors and therefore, predicting them may not lead into the most correct conclusion. Tucker et al. (David, Masri, and Lee 2000) compared the oil yields when retorting under CO_2 and N_2 and reported that oils produced from them are quite similar. They also found that the most substantial difference is that the yield under CO_2 contains more mid-distillate fractions and also has a narrower molecular-weight distribution, and thus is a higher quality oil. The latter result was similar to what Polasy and Lee (Polasky and Lee 1988) obtained in their study on initial and final boiling points as well as the boiling range distribution of various shale oils under CO_2 and N_2 retorting and suggested that using CO_2 as a sweep gas increased the quality and quantity of the shale oil. Furthermore, other researchers (Lee, Polasky, and Fullerton 1991) investigated oil shale retorting under CO_2 and N_2 and found that the chemical compositions of the derived shale oils were different. They also concluded that retorting in CO_2 resulted in production of oils with shorter aliphatic chains compared with N_2, and reduced the abundance of n-alkanes and n-alkenes and suggested that CO_2 tends to preserve the aromatic structure of kerogen, whereas N_2 retorting tends to promote the formation of aliphatic compounds. Therefore, CO_2 appears to play an important role on final products when utilized in the pyrolysis process. The aim of the present research is to study the thermal behavior of kukersite oil shale under a CO_2 atmosphere and compare the yields and properties with those from retorting in N_2 to acquire a deeper understanding of the decomposition process and its impact on liquid products. The evolution and analysis of

gaseous products were presented in the second part of this study.(Moaffari, Järvik, and Baird 2021)

Materials and Methods

Fischer Assay

The Fischer assay is a standard laboratory method used to estimate the oil yield of an oil shale. 50 g of kukersite oil shale with a particle size of 500–710 μm was placed in a Fischer Assay retort. The Fischer assay retort was subjected to four different gaseous environments; CO_2, CO_2/steam, N_2 and N_2/steam. These gases were injected into the reactor using a tube which was placed through the retort lid. The flowrate used for tests without steam was 21 ml/min and for the runs with water vapor, water was injected at 0.1 ml/min and the flowrates of CO_2 and N_2 were set at 10 ml/min. In order ensure that the system was fully purged, the sweep gases were fed through the retort for one hour before beginning the experiment. Also, for the tests in the presence of water vapor, the water was first preheated to 150°C before entering into the retort. The retort was then heated up to 500°C at 10°C/min, from 500 to 520°C for 20 minutes and held at 520°C for another 20 minutes. To take the possible loss of water into account, three blank runs were made with water injection only. The Fischer Assay enables us to calculate the amount of oil and water, gas, and solid residue produced. The weight of gas produced was computed by difference based on the material balance.

Other Analytical Methods

Thermal Analysis

Thermogravimetric analysis (TGA) of the oil shale samples was conducted using a Netzsch STA 449 F3 Jupiter and differential scanning calorimetry (DSC) analysis was performed using a NETZSCH 204HP Phoenix DSC. The tests were performed under the same conditions as the Fischer Assay in both N_2 and CO_2 environments. The crucibles were filled with about 10 mg of the shale sample. In TGA Pt/Rh alloy crucibles with removable thin-walled Al_2O_3 liners were used, while in DSC open Al-crucibles were used. To ensure reproducibility, the tests for each atmosphere were conducted at least three times.

FTIR

An Interspec 301-X spectrometer fitted with an ATR accessory were used to measure the IR spectra for the oil samples. The sample spectra were analyzed in the wavenumber range of 600–4000 cm^{-1} at a resolution of 1 cm^{-1}. For each sample, the average of 10 scans was used to ensure the repeatability of the spectra and also to reduce the effect of noise. The estimated standard uncertainty and estimated expanded uncertainty (95% level) are 0.00053 and 0.0012 absorbance units (on average), respectively.

Elemental Analysis

Elemental analysis was performed using a Vario MACRO CHNS Cube system. The estimate of expanded relative uncertainty for each element would be as follows: carbon (1.11%), nitrogen (16.56%), hydrogen (2.56%) and sulfur (5.7%). Note that these are relative

uncertainties. The relative uncertainty of the nitrogen content seems high simply because the nitrogen content in the samples is low.

MW, RI, and Density

Other oil properties such as the density, molecular weight and refractive index were also measured. The densities of the oil samples were measured at 15 and 20°C using a DMA 5000 M (Anton Paar GmbH, Austria). In order to check the performance of the device, before and after each experiment the density of air and water were measured. The estimated standard uncertainty and expanded uncertainty (95% level) of the measurements for oil samples is 0.00015 g/cm^3 and 0.0003 g/cm3, respectively. The refractive index of the samples was measured using an Abbemat HT refractometer (Anton Paar GmbH) at 20°C and 589.592 nm. Also, water was used before and after each sample to check the performance of the device. The standard uncertainty and expanded uncertainty (95% level) for the device are estimated to be 0.0011 and 0.0021. Molecular weight was measured using a Knauer K-7000 vapor pressure osmometer (Wissenschaftliche Gerätebau Dr Ing Herbert KNAUER GmbH, Germany). Also, it should be noted that estimated standard uncertainty and the expanded uncertainty (95% level) are 7 g/mol and 14 g/mol.

Results and Discussion

Oil Shale Analysis

Kukersite oil shale from the Ojamaa mine was used throughout the study. The characteristics of kukersite oil shale used in this work are given in Table 1. More detailed analysis of the oil shale can be found in the literature. (Maaten et al. 2020) The elemental analysis of the shale sample indicated that the sample contains 28.5% organic matter. Also, the total organic carbon and total inorganic carbon are 19.71 and 5.83%, respectively. Due to its low H/C (1.26) and high O/C (0.09) molar ratio, kukersite oil shale can be classified as Type II oil shale.

Table 2 presents the yields from Fischer Assay under N_2, CO_2 and also with injected steam. Since the yield of liquid products from the tests were small, it was not possible to separate the oil and water. The results are the average of at least two tests for each test atmosphere. The variation of values for parallel measurements did not exceed 10%.

Table 1. Elemental and proximate analysis for the oil shale and the organic matter in the oil shale.

Elemental analysis	Dry basis, wt %	Organic matter, wt %
C	25.54	69.1
H	2.38	8.3
N	0.06	0.2
S	1.73	2.1
Cl	0.15	0.5
O	18.69	19.8
Proximate analysis		
Volatile matter	31.36%	
Moisture content	0.44%	
Ash content at 950°C	51.59%	
Fixed carbon	16.61%	
Lower heating value	8891.5 J/g	

Table 2. Fischer assay yields under all test environments.

Dry oil shale basis, wt%	N_2	N_2/steam	CO_2	CO_2/steam
Oil+Water	15.9	17.2	16.1	17.4
Gas	6.7	7.8	6.8	7.6
Semicoke	77.3	75.0	77.1	75.0

As can be seen from the table, the liquid and gas yields increased when steam was injected along with the sweep gases. EL Harfi et al. (El, Mokhlisse, and Ben Chanâa 1999) suggested that steam enhances oil evaporation and decreases coke formation. In addition, injection of steam caused more mass loss in the sample. The loss could be a result of reactions between water vapor and the oil shale organic matter. These results agree with the findings from other studies (El, Mokhlisse, and Ben Chanâa 1999; S. Al-Ayed 2006). Furthermore, water vapor speeds up the process of vaporization, desorption and diffusion of low molecular weight components in the pores by breaking their bonds with the macromolecular part and separating them as volatiles (Minkova et al. 1991). Other researchers have also studied the effect of steam as a sweep gas in pyrolysis. Williams and Nazzal (P. T. Williams and Nazzal 1998) pyrolyzed oil shale in a fixed bed reactor from 400–620°C under nitrogen and nitrogen/steam atmospheres and found that the presence of steam increases the oil yield significantly at all temperatures. For instance, at 520°C and using nitrogen the liquid yield was 11.84%, whereas the presence of steam increased the liquid yield up to 13.89%. Steam enhances the liquid yield by preventing retrogressive reactions that lead to char formation, probably via dehydrogenation of alkanes to alkenes and cyclization (Ekinci et al. 1991).

Oil Properties

Table 3 presents the elemental composition of the derived oils. The results show that the elemental composition for all oils is similar. It can be seen from the table the nitrogen content is lower when steam was added to the retort. This is because the nitrogen is contained in aromatic molecules of the oil and these molecules, because of their higher stability, are resistant to thermal cracking (Burnham et al. 1981). Thermodynamically speaking, aromatic compounds are more stable than aliphatic compounds. So, when cracking reactions increasingly take place, aliphatic compounds – which at high temperature undergo gas phase cracking – are converted to low molecular weight hydrocarbons. As a result, oils with more aromatic compounds are produced. Hence, aromatic nitrogen compounds are selectively concentrated (Paul T. Williams and Nazzal 1995; P. T., 1998; Wang et al. 2013; Burnham et al. 1981). On the other hand, other researchers also reported a similar result and proposed that the reduction of nitrogen content could be a result of steam ability to react with part of the organic nitrogen (Nazzal 2008). They also linked this

Table 3. Elemental analysis on derived oils.

Oil Sample	N [%]	C [%]	H [%]	S [%]	O [%]	H/C
N_2	0.18	81.30	9.35	0.84	8.33	1.380
N_2/steam	0.13	82.78	10.10	0.88	6.11	1.464
CO_2	0.18	80.84	9.35	0.85	8.78	1.387
CO_2/steam	0.14	83.75	10.11	0.8	5.29	1.448

occurrence with the ability of steam to recover the very light fractions which are low in nitrogen (Carter and Taulbee 1985). Furthermore, it is apparent that injection of steam increases the atomic H/C ratio. The H/C ratio is helpful to identify whether the oil sample is aromatic- or aliphatic-rich (Asemani and Rabbani 2020). In general, a lower H/C ratio indicates that the produced oil contains more aromatics compounds (P. T. Williams and Nazzal 1998; Nazzal 2008; Ekinci et al. 1991; Paul T. Williams and Nazzal 1995; Wang et al. 2013). A decrease in H/C ratio could be as a result of decrease in long-chain alkanes and increase in alkenes and aromatic content (Burnham et al. 1980). Furthermore, Olukcu also reported that using water vapor as the sweep gas results in a higher production of aliphatic hydrocarbons in the derived oils (Olukcu et al. 2002). According to Basu, introducing steam increases the H/C ratio, resulting in more gaseous products and less solid char (Basu 2010). Table 2 also shows that more gas was produced under pyrolysis in the presence of steam.

Table 4 shows the molecular weight, density and refractive index measured for the produced oils. Several researchers found that the oil from pyrolysis with steam contains lighter hydrocarbons. This may be a result of enhancement of secondary reactions with steam. This is due to the reaction with carbon and the catalyzing effect that some minerals have. They also suggested that water vapor speeds up the process of desorption of low molecular weight products from the mineral matrix (Al-Ayed and Matouq 2009; El, Mokhlisse, and Ben Chanâa 1999; S. Al-Ayed 2006). Furthermore, steam aids evaporation of the oil and decreases coke formation (Dung 1990).

Järvik and Oja (Järvik and Oja 2017) studied the shale oils from four different deposits produced using a modified Fischer assay method and suggested that the average molecular weight for the Fischer assay oils is about 279 ± 26 $g.mol^{-1}$. They also narrowed down the range further to 290 ± 13 $g.mol^{-1}$ for high yield oil shales and also suggested that oils with a higher aliphatic content (or oils with higher H/C) tend to have higher molecular weights. William and Nazzal (Paul T. Williams and Nazzal 1995) also measured the molecular weight of pyrolysis oils in the temperature range of 400–620°C and reported that an increase in pyrolysis temperature lowers the MW range of the oils. They attributed the reduction in MW range to an increase in the concentration of aromatic compounds and a lower concertation of higher MW aliphatic compounds when the temperature increases.

TGA and DSC Analysis

TGA and DSC were performed to study the behavior of thermal decomposition of oil shale kerogen when the temperature is increased. Figure 1 shows the mass loss behavior of kukersite oil shale in N_2 and CO_2 as a function of temperature. It can be seen from the figure that at temperatures below 200°C only a little weight loss occurred, mainly due to the evaporation of moisture. Below 350°C the mass loss is small and almost identical for both.

Table 4. Molecular weight, density and refractive index measurements of produced oils.

Fischer assay test	MW (g/mol)	Density @15.6°C (g/cm3)	Density @20°C (g/cm3)	RI @ 589.3 nm
N_2	290	0.9698	0.9661	1.5349
N_2/steam	282	0.9788	0.9749	1.5394
CO_2	283	0.9769	0.9730	1.5372
CO_2/steam	278	0.9776	0.9737	1.5369

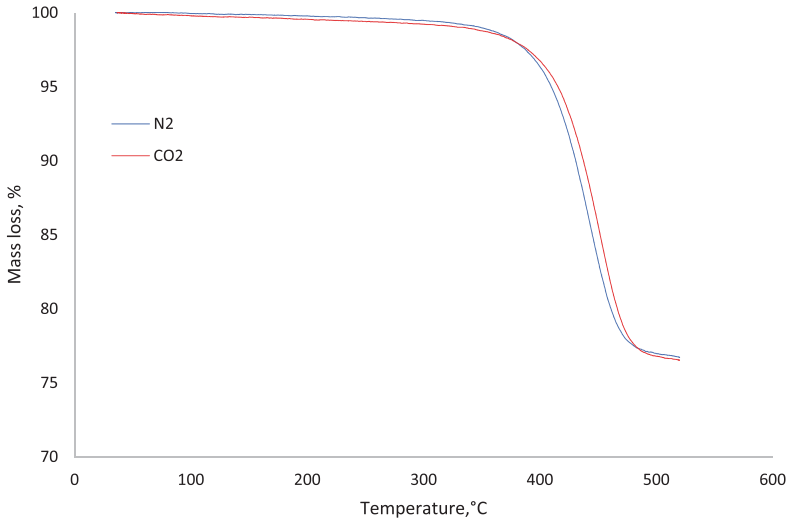

Figure 1. TGA curves of Ojamaa oil shale in N_2 and CO_2.

However, above 350°C the process of pyrolysis largely begins with mass loss at a higher rate. This happens due to the decomposition of organic matter and continues up to 520°C, at which point most of the hydrocarbons have been released.

As shown in the figure, the weight loss in the CO_2 environment was observed to be larger in comparison with N_2 even though, this difference is not significant. Also, this small difference at low temperatures could also be a result of heterogeneity of the sample. Jaber and Probert suggest that the presence of alkali metals – which play a role in carbon dioxide and H_2O reactions with carbon – cause higher reactivity in CO_2, and thus, a higher mass loss (Jaber and Probert 2000). This result matches other work given in the literature (Avid et al. 2003; Fang-Fang et al. 2010; Jaber and Probert 2000, 1999).

In order to create conditions similar to the Fischer assay tests, TGA tests were also run with the injection of steam so that the effect of water vapor on weight loss could be studied as well. Figures 2andFigures 3 illustrate the results for the oil shale sample in the presence of steam. As can be seen, more mass loss was observed after injection of steam into both environments. Also, despite almost identical mass loss rates, steam seemed to shift the pyrolysis process to a lower temperature than the test without steam. Additionally, running TGA tests under N_2/steam and CO_2/steam atmospheres increased the weight loss by about 2% and 3%, respectively.

Figure 4 compares the DSC curves obtained for oil shale under CO_2 and N_2 and both curves show similar trends in general. As the temperature increased to 150°C, endothermic behavior can be seen from the curves as heat is required to evaporate water particles from clay minerals (Qing et al. 2007). At about 200°C, the process of conversion of kerogen to bitumen starts by softening and changing the molecular structure of kerogen. This is followed by the release of gases as well (Jaber and Probert 2000). Subsequently, from 200 to 500°C, thermal decomposition of kerogen to bitumen and then to oil and gas can be seen as an endothermic peak. Also, the figure shows that the slope for the CO_2 run continuously increased until the end of the decomposition process while for N_2 it started with a moderate

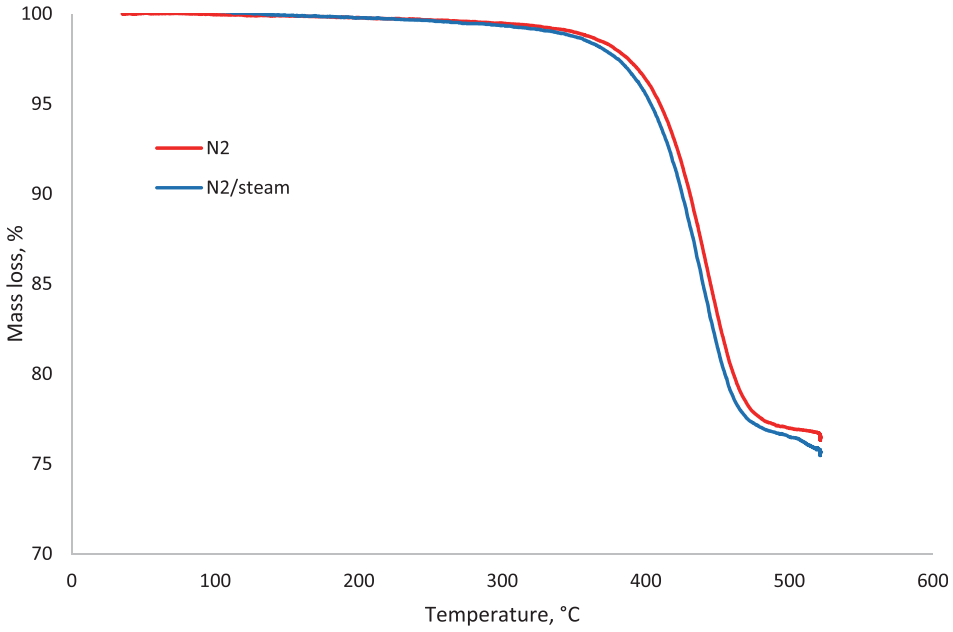

Figure 2. Comparison between the TGA in N_2 and N_2/steam.

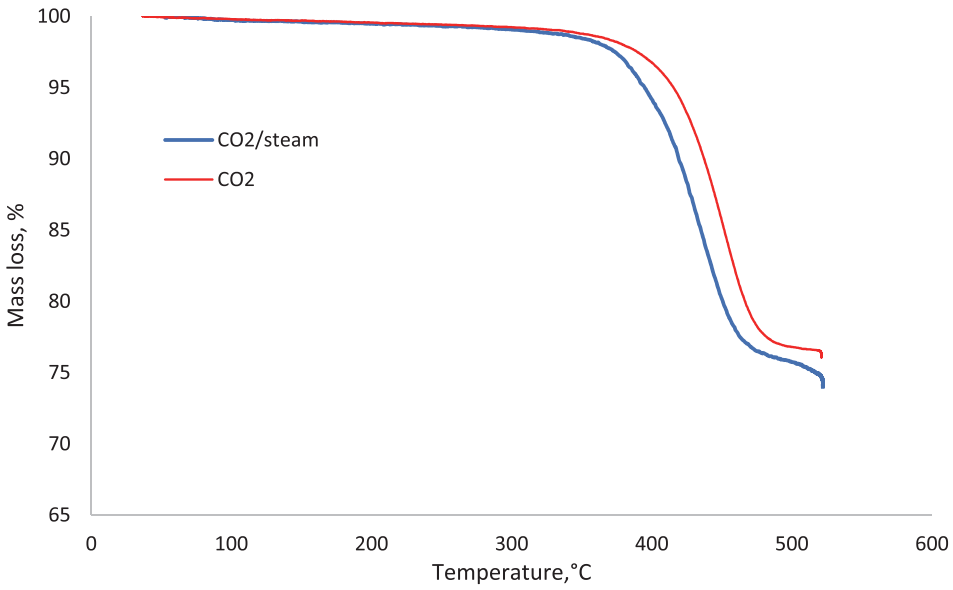

Figure 3. Comparison between the TGA in CO_2 and CO_2/steam.

slope which seems to be the releasing of light organic content up to 200°C and then a sharp increase for N_2 took place from 350°C. After pyrolysis, or after the pyrolysis peak temperature (around 450°C), the heat requirement reduced which means some material the

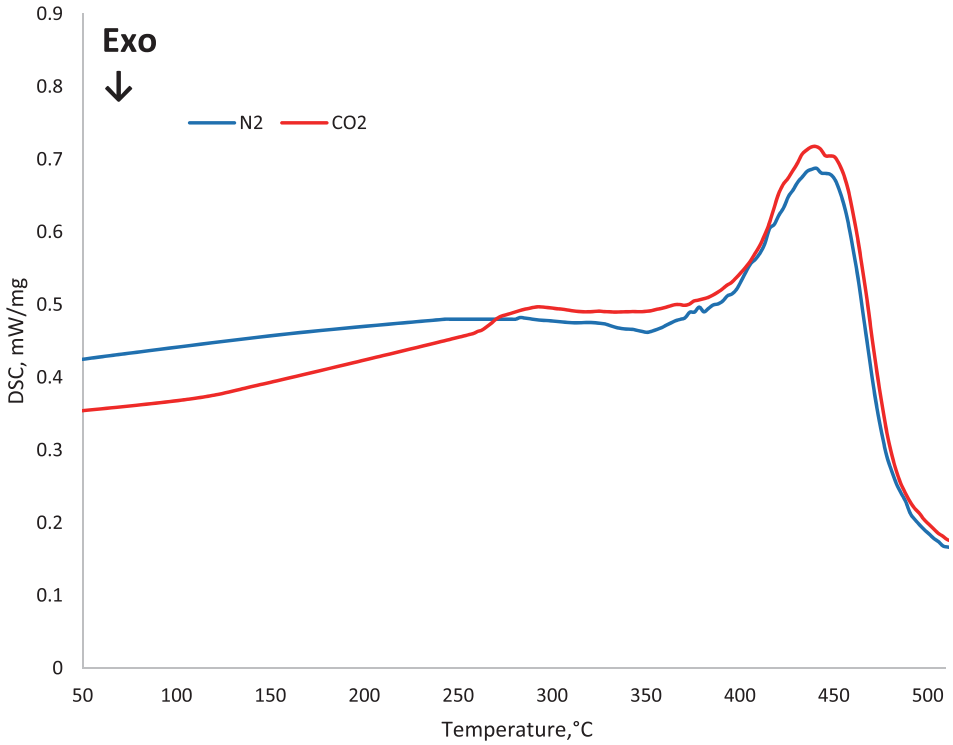

Figure 4. DSC curves for the oil shale sample under CO_2 and N_2.

pyrolysis is completed. In general, comparing the DSC results indicate that both curves behave similarly and the thermal decomposition is not affected by the carrier gas.

Fourier-transform Infrared Spectroscopy (FTIR)

FTIR spectra of the shale oils produced in CO_2 and N_2 atmospheres are shown in Figure 5. From the figure it can be seen that the spectra are relatively similar for both samples. The highest peak area is within the band range of 2750–3000 cm^{-1}, which is indicative of the aliphatic C-H functional group in the oil. In addition, two distinct differences can be seen between the curves at wavenumbers of 700–1800 cm^{-1} and 3200–3600 cm^{-1}. The former range can be used to mainly characterize C-H bonds and obtain information about the aromaticity and chain length. More specifically, absorptions for methyl C-H (CH_3 at 1365 cm^{-1}), methylene and methyl groups C-H (CH_3 + CH_2 at 1465 cm^{-1}), aromatic C-H bonds including CH out-of-plane bending; solo, duet, trio and quartet (700–900 cm^{-1}) as well as C-H in-plane bending (950–1225 cm^{-1}) can be observed within this region. Two bands at 1500 cm^{-1} and 1600 cm^{-1} are ascribed to aromatic ring vibration and the presence of a weak band at 3000–3150 cm^{-1} confirms their assignment. Also, the region 3200–3600 cm^{-1} is assigned to the presence of O-H functional groups (Borrego et al. 2000; Coates 2006).

The figure shows that the intensity of the absorbance peaks in the regions 700–1000 cm^{-1} as well as that of the hydroxyl groups band is significantly lower in CO_2 than N_2. This suggests that

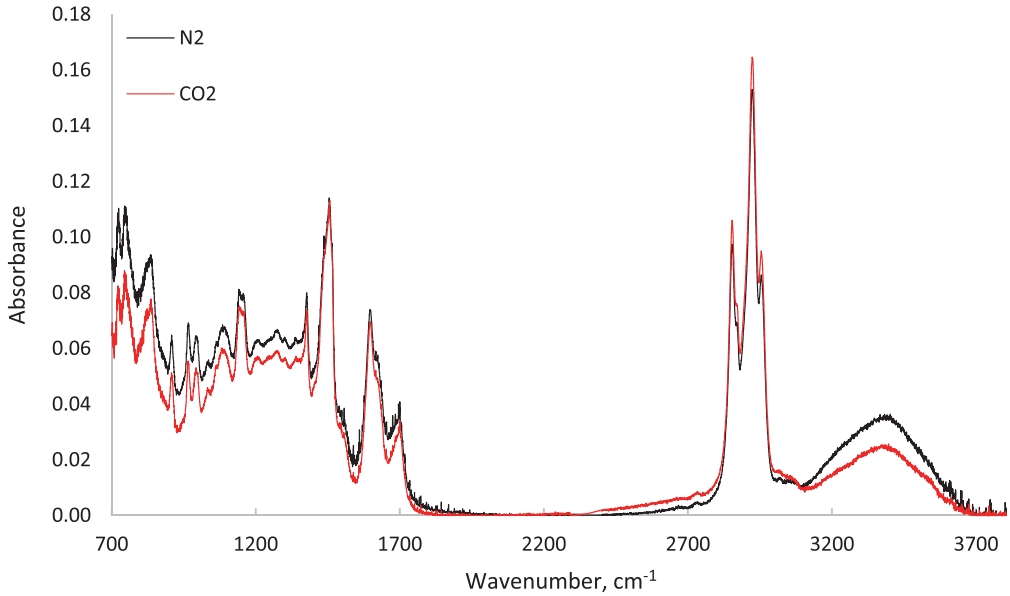

Figure 5. Infrared spectra of the oils produced in a Fischer assay under CO_2 and N_2.

CO_2 enhanced the cracking of hydroxyl groups and converted them into volatile matter (Luo et al. 2019). Also, it can be seen that the intensity of aliphatic peak at 2750–3000 cm^{-1} for the oil from CO_2 pyrolysis is higher, whereas the oil from N_2 pyrolysis showed bigger peaks in the aromatic regions. This indicates that using CO_2 as the carrier gas produced a more aliphatic oil. The higher aromatic peak under N_2 may be a result of the selective concentration of existing aromatics and aromatization of aliphatic compounds in the shale oil (Lai et al. 2016).

Figures 6 and Figures 7 show the spectrum of oils produced in the presence of steam. It seems that the presence of steam did not markedly affect the intensity of the hydroxyl group bands for both environments; however, the aliphatic peak slightly increased for the oil under N_2 when steam was added. By contrast, steam significantly decreased the aliphatic peak in CO_2. Furthermore, looking at the band region 700–1700 cm^{-1}, the band for N_2 is noticeably higher than that of in N_2/steam. On the other hand, steam significantly reduced the intensity of the alkenes and aromatic C-H bonds peaks in N_2 oil, whereas for CO_2, steam had slight effect on these chemical structures in the oil. The aliphatic peaks of the spectra in both figures indicate an inverse effect of steam in N_2 and CO_2. The figure shows that the presence of steam in CO_2 reduced the aliphatic peak of the oil, which is the opposite of N_2 where steam caused a little increase in the aliphatic peak. William and Nazzal (Nazzal and Williams 2002) concluded that formation of aromatic compounds during pyrolysis is due to secondary reaction in which gas-phase cracking of long-chain aliphatic compounds leads to conversion to low molecular weight hydrocarbons. Carter and Taulbee (Carter and Taulbee 1985) also suggested that an increase in oil aromaticity is a result of an increase in secondary reactions, which is caused by an increase in bed temperature. Burnham and Happe (Burnham and Happe 1984) proposed a mechanism for the conversion of aliphatic and aromatic content to oil, gas and carbonaceous residue. They expressed that during pyrolysis both aromatic and aliphatic

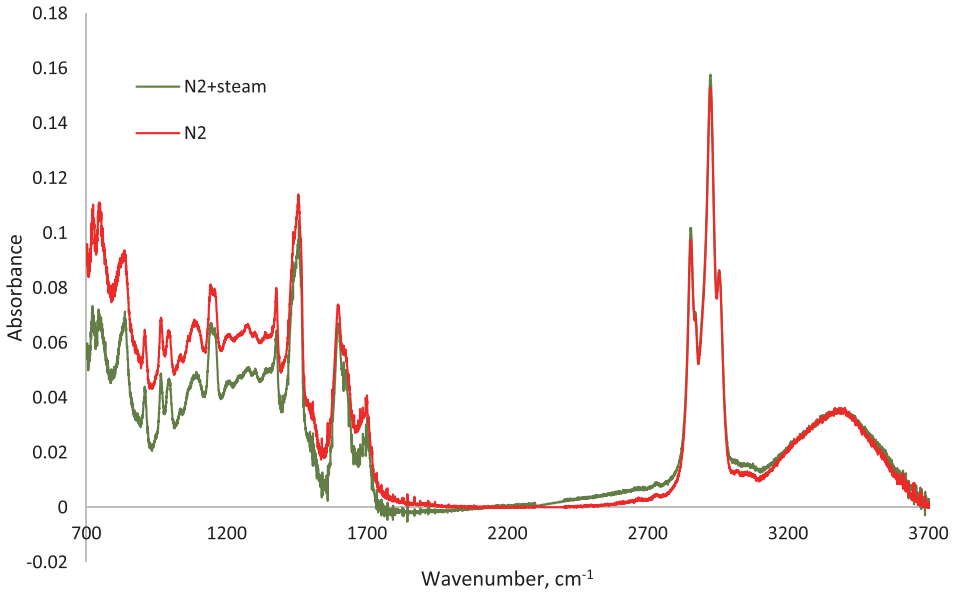

Figure 6. Comparison between the FTIR results for the Fischer assay oils in N_2 and N_2/steam.

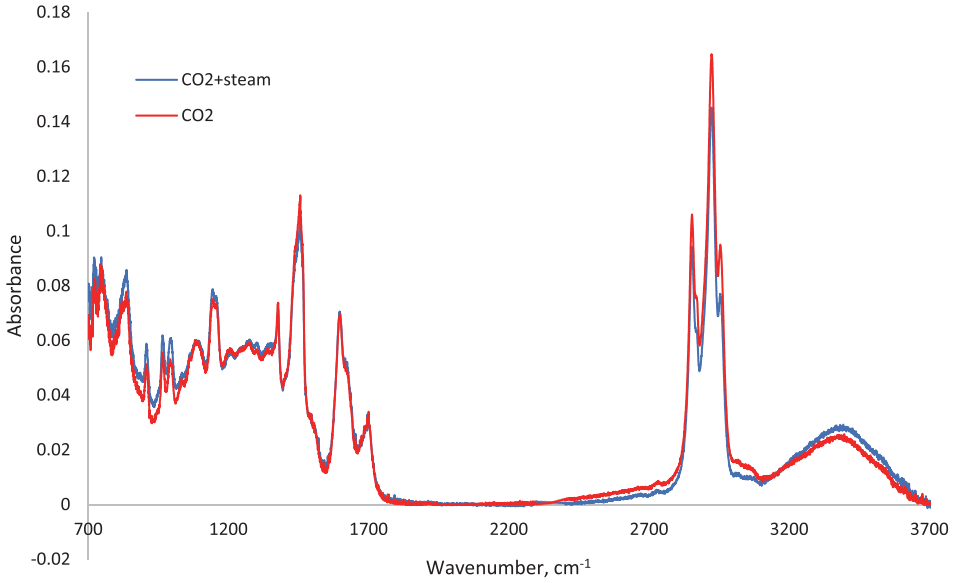

Figure 7. Comparison between the FTIR results for the Fischer assay oils in CO_2 and CO_2/steam.

structures in kerogen play a role in producing aromatic oil, and some of this oil is subsequently converted to coke. However, the main difference between these two kerogen portions is that the aliphatic content of kerogen is converted to aliphatic oil and gas while the aromatic content of kerogen has more of a tendency to remain in the char. On the other hand, during oil vapor cracking, some of the long-chain aliphatic structures are

converted to short-chain alkanes and alkenes as well as gas, which results in the production of hydrocarbons with a lower carbon content (Lai et al. 2016). But, the aromatic carbon in oil shale remains greatly unaffected by thermal decomposition, which means they have a higher tendency to become carbon residue (Lai et al. 2017). Therefore, it can be perceived that during thermal cracking, aliphatic compounds are transformed into aromatic compounds. This may be the primary reason that the amount of aromatic carbons in the recovered oil and solid residue is higher than that in raw oil shale: aromatization of aliphatic carbons. Accordingly, the process of conversion of aliphatic to aromatic is considered to have undesirable effect on generation of oil and thus inhibits achieving high oil yield (Hershkowitz et al. 1983; Shi et al. 2017).

Conclusion

In this study, Estonian kukersite oil shale was pyrolyzed using the Fischer assay method under N_2, N_2/steam, CO_2 and CO_2/steam environments. The results showed that the presence of steam in both environments produced more liquid and gaseous products. Also, injection of steam caused an increase in mass loss in comparison with the tests without steam and this loss was greater in the CO_2 atmosphere. In addition, oils produced under all environments had similar properties. However, the FTIR results indicated that the chemical structure of the derived oils was affected to some extent depending on the environment used. Overall, analysis of the oils from pyrolysis shows that at low temperatures CO_2 retorting and N_2 retorting yield oils with fairly similar characteristics. Though, according to the results obtained from TGA, using CO_2 as the sweep gas could possibly increase the shale weight loss, which means more of oil shale is converted into hydrocarbons. Comparing the results with the test in N_2, CO_2 seems to produce more liquid products, even though the difference is slight. This was reported previously by several researchers as well. In addition, over the studied temperature range, the effect of steam seems to be considerable. Injection of steam along with the sweep gas produced oils of a higher quality. That is due to the fact that steam increased the H/C ratio and also reduced the amount of nitrogen and oxygen atoms. Steam did not show remarkable impact on sulfur content of shale oil, however. As mentioned earlier, due to the higher availability and low cost of N_2, using nitrogen as carrier gas has been extensively studied and discussed. Conversely, the number of research works on pyrolysis of oil shale in a CO_2 atmosphere is not large. Current results available in the literature on using CO_2 as a sweep gas has been indicating promising results in terms of improving the quantity and quality of the derived oils. As seen in the results, CO_2 is one of the main components of pyrolysis gas. Furthermore, using CO_2 is known to have environmental impact as well. Therefore, the feasibility of development of recycling and utilizing CO_2 produced from oil shale pyrolysis could possibly be an attractive way to mitigate the emission of CO_2 to some extent and also to make its usage more economically viable. Consequently, with reference to previously stated points – chemical changes to the products, environmental issues, potential economic benefits – the products from pyrolysis in CO_2 may be of interest to corresponding industries.

Acknowledgments

This research was funded by Estonian Research Council from National Programme for Addressing Socio-Economic Challenges through R&D (RITA), which is supported by the Estonian Government and European Regional Development Fund."

ORCID

Sepehr Mozaffari http://orcid.org/0000-0002-9412-2820

References

Al-Ayed, O. S., and M. Matouq. 2009. Influence of Pyrolysis Environment on Liquid Product and Sulfur of Oil Shale. *Energy Sources, Part A: Recovery, Utilization and Environmental Effects* 31 (8):679–86. doi:10.1080/15567030701752529.

Al-Ayed, S. 2006. Pyrolysis of Ellajjun Oil Shale Under the Influences of Nitrogen and Water Vapor. *JES. Journal of Engineering Sciences* 34(1):275–81. Omar. doi:10.21608/jesaun.2006.110277.

Asemani, M., and A. R. Rabbani. 2020. Detailed FTIR Spectroscopy Characterization of Crude Oil Extracted Asphaltenes: Curve Resolve of Overlapping Bands. *Journal of Petroleum Science and Engineering* 185 October 2019:106618. doi:10.1016/j.petrol.2019.106618

Avid, B., M. Born, B. Purevsuren, N. Undrakh, and A. Tuvshinjargal. 2003. Thermal Behavior of Khoot Oil Shale in Different Conditions. *Oil Shale* 20 (1):47–55.

Baird, Z. S., P. Uusi-Kyyny, O. Järvik, V. Oja, and V. Alopaeus. 2018. Temperature and Pressure Dependence of Density of a Shale Oil and Derived Thermodynamic Properties. *Industrial & Engineering Chemistry Research* 57 (14):5128–35. doi:10.1021/acs.iecr.7b05018.

Basu, P. 2010. *Biomass Gasification and Pyrolysis. Biomass Gasification and Pyrolysis*. Academic Press. https://doi.org/10.1016/C2009-0-20099-7 .

Borrego, A. G., J. G. Prado, E. Fuente, M. D. Guillén, and C. G. Blanco. 2000. Pyrolytic Behaviour of Spanish Oil Shales and Their Kerogens. *Journal of Analytical and Applied Pyrolysis* 56 (1):1–21. doi:10.1016/S0165-2370(99)00092-3.

Burnham, A. K., R. H. Sanborn, R. W. Crawford, J. C. Newton, and J. A. Happe. 1980. Shale Oil Cracking. 2. Effect on Oil Composition. *Lawrence Livermore National Laboratory* Livermore, CA, UCID-18763 doi:10.1201/b16782-13.

Burnham, A. K., R. H. Sanborn, R. W. Crawford, J. C. Newton, and J. A. Happe. 1981. Chemistry of Shale Oil Cracking. In *Oil Shale, Tar Sands, and Related Materials, American Chemical Society Symposium Series*, ed.. H. C. Stauffer, Vol. 163, 39–60. American Chemical Society. doi:10.1021/bk-1981-0163.ch004.

Burnham, A. K., and J. A. Happe. 1984. On the Mechanism of Kerogen Pyrolysis. *Fuel* 63 (10):1353–56. doi:10.1016/0016-2361(84)90336-3.

Carter, S. D., and D. N. Taulbee. 1985. FLUIDIZED BED STEAM RETORTING OF KENTUCKY OIL SHALE. *Fuel Processing Technology* 11 (3):251–72. doi:10.1016/0378-3820(85)90004-9.

Coates, J. 2006. Interpretation of Infrared Spectra, A Practical Approach. *Encyclopedia of Analytical Chemistry* 1–23. doi:10.1002/9780470027318.a5606.

David, T. J., B. Masri, and S. Lee. 2000. Comparison of Retorting and Supercritical Extraction Techniques on El-Lajjun Oil Shale. *Energy Sources* 22 (5):453–63. doi:10.1080/00908310050013866.

Demirbas, A., H. Alidrisi, and M. A. Balubaid. 2015. API Gravity, Sulfur Content, and Desulfurization of Crude Oil. *Petroleum Science and Technology* 33 (1):93–101. doi:10.1080/10916466.2014.950383.

Dijkmans, T., M. R. Djokic, K. M. Van Geem, and G. B. Marin. 2015. Comprehensive Compositional Analysis of Sulfur and Nitrogen Containing Compounds in Shale Oil Using GC x GC - FID/SCD/NCD/TOF-MS. *Fuel* 140:398–406. doi:10.1016/j.fuel.2014.09.055.

Dung, N. V. 1990. Yields and Chemical Characteristics of Products from Fluidized Bed Steam Retorting of Condor and Stuart Oil Shales: Effect of Pyrolysis Temperature. *Fuel* 69 (3):368–76. doi:10.1016/0016-2361(90)90102-V.

Ekinci, E., A. E. Putun, M. Citiroglu, C. J. Lafferty, and C. E. Snape. 1991. "Effect of Steam and Hydrogen Pressure on Fixed-Bed Pyrolysis of Lignites and Oil Shales." *1991 International Conference on Coal Science Proceedings*, University of Newcastle-Upon-Tyne, United Kingdom, 520–23. https://doi.org/10.1016/b978-0-7506-0387-4.50132-7 .

El, H. K., A. Mokhlisse, and M. Ben Chanâa. 1999. Effect of Water Vapor on the Pyrolysis of the Moroccan (Tarfaya) Oil Shale. *Journal of Analytical and Applied Pyrolysis* 48 (2):65–76. doi:10.1016/S0165-2370(98)00108-9.

Fang-Fang, X., Z. Wang, L. Wei-Gang, and S. Wen-Li. 2010. Study on Thermal Conversion of Huadian Oil Shale under N2 and CO2 Atmospheres. *Oil Shale* 27 (4):309–20. doi:10.3176/oil.2010.4.04.

Gülamber, C., K. M. Ibrahim, S. Aljurf, and H. A. Rahman. 2019. "Introduction of Analytical Methods for Oil Shale Resource Evaluation." *IMCET 2019 - Proceedings of the 26th International Mining Congress and Exhibition of Turkey*, Antalya, Turkey, no. February 2020: 1154–68.

Hershkowitz, F., W. N. Olmstead, R. P. Rhodes, and K. D. Rose. 1983. "Molecular Mechanism of Oil Shale Pyrolysis in Nitrogen and Hydrogen Atmospheres." *American Chemical Society Symposium Series, USA* 230: 301–16. 10.1021/bk-1983-0230.ch015.

Jaber, J. O., and S. D. Probert. 1999. Pyrolysis and Gasification Kinetics of Jordanian Oil-Shales. *Applied Energy* 63 (4):269–86. doi:10.1016/s0306-2619(99)00033-1.

Jaber, J. O., and S. D. Probert. 2000. Non-Isothermal Thermogravimetry and Decomposition Kinetics of Two Jordanian Oil Shales under Different Processing Conditions. *Fuel Processing Technology* 63 (1):57–70. doi:10.1016/S0378-3820(99)00064-8.

Järvik, O., and V. Oja. 2017. Molecular Weight Distributions and Average Molecular Weights of Pyrolysis Oils from Oil Shales: Literature Data and Measurements by Size Exclusion Chromatography (SEC) and Atmospheric Solids Analysis Probe Mass Spectroscopy (ASAP MS) for Oils from Four Di. *Energy and Fuels* 31 (1):328–39. doi:10.1021/acs.energyfuels.6b02452.

Kann, J., A. Elenurm, I. Rohtla, N. Golubev, A. Kaidalov, and B. Kindorkin. 2004. About Thermal Low-Temperature Processing of Oil Shale by Solid Heat Carrier Method. *Oil Shale* 21 (3):195–203.

Lai, D., Y. Shi, S. Geng, Z. Chen, S. Gao, J. H. Zhan, and X. Guangwen. 2016. Secondary Reactions in Oil Shale Pyrolysis by Solid Heat Carrier in a Moving Bed with Internals. *Fuel* 173:138–45. doi:10.1016/j.fuel.2016.01.052.

Lai, D., J. H. Zhan, Y. Tian, S. Gao, and X. Guangwen. 2017. Mechanism of Kerogen Pyrolysis in Terms of Chemical Structure Transformation. *Fuel* 199:504–11. doi:10.1016/j.fuel.2017.03.013.

Lee, S., and R. Joshi. 1985. "Enhanced Oil Recovery from Western United States Type Oil Shale Using Carbon Dioxide Retorting Technique." *U.S. Patent No. 4,502,942*.

Lee, S., M. E. Polasky, and K. L. Fullerton. 1991. Chemical Composition of Oil Shale II. Dependence on the Extraction Process. *Fuel Science and Technology International* 9 (9):1151–79. doi:10.1080/08843759108942316.

Luo, Y., H. Ben, W. Zhihong, K. Nie, G. Han, and W. Jiang. 2019. Impact of CO2 on Pyrolysis Products of Bituminous Coal and Platanus Sawdust. *Polymers* 11 (8):1–12. doi:10.3390/polym11081370.

Maaten, B., O. Järvik, O. Pihl, A. Konist, and A. Siirde. 2020. Oil Shale Pyrolysis Products and the Fate of Sulfur. *Oil Shale* 37 (1):51–69. doi:10.3176/oil.2020.1.03.

Minkova, V., M. Razvigorova, M. Goranova, L. Ljutzkanov, and G. Angelova. 1991. Effect of Water Vapour on the Pyrolysis of Solid Fuels. 1. Effect of Water Vapour during the Pyrolysis of Solid Fuels on the Yield and Composition of the Liquid Products. *Fuel* 70 (6):713–19. doi:10.1016/0016-2361(91)90067-K.

Moaffari, S., O. Järvik, and Z. S. Baird. 2021. "Composition of Gas from Pyrolysis of Estonian Oil Shale under N2 and CO2 Fischer Assay." https://doi.org/10.31219/osf.io/2wv3h .

Mozaffari, P., Z. S. Baird, M. Listak, and V. Oja. 2020. Vapor Pressures of Narrow Gasoline Fractions of Oil from Industrial Retorting of Kukersite Oil Shale. *Oil Shale* 37 (4):288–303. doi:10.3176/oil.2020.4.03.

Mozaffari, P., O. Järvik, and Z. S. Baird. 2020. Vapor Pressures of Phenolic Compounds Found in Pyrolysis Oil. *Journal of Chemical and Engineering Data* 65 (11):5559–66. doi:10.1021/acs.jced.0c00675.

Nazzal, J. M. 2008. The Influence of Grain Size on the Products Yield and Shale Oil Composition from the Pyrolysis of Sultani Oil Shale. *Energy Conversion and Management* 49 (11):3278–86. doi:10.1016/j.enconman.2008.03.028.

Nazzal, J. M., and P. T. Williams. 2002. Influence of Temperature and Steam on the Products from the Flash Pyrolysis of Jordan Oil Shale. *International Journal of Energy Research* 26 (14):1207–19. doi:10.1002/er.845.

Oja, V., R. Rooleht, and Z. S. Baird. 2016. Physical and Thermodynamic Properties of Kukersite Pyrolysis Shale Oil: Literature Review. *Oil Shale* 33 (2):184–97. doi:10.3176/oil.2016.2.06.

Olukcu, N., J. Yanik, M. Saglam, and M. Yuksel. 2002. Liquefaction of Beypazari Oil Shale by Pyrolysis. *Journal of Analytical and Applied Pyrolysis* 64 (1):29–41. doi:10.1016/S0165-2370(01)00168-1.

Polasky, M. E., and S. Lee. 1988. Boiling Range Distributions of Various Shale Oils and Influence of Carbon Dioxide Retorting. *Fuel Science and Technology International* 6 (1):83–94. doi:10.1080/08843758808915875.

Pomerantz, A. E., K. D. Bake, P. R. Craddock, K. W. Kurzenhauser, B. G. Kodalen, S. Mitra-Kirtley, and T. B. Bolin. 2014. Sulfur Speciation in Kerogen and Bitumen from Gas and Oil Shales. *Organic Geochemistry* 68:5–12. doi:10.1016/j.orggeochem.2013.12.011.

Qing, W., S. U. N. Baizhong, H. U. Aijuan, B. A. I. Jingru, and L. I. Shaohua. 2007. Pyrolysis Charactersitics of Huadian Oil Shales. *Oil Shale* 24 (2):147–57.

Shadle, L. J., K. S. Seshadri, and D. L. Webb. 1994. Characterization of Shale Oils. 1. Analysis of Fischer Assay Oils and Their Aromatic Fractions Using Advanced Analytical Techniques. *Fuel Processing Technology* 37 (2):101–20. doi:10.1016/0378-3820(94)90010-8.

Shi, J., M. Yue, L. Shuyuan, W. Jianxun, Y. Zhu, and J. Teng. 2017. Characteristics of Estonian Oil Shale Kerogen and Its Pyrolysates with Thermal Bitumen as a Pyrolytic Intermediate. *Energy and Fuels* 31 (5):4808–16. doi:10.1021/acs.energyfuels.7b00054.

Strizhakova, Y. A., and T. V. Usova. 2008. Current Trends in the Pyrolysis of Oil Shale: A Review. *Solid Fuel Chemistry* 42 (4):197–201. doi:10.3103/S0361521908040022.

Tang, L., Y. Yan, Y. Meng, J. Wang, P. Jiang, C. H. Pang, and W. Tao. 2019. CO2 Gasification and Pyrolysis Reactivity Evaluation of Oil Shale. *Energy Procedia* 158:1694–99. doi:10.1016/j.egypro.2019.01.394.

Vandenbroucke, M., and C. Largeau. 2007. Kerogen Origin, Evolution and Structure. *Organic Geochemistry* 38 (5):719–833. doi:10.1016/j.orggeochem.2007.01.001.

Wang, S., X. Jiang, X. Han, and J. Tong. 2013. Effect of Residence Time on Products Yield and Characteristics of Shale Oil and Gases Produced by Low-Temperature Retorting of Dachengzi Oil Shale. *Oil Shale* 30 (4):501–16. doi:10.3176/oil.2013.4.04.

Wang, W., L.-Y. Li, Y. M. A. C-t Yue, and J.-L. He. 2014. Pyrolysis Kinetics of North-Korean Oil Shale. *Oil Shale* 31 (3):250. doi:10.3176/oil.2014.3.05.

Williams, P. T., and J. M. Nazzal. 1995. Polycyclic Aromatic Compounds in Oils Derived from the Fluidised Bed Pyrolysis of Oil Shale. *Journal of Analytical and Applied Pyrolysis* 35 (2):181–97. doi:10.1016/0165-2370(95)00908-9.

Williams, P. T., and J. M. Nazzal. 1998. Polycyclic Aromatic Compounds in Shale Oils: Influence of Process Conditions. *Environmental Technology (United Kingdom)* 19 (8):775–87. doi:10.1080/09593331908616734.

Zhao, S., Y. Sun, X. Lü, and L. Qiang. 2021. Kinetics and Thermodynamics Evaluation of Carbon Dioxide Enhanced Oil Shale Pyrolysis. *Scientific Reports* 11 (1):1–14. doi:10.1038/s41598-020-80205-4.

Publication II

S. Mozaffari, O. Järvik, and Z. S. Baird, “Composition of gas from pyrolysis of Estonian oil shale with various sweep gases” *Oil Shale*, vol. 38, no. 3, pp. 215–227, 2021, doi: 10.3176/oil.2021.3.03.

Oil Shale, 2021, Vol. 38, No. 3, pp. 215–227
doi: https://doi.org/10.3176/oil.2021.3.03
ISSN 0208-189X

Composition of gas from pyrolysis of Estonian oil shale with various sweep gases

Sepehr Mozaffari*, Oliver Järvik, Zachariah Steven Baird

Department of Energy Technology, Tallinn University of Technology, Ehitajate tee 5, 19086 Tallinn, Estonia

Received 12.02.2021, accepted 23.07.2021, available online 10.09.2021

Abstract. *Studying the evolution of gas during the decomposition process of oil shale provides information about the changes of its composition, as well as an understanding of the mechanism of the pyrolysis process. Earlier mainly the CO_2 atmosphere was used to observe the effect of the sweep gas on the production of pyrolysis products. In the current study, the Fischer assay method was used to analyze the pyrolysis of Estonian kukersite oil shale with CO_2, CO_2/steam, N_2 and N_2/steam sweep gases. The gaseous products were collected offline using a sample bag. Gas chromatography (GC) was performed to investigate the evolution of C_1–C_3 gases, H_2, CO_2 and CO. Subsequently, the results from each test were analyzed and compared. It was shown that in comparison with N_2, pyrolysis in CO_2 increased the production of alkanes and hydrocarbon (HC) gases. Also, the generation of CH_4 and CO gases was enhanced with CO_2, while the concentration of H_2 in the pyrolysis gas did not significantly change with either environment. The tests carried out in the presence of steam showed that unlike the N_2 atmosphere, CO_2/steam decreased the production of total hydrocarbons, H_2, CO_2 and CO.*

Keywords*: Estonian kukersite oil shale, Fischer assay, pyrolysis, gas evolution.*

1. Introduction

Compared with other energy sources such as coal and biomass, oil shale is considered to have great potential due to its large known deposits [1]. In addition to serving as an alternative fuel, utilization of oil shale may help keep the balance between energy production and consumption, ensure energy security and benefit countries economically [2]. As a result, the oil shale-based energy production has been acquiring importance in several countries

* Corresponding author: e-mail *sepehr.mozaffari@taltech.ee*

to meet their energy demands [3]. Estonia, for instance, has been producing heat, electricity and power as well as diesel fuel from oil shale for almost a century already, while its respective reserves make up only 1.1% of the world reserves [4]. However, the continual use of fossil fuels causes an increase in the emission of greenhouse gases into the environment, which leads to climate change [5]. Studying various aspects of the processing of oil shale would be helpful to assess and mitigate the environmental risks [6]. In light of these reasons, investigating alternative fuels has raised interest among researchers and accordingly, abundant analysis has been done on shale oil derived from oil shale pyrolysis. However, detailed analyses of and data about the shale gas from pyrolysis are quite rare. The yields and concentrations of pyrolysis gases are important parameters to learn about the quality of the shale gas produced. Data on shale gas can be helpful to give a better understanding about the chemistry related aspects of gas and oil production [7]. This, in fact, depends on many factors such as the final temperature, residence time, heating rate, production approach applied, oil shale characteristics, condenser used, etc. Since the decomposition of kerogen and conversion to oil take place mainly at temperatures below 500 °C, studying the evolution of gas gives more information about its composition as well as the mechanism of the decomposition process. The analysis of oil yield is provided in the first part of the study.

In this paper, the concentrations of H_2, CO, CO_2 and C_1–C_3 hydrocarbons (HC) in the gaseous product, as well as the evolution of these gases at different temperatures during pyrolysis are reported. The results give evidence of the dependency of the release of the gases on temperature.

2. Experimental section

2.1. Fischer assay

In pyrolysis experiments, a kukersite oil shale sample obtained from the Ojamaa mine located in northeast Estonia was used. The experiments were carried out in a Fischer assay retort. The 50 g oil shale sample was crushed to a particle size of 500–710 μm. The pyrolysis tests were conducted using the following sweep gases: CO_2, CO_2/steam, N_2 and N_2/steam. These sweep gases were introduced into the retort at a rate of 21 ml/min and in steam tests the gas and water flow rates were 10 and 0.1 ml/min, respectively. The sweep gases were injected into the system one hour before the pyrolysis began to ensure that the air was totally flushed out of the retort. Then, the retort was heated up to 500 °C at 10 °C/min and to 520 °C at 1 °C/min and held at 520 °C for 20 minutes. The total run took 90 min. Steam tests used a small heater to convert the injected water into steam before it reached the retort.

2.2. Gas chromatography

A Shimadzu GC-2014 gas chromatograph with a thermal conductivity detector (GC-TCD) and a valve system was used to analyze the release of various gases in a single run. The amounts of O_2, N_2 and CO were determined using a 3 m packed column with a 5 Å molecular sieve (OD 1/8″, ID 2 mm, 80/100 mesh), while a 9 m 25% DC-200/Shimalite packed column (60/80 mesh, OD 1/8″, ID 2 mm) was employed to determine the amount of CO_2. Determining the amounts of the aforementioned gases was possible by calibration. The calibration of GC was done by injecting 3 ml of gas with different concentrations of O_2, N_2, CO and CO_2. The column oven program started at a temperature of 35 °C (held isothermally for 3 minutes), followed by heating up to 85 °C at 5 °C/min (also held isothermally for 3 minutes), and finally by a ramp up to 125 °C at 10 °C/min. The total program time was 20 min. The injection temperature was 250 °C and the split ratio was 10:1. A Gazohrom-3101 gas chromatograph with a thermal conductivity detector was employed to determine the quantities of H_2, CO and CH_4 by using air as the carrier gas at a flow rate of 65 mL/min. A packed column (ID 3.5 mm, length 2.5 m), which operated at room temperature, was used for separation of gases. The injection volume was 2 mL and the relative standard deviation for parallel measurements for both GCs did not exceed 10% and 5%, respectively. With a Shimadzu GC-2014, peaks of hydrocarbons of higher quantities could be observed. As calibration was not applicable to C_2 and C_3 hydrocarbons, their concentrations were determined using the CH_4 peak area from a Gazohrom 3101 GC as a reference, while the different thermal conductivities of the gases accounted for their different properties. To calculate the concentration of C_2 and C_3 hydrocarbon gases, it was assumed that the peak areas of the gases were directly proportional to their thermal conductivity at corresponding temperatures. Although this leads to a somewhat higher uncertainty, it also allowed us to obtain information on the concentrations of these gases which would have otherwise got lost. Consequently, the concentration values of these gases would more likely provide qualitative data about the respective trends throughout the experiments.

3. Results and discussion

3.1. Gas analysis

Tables 1 and 2 present the quantities of gases evolved at different test temperatures in different atmospheres as a function of temperature. The major gases evolved were CO, CO_2, H_2, and C_1–C_3 hydrocarbons.

Campbell et al. [8], studying oil shale pyrolysis mechanisms from 25 °C to 900 °C, described it as a simplified two-step process of kerogen, during which the matter was transformed to bitumen and then bitumen to oil. In addition, the

Table 1. Evolution of gases at different temperatures of the Fischer assay test in N_2 and N_2/steam atmospheres, %

	N_2				N_2/steam			
Gas	200–400 °C	400–500 °C	500–520 °C	520 °C	200–400 °C	400–500 °C	500–520 °C	520 °C
CO	0.2	5.1	5.1	1.8	0.1	5.2	5.1	2.4
CO_2	2.3	12.3	10.7	5.8	1.3	17.0	14.9	16.2
H_2	0.0	1.3	4.9	4.7	0.0	1.6	4.5	2.7
CH_4	0.4	3.5	16.4	11.7	0.5	7.0	19.1	11.1
C_2H_4	0.0	0.7	2.3	0.9	0.0	1.3	2.6	1.0
C_2H_6	0.0	1.9	7.7	3.0	0.0	4.3	8.7	3.0
C_3H_6	0.0	2.5	3.4	0.9	0.0	6.8	5.0	2.1
C_3H_8	0.0	1.6	5.5	1.8	0.0	3.6	6.3	1.9
Total HC gases	0.4	10.1	35.3	18.3	0.6	23.0	41.8	19.2
Alkanes	0.4	7.0	29.7	16.5	0.5	14.8	34.1	16.1
Alkenes	0.0	3.1	5.7	1.7	0.0	8.1	7.6	3.1
Alkenes/alkanes ratio	0.1	0.4	0.2	0.1	0.0	0.5	0.2	0.2

Table 2. Evolution of gases at different temperatures of the Fischer assay test in CO_2 and CO_2/steam atmospheres, %

	CO_2				CO_2/steam			
Gas	200–400 °C	400–500 °C	500–520 °C	520 °C	200–400 °C	400–500 °C	500–520 °C	520 °C
CO	0.1	7.9	7.7	2.9	0.4	6.2	5.0	2.8
H_2	0.0	1.8	4.7	3.6	0.0	1.3	4.6	4.4
CH_4	0.4	8.2	16.0	11.9	0.4	5.5	18.8	18.1
C_2H_4	0.1	1.6	4.8	0.7	0.2	1.2	3.0	2.0
C_2H_6	0.1	5.1	16.3	2.0	0.1	3.8	9.5	5.6
C_3H_6	0.0	5.7	7.8	0.0	0.0	7.5	7.1	4.4
C_3H_8	0.0	4.0	11.2	0.5	0.0	3.4	7.2	4.1
Total HC gases	0.6	24.6	56.2	15.1	0.8	21.5	45.6	34.2
Alkanes	0.5	17.3	43.5	14.3	0.6	12.7	35.5	27.8
Alkenes	0.1	7.3	12.7	0.7	0.2	8.8	10.1	6.4
Alkenes/alkanes ratio	0.2	0.4	0.3	0.1	0.4	0.7	0.3	0.2

researchers suggested that only small amounts of non-condensable gases are produced during the process of conversion of kerogen to bitumen; however, during the conversion of bitumen to oil, the evolution of significant amounts of non-condensable gases takes place [8]. This can also be observed in the current work as seen from Table 1. Only traces of non-condensable gases were produced below 400 °C whereas above this temperature and up to 500 °C the main evolution of oil and gas can be observed.

The detailed analysis of evolution of hydrocarbon gases during the pyrolysis as a function of temperature in the presence of steam is shown in Figures 1–3. As seen from the figures, in all test environments the production of total HC gases, alkanes and alkenes was increased by increasing the retort temperature. Moreover, these figures indicate that the inclusion of steam in the N_2 atmosphere caused an increase in the concentration of hydrocarbon gases, alkanes and alkenes in the gaseous pyrolysis products. These results agree with those of several other researchers' works [9–11]. Nazzal [12] suggested that the presence of steam in oil shale pyrolysis could play an important role in the exit gas composition because, in addition to having a high heat capacity, steam speeds up the pyrolysis process. Also, steam increases the heating value of gaseous products after condensation as a result of increase in the concentrations of CO and H_2.

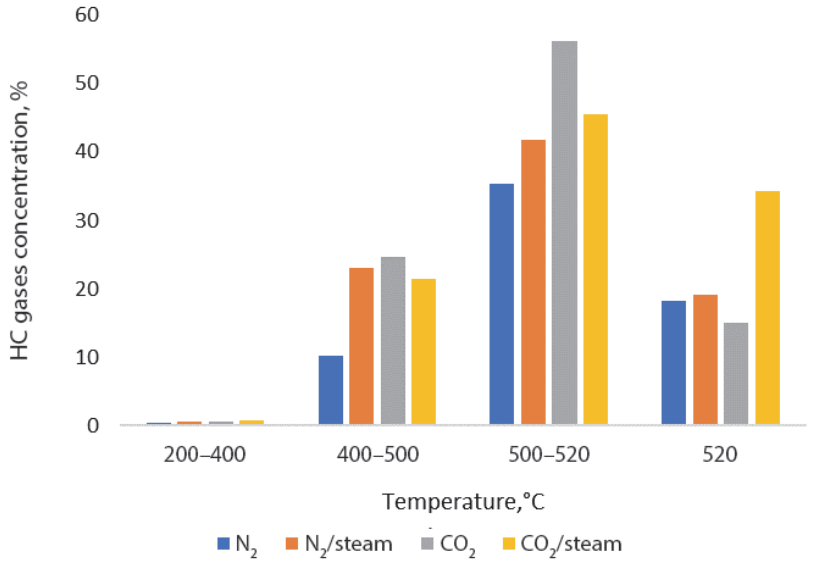

Fig. 1. Evolution of hydrocarbon gases during pyrolysis.

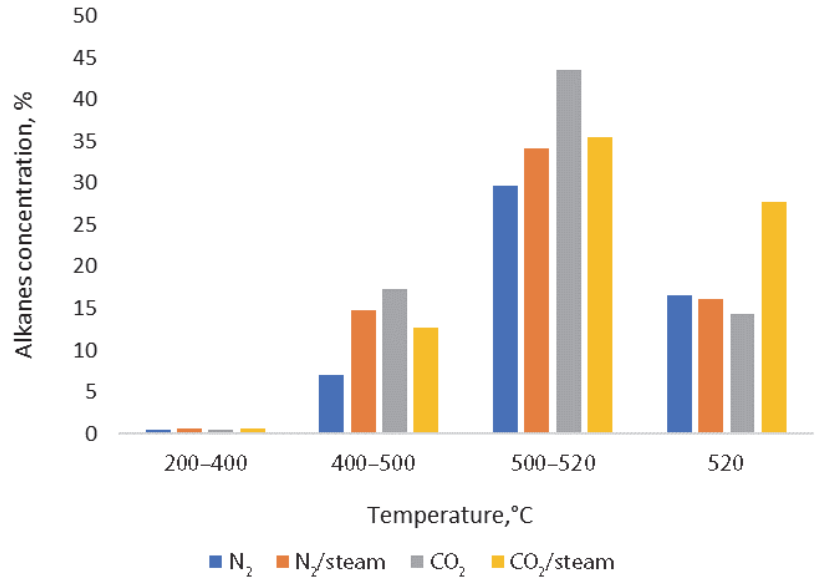

Fig. 2. Evolution of alkane gases during pyrolysis.

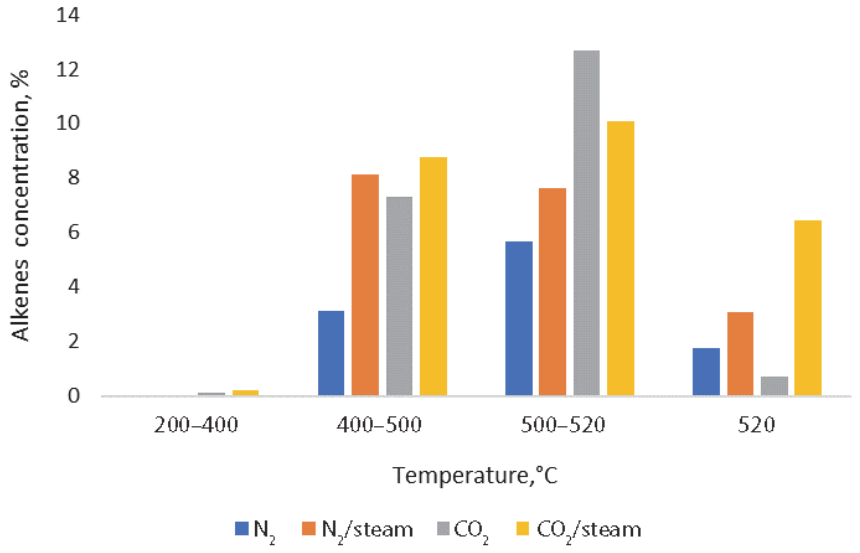

Fig. 3. Evolution of alkene gases during pyrolysis.

However, looking at the graphs more closely, it is obvious that steam has the opposite effects when injected into the N_2 and CO_2 environments. In the N_2 atmosphere, steam enhanced the total amounts of HC gases, alkanes and

alkenes. These results agree with Nazzal's findings [12] where a small increase in total HC gases and alkenes and a slight difference in alkanes production was observed between 400 °C and 520 °C in the N_2/steam environment. As stated earlier, steam exerts a different effect in the CO_2 atmosphere. In CO_2, it caused a decrease in the total hydrocarbon and alkane gases production; however, the presence of steam initially increased the concentration of alkene gases (up to 400 °C) and then reduced it as the evolution of oil began (450 °C). Subsequently, steam decreased the concentration of alkenes at higher temperatures.

Table 1 also presents the alkenes/alkanes ratios for all tests during the HC gases evolution. The said ratio has been used to determine reaction mechanisms and indicates pyrolysis conditions [11, 13]. Several researchers have suggested that an increase in the alkene/alkane ratio is a result of secondary cracking reactions [9, 11, 12] and lower ratios are associated with coking reactions [1, 2]. During pyrolysis the alkenes/alkanes ratio initially increased and then decreased. The highest values of the ratio may be due to the occurrence of secondary gas phase reactions in the temperature range of 400–500 °C where the evolution of oil and gas largely takes place. Moreover, these ratios were mostly higher in the pyrolysis with steam. Williams and Nazzal [9] suggested that even though steam increases the oil yield by decreasing the occurrence of secondary coking reactions, it also increases the alkenes/alkanes ratio, which means an increase in the taking place of secondary vapor phase cracking reactions.

Figure 4 exhibits the evolution of CO_2 during pyrolysis in N_2 and N_2/steam as a function of temperature. Even though studying CO_2 evolution in the

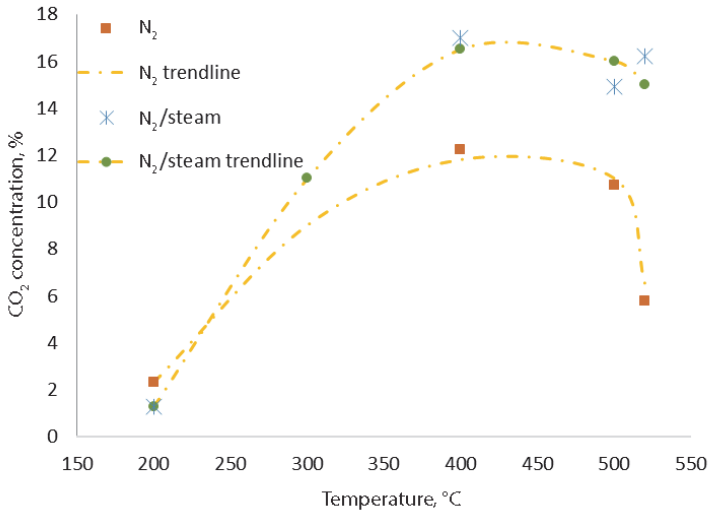

Fig. 4. Evolution of CO_2 during pyrolysis as a function of temperature.

tests in CO_2 was not applicable, such measurements were made in the N_2 and N_2/steam environments. It can be seen from the figure that the yield of CO_2 was greatly increased in the run with steam. This could be a result of various reactions such as the water-gas shift reaction, mineral carbonate decomposition reactions as well as steam-hydrocarbon reactions. By increasing the pyrolysis temperature, the decomposition of mineral carbonates and production of water increase, which leads to the higher production of CO_2 [12]. Looking at the yield of gases throughout the pyrolysis process (up to 500 °C) indicates that CO_2 made up the largest portion of the gaseous products. This may suggest that water vapor plays a certain role in oxidation reactions.

Williams and Nazzal [9] related the higher gas yield in N_2/steam to the higher CO_2 concentration that is produced at higher temperatures and suggested that this is coupled with a series of reactions, namely the char-steam, water gas-shift, hydrocarbon steam and mineral carbonate-steam reactions.

Figures 5–7 compare the yields of CO, H_2 and CH_4 during the decomposition of kerogen. Since the gas sampling was offline, it was not possible to find the precise peak temperature at which the evolution of gas took place. From the figures it can be perceived that the peak for carbon monoxide, hydrogen and methane evolution occurs at around 400–450 °C, 480–510 °C and 500 °C, respectively. Huss and Burnham [14] also studied the gas evolution of different shale samples during pyrolysis in a reactor under an argon atmosphere over a temperature range of 25–950 °C at a heating rate of 2 °C/min. The researchers' findings show that the evolution of CO, H_2 and CH_4 mostly happens at 425–435 °C, 465 °C and 480–520 °C, respectively. They associated this phenomenon with oil generation which occurred at the maximum rate at 430–435 °C.

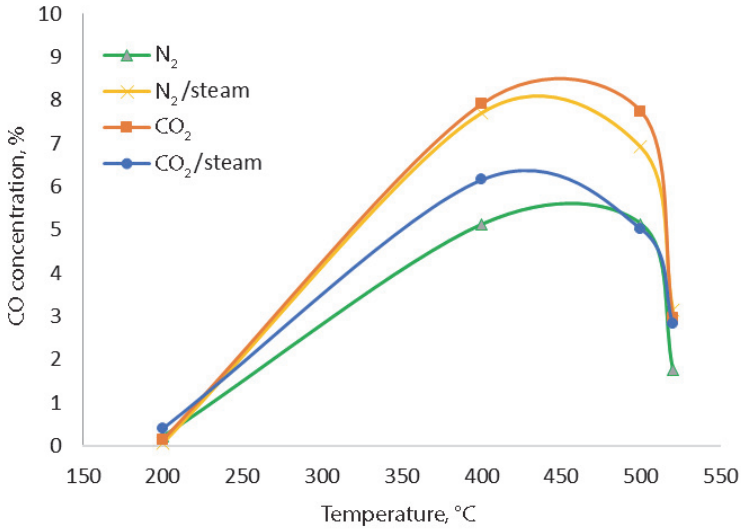

Fig. 5. Evolution of CO during kerogen decomposition.

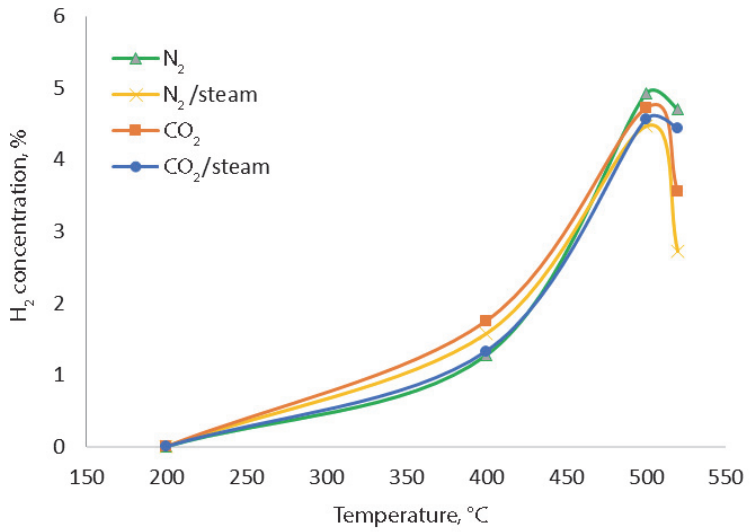

Fig. 6. Evolution of H_2 during kerogen decomposition.

The experimental results of the current work revealed that in the presence of steam CO started to be produced at around 400 °C and had its highest content when the oil was about to be generated. It appears that the concentration of CO in N_2 pyrolysis was lower than that in N_2/steam. That is partially because of the reactions that the produced water and injected steam initiate with the char to produce hydrogen and carbon monoxide. Also, in the water gas shift reaction, steam and CO produce hydrogen and CO_2. These reactions have an obvious effect on the concentrations of CO and H_2 in the retort. In addition, at higher temperatures, the concentration of CO is reduced and that of hydrogen increased. Also, it appears from the results of the test carried out in N_2 that using CO_2 as a sweep gas significantly increased the amounts of CO and H_2 in the gaseous products. Generally, it was observed that steam injected into the CO_2 atmosphere lowered the concentrations of H_2 and CO in the pyrolysis gas but in the N_2 atmosphere increased them.

Comparison of methane concentrations in the pyrolysis products indicates that its formation is higher in the CO_2 atmosphere than in N_2. It is apparent that the presence of steam yielded higher methane concentrations in N_2 at all temperatures while in CO_2 the methane formation only increased at higher temperatures. This can be explained by the reaction between steam and hydrocarbon gases in which oxygen and methane are formed:

$$2HC + H_2O \rightarrow O_2 + CH_4$$

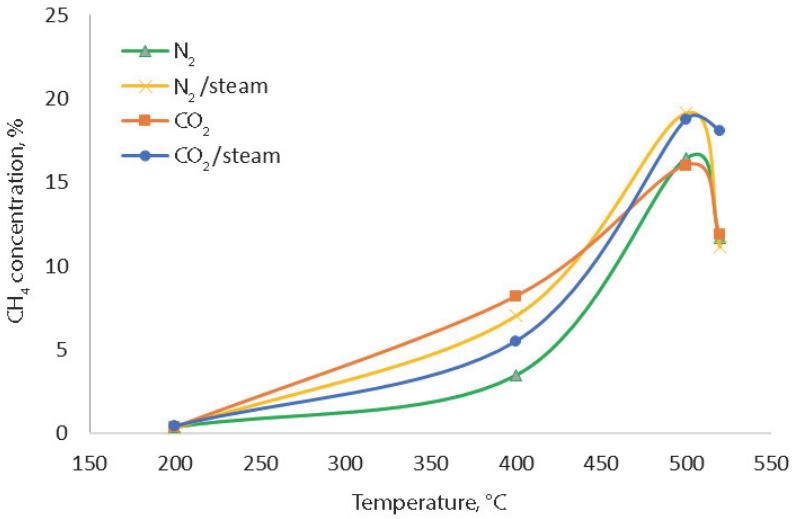

Fig. 7. Evolution of CH_4 during kerogen decomposition.

It is for this reason that the yield of methane in pyrolysis with steam is higher.

It is worth noting that a sharp increase in the formation of said gases can be observed from about 400 °C onward. This is the approximate temperature at which bitumen is converted to oil and shale oil generation begins. As explained before, with increasing temperature the total concentration of HC gases increased and consequently, the formation of H_2 and CH_4 in the retort increased as well. During the last phase of the test, in which the retort temperature was held at 520 °C for 20 minutes, and due to the consumption of the shale sample over time, less hydrocarbons were produced, as a result of which the formation of methane decreased.

4. Conclusions

This research focused on the gaseous products of the pyrolysis of Estonian kukersite oil shale by using the Fischer assay method. The tests were conducted in four different atmospheres: CO_2, CO_2/steam, N_2 and N_2/steam. Gas chromatography was used to measure the amounts of the gases evolved. The analysis showed that more hydrocarbon gases were produced when steam was injected into N_2. Conversely, the presence of steam caused a reduction in total hydrocarbon gases and alkane gases in the CO_2 atmosphere. Moreover, the results indicated that in CO_2/steam the concentrations of H_2 and CO were

lowered by steam differently from the CO_2 atmosphere. Furthermore, the alkenes/alkanes ratio, which is used to determine reaction mechanisms, first increased and then decreased. Analyzing the outcomes obtained from studying gases evolution during oil shale pyrolysis may contribute to the development and advancement of processes and technology to enhance the oil and gas yields from the retorting of oil shale.

Acknowledgments

This research was funded by the Estonian Research Council within the National Programme for Addressing Socio-Economic Challenges through R&D (RITA), which is supported by the Estonian Government and the European Regional Development Fund.

REFERENCES

1. Wang, S., Liu, J., Jiang, X. Han, X., Tong, J. Effect of heating rate on products yield and characteristics of non-condensable gases and shale oil obtained by retorting Dachengzi oil shale. *Oil Shale*, 2013, **30**(1), 27–47. https://doi.org/10.3176/oil.2013.1.04
2. Wang, S., Jiang, X., Han, X., Tong, J. Effect of residence time on products yield and characteristics of shale oil and gases produced by low-temperature retorting of Dachengzi oil shale. *Oil Shale*, 2013, **30**(4), 501–516. https://doi.org/10.3176/oil.2013.4.04
3. Baird, Z. S., Uusi-Kyyny, P., Järvik, O., Oja, V., Alopaeus, V. Temperature and pressure dependence of density of a shale oil and derived thermodynamic properties. *Ind. Eng. Chem. Res.*, 2018, **57**(14), 5128–5135. https://doi.org/10.1021/acs.iecr.7b05018
4. Ristic, N. D., Djokic, M. R., Konist, A., Van Geem, K. M., Marin, G. B. Quantitative compositional analysis of Estonian shale oil using comprehensive two dimensional gas chromatography. *Fuel Process. Technol.*, 2017, **167**, 241–249. https://doi.org/10.1016/j.fuproc.2017.07.008
5. Mozaffari, P., Järvik, O., Baird, Z. S. Vapor pressures of phenolic compounds found in pyrolysis oil. *J. Chem. Eng. Data*, 2020, **65**(11), 5559–5566. https://doi.org/10.1021/acs.jced.0c00675
6. Mozaffari, P., Baird, Z. S., Listak, M., Oja, V. Vapor pressures of narrow gasoline fractions of oil from industrial retorting of Kukersite oil shale. *Oil Shale*, 2020, **37**(4), 288–303. https://doi.org/10.3176/oil.2020.4.03
7. Coburn, T. T. Eastern oil shale retorting: Gas evolution during pyrolysis of northeastern Kentucky shales. *Energ. Source.*, 1983, **7**(2), 121–150. https://doi.org/10.1080/00908318308908080

8. Campbell, J. H., Koskinas, G. J., Gallegos, G., Gregg, M. Gas evolution during oil shale pyrolysis. 1. Nonisothermal rate measurements. *Fuel*, 1980, **59**(10), 718–726. https://doi.org/10.1016/0016-2361(80)90027-7
9. Williams, P. T., Nazzal, J. M. Polycyclic aromatic compounds in shale oils: Influence of process conditions. *Environ. Technol. (United Kingdom)*, 1998, **19**(8), 775–787. https://doi.org/10.1080/09593331908616734
10. Wang, S., Jiang, X., Han, X., Tong, J. Effect of retorting temperature on product yield and characteristics of non-condensable gases and shale oil obtained by retorting Huadian oil shales. *Fuel Process. Technol.*, 2014, **121**, 9–15. https://doi.org/10.1016/j.fuproc.2014.01.005
11. Williams, P. T., Ahmad, N. Influence of process conditions on the pyrolysis of Pakistani oil shales. *Fuel*, 1999, **78**(6), 653–662. https://doi.org/10.1016/S0016-2361(98)00190-2
12. Nazzal, J. M. Gas evolution from the pyrolysis of Jordan oil shale in a fixed-bed reactor. *J. Therm. Anal. Calorim.*, 2001, **65**(3), 847–857. https://doi.org/10.1023/A:1011936401407
13. Williams, P. T., Nazzal, J. M. Polycyclic aromatic compounds in oils derived from the fluidised bed pyrolysis of oil shale. *J. Anal. Appl. Pyrol.*, 1995, **35**(2), 181–197. https://doi.org/10.1016/0165-2370(95)00908-9
14. Huss, E. B., Burnham, A. K. Gas evolution during pyrolysis of various Colorado oil shales. *Fuel*, 1982, **61**(12), 1188–1196. https://doi.org/10.1016/0016-2361(82)90018-7

Publication III

H. Astra, T. Albert, **S. Mozaffari**, O. Järvik, A. Yanchilin, S. Kamenev, S. Karagöz, V. Oja, “Yields and the selected physicochemical properties of thermobitumen as an intermediate product of the pyrolysis of Kukersite oil shale” vol. 38, no. 4, pp. 295–316, 2021, doi: 10.3176/oil.2021.4.02.

Oil Shale, 2021, Vol. 38, No. 4, pp. 295–316
doi: https://doi.org/10.3176/oil.2021.4.02
ISSN 0208-189X

Yields and the selected physicochemical properties of thermobitumen as an intermediate product of the pyrolysis of Kukersite oil shale

Hanna-Liina Astra[(a)], Tiina Albert[(a)], Sepehr Mozaffari[(b)], Oliver Järvik[(a,b)], Alexey Yanchilin[(a)], Sven Kamenev[(b)], Selhan Karagöz[(c)], Vahur Oja[(a,b)]*

Received 21 January 2021, accepted 10 November 2021, available online 10 December 2021

(a) Department of Chemical Engineering, Tallinn University of Technology, Ehitajate tee 5, 19086 Tallinn, Estonia
(b) Department of Energy Technology, Tallinn University of Technology, Ehitajate tee 5, 19086 Tallinn, Estonia
(c) Department of Chemistry, Karabük University, 78050 Karabük, Turkey

Abstract. *In the pyrolytic decomposition of kerogen, a macromolecular cross-linked material of oil shale, the formation of thermobitumen is often considered an important intermediate step in pyrolysis modelling. The authors' literature review indicated that information regarding the yield of thermobitumen from Kukersite oil shale was somewhat contradictory, and data on physical-thermodynamic properties, which is to be used in engineering calculations, was limited. Therefore the present work provides further information on thermobitumen yield levels and properties, along with empirical correlations, which serve to link together pyrolysis temperature, time, and/or selected properties (molecular weight, H/C, density, refractive index, and heat capacity). No information can be found on the last three properties for thermobitumens, derived from either Kukersite oil shale or other oil shale. The paper contributes to the topic by presenting information under conditions in which volatile pyrolytic products (oil and water) were removed from a pyrolysis system by an inert gas flow. So far, the formation of thermobitumen in Kukersite oil shale pyrolysis has been studied in either closed or open systems with no inert gas flow. To further generalise the results, the article also presents some comparisons with Green River formation oil shale thermobitumens, which were produced under similar conditions.*

Keywords: *thermobitumen, molecular weight, density, refractive index, hydrogen-carbon ratio, heat capacity.*

* Corresponding author: e-mail *vahur.keemteh@outlook.com*

1. Introduction

Oil shale, a solid fossil fuel, is a potentially important source of chemicals and oil due to the large amount of oil shale resources available. The world's oil shale resources are estimated to be equivalent to more than 2.9 trillion barrels of oil (one barrel = 0.159 m^3), and these resources are distributed widely across the world [1]. To be able to produce the oil, the kerogen, or macro molecular organic component, in oil shale must be thermally decomposed in an inert environment [2]. In this process, depending upon the type of oil shale, the formation of thermobitumen, which can also be referred to as pyrolytic bitumen or a 'metaplast' in coal chemistry, is often considered as an important intermediate step of pyrolysis [2–5]. Consequently, the formation of thermobitumen has been included in pyrolytic schemes (multi-step pyrolytic schemes which show yields of major intermediate and final macro-products). Generally the decomposition step in converting kerogen to thermobitumen precedes the major formation of volatiles and char, in either sequential or simultaneous reaction schemes [2, 5, 6]. Moreover, the formation of the intermediate product thermobitumen is considered more significant for oil shales with high oil yields (as it contains the kerogen that softens during the pyrolysis process), such as Kukersite oil shale from Estonia or Green River formation oil shale from the USA [7–11]. For example, in relation to the industrial-scale retorting of Kukersite oil shale, the thermobitumen formation has historically caused operational problems due to its sticky character in slow-pyrolysis fixed-bed gasifier type retorts. The formation of thermobitumen is also related to the phenomenon of thermal swelling [7]. Therefore the yields and properties of thermobitumen from Kukersite oil shale (such as the Estonian deposit or the Gdov deposit) have been of interest for the best part of the past century [2, 10, 12–27].

A review of the literature shows that thermobitumen formation in the pyrolysis of Kukersite oil shale has been studied in either open systems (with the removal of volatiles that are driven by volatile formation itself, such as with a Fischer retort or similar systems [12–16], and no inert gas flowing through the material has been used), or closed systems (with no removal of volatiles such as, for instance, autoclaves [17, 18]). While the practical purpose of the first approach is related to retort-based technological research, the second is more suitable for technological research on thermal dissolution [2]. These studies have been carried out over a wide range: utilising temperatures from 275 °C [12] to 420 °C [13], and residence times from 0.08 hours (at 386 °C) [14] to 456 hours (at 275 °C) [12]. The yields and properties of the formed thermobitumen depend upon both the process conditions and the characteristics of kerogen, and also upon how thermobitumen has been operationally defined.

In general, thermobitumen is defined as an intermediate reaction product of kerogen pyrolytic decomposition that is non-volatile in its process condition and is soluble in organic solvents [10, 11]. Very often it is the more specific

definition that serves specifically to denote the solvent as being benzene, although extraction with other solvents such as methanol, acetone, and petroleum ether has also been used [12]. This definition of thermobitumen has historically been more or less followed by scientists but, in practice however, a specific thermobitumen is operationally definable, largely depending upon the purpose of the study. However, it could be emphasised here that the thermobitumen as an extraction product that had been obtained from the autoclave (a closed system) was often operationally defined as being a mixture of oil and thermobitumen, even down to including pyrolysis water.

By contrast, oil is defined as the organic pyrolytic decomposition product that is volatile in its process conditions and is condensable at room temperature. On that basis oil is volatile, and it can undergo secondary reactions at longer residence times if not removed rapidly. Therefore, an important factor in defining thermobitumen is whether those components that are vaporisable during pyrolysis (more specifically oil) are removed from the reactor and how fast this process occurs. In principle a complete oil removal with the shortest residence time can be obtained from the system by allowing inert gas to flow through the material that is undergoing pyrolysis. Therefore any thermobitumen that is obtained in this way more closely represents the definition 'based', or 'actual', thermobitumen. This approach has, for example, been used by Miknis et al. [11] in thermobitumen studies involving USA oil shales (western oil shales of the Green River formation such as the Colorado Anvil Points, Wyoming Tipton, and the Colorado Exxon-Colony, and Eastern oil shales such as those of Kentucky New Albany). Oil shale from the Green River deposit has a high oil yield and kerogen that softens during pyrolysis, as does Kukersite oil shale. On the other hand, New Albany oil shale (similarly to another Estonian oil shale – Dictyonema) has a low oil yield and kerogen that does not soften during pyrolysis, unlike Green River oil shale or Kukersite oil shale [7, 27, 28].

Because Kukersite oil shale studies in relation to thermobitumen have only been conducted in closed systems or in open systems without an inert gas stream (such as with a Fischer retort or similar systems), this paper contributes to the topic by providing information in conditions under which volatiles were removed from the pyrolysis system by means of inert gas flow (with this flowing through the material that is undergoing pyrolysis). As the review showed that there was little information on the physical properties of thermobitumen in the available literature, our research team's interest in this topic was based on the physical properties that were seen as being important in chemical engineering calculations (especially those that are used to calculate other properties using thermodynamic property prediction approaches which are based on bulk properties). So far the most often measured characteristic parameters for Kukersite thermobitumens have been elemental composition in the first place (and/or the resultant H/C ratio), followed by molecular weight [12–21]. In addition, there was also found some (not systematic) information regarding

solvent fractionation [12, 22], spectroscopic data (infrared spectra [23, 24], nuclear magnetic resonance (NMR) spectra [24, 25], X-ray photoelectron spectra [24]), OH group content [12], and some information on the individual components [24–26]. The purpose of this study is to supplement the available information on average molecular weights and elemental composition, and to provide information on density, refractive index, and heat capacity that was not yet available. The work maps out the variations in these thermobitumen properties obtained at different pyrolysis temperatures and with different residence times, and provides easy-to-use empirical equations when it comes to determining these properties.

2. Experimental

2.1. Oil shale sample

Thermobitumens were produced from the freshly ground Estonian Kukersite oil shale sample with a particle size between 0.315 and 0.8 mm (the choice was based on experimental concerns such as pressure drop, uniform flow over the cross-sectional area, etc.) and an average organic content of 23.2%, with a variation of 2% in the test samples. For confirmation, some subsequent comparative experiments were performed on another oil shale sample with the same particle size range, and these results were normalized to the original oil shale sample. The ultimate analysis for the oil shale with an organic content of 23.2% delivered the following results on a dry basis (wt%): 51.94% ash, 21.36% carbon, and 1.59% hydrogen. As the carbonaceous CO_2 content was 24.88 wt%, the estimated carbon and hydrogen composition of the organic matter was 75.42 wt% C and 9.36 wt% H (with an atomic H/C ratio of 1.49). Additional information about the structure and composition of Kukersite oil shale and the properties of the retort products can be found via the following references [27, 29–33]. It is important to note again that Kukersite oil shale has a high oil yield and contains kerogen, which softens thermally [6]. Exemplary yields of pyrolysis products from Fischer Assay retorting under standard conditions (at a temperature of 520 °C) for Kukersite kerogen on a dry basis are as follows: 59.7 wt% oil, 6.1 wt% pyrogenous water, 12.7 wt% gas, and 21.5 wt% semicoke (char) [21]. For indication purposes, the Fischer Assay oil properties are reported with the following sample figures: a relative density of about 0.964, with an H/C of about 1.43, and a molecular weight of about 230 g/mol [27, 30, 31].

2.2. Thermobitumen production

Thermobitumens were produced from Kukersite oil shale by means of isothermal pyrolysis at temperatures of 340 °C, 380 °C, and 420 °C. A U-shaped reactor which had been formed from a stainless steel pipe (9.4 × 2.3 mm)

and Swagelok fittings with a total volume of about 30 ml were inserted in a convection oven that was preheated to the required temperature (as listed above). In principle, the set-up has the same design as that used by Miknis et al. [11]. Therefore the drawing for this set-up is not specifically shown. The pyrolysis temperatures were measured using a K-type thermocouple (accuracy ±0.5 °C), which was inserted from the nitrogen inlet zone to a depth of about 10 cm into the oil shale layer in the U-shaped reactor. Pyrolysis times were between 15 minutes to 16 hours, counted from the moment at which the sample temperature was no more than 5 °C lower than the oven temperature. Average heating-up rates were about 20–25 °C/min as it took an average of 13, 16 or 18 minutes to heat up the reactor that had been inserted into the preheated oven, from room temperature to temperatures of 340 °C, 380 °C and 420 °C, respectively. The pyrolysis process was stopped by removing the reactor from the oven and quickly cooling it in a water bath. Nitrogen (with a purity level of 99.995%), which was pre-heated in the same convective oven until it reached the pyrolysis temperature, was allowed to flow through the packed bed of oil shale particles at a flow rate of about 100 ml/min and served to carry away (out of the reactor) the pyrolysis gases, water and oil vapours that had formed.

2.3. Collecting oil and pyrolysis water

The pyrolysis water and oil vapours from the reactor were condensed using water cooling and were collected in a container that had been placed in ice water. The container was weighed before and after each experiment to be able to ascertain water and oil mass as produced during pyrolysis. To prepare the oil for characterisation (involving measurements of its molecular weight and elemental composition), the oil was separated from the water by means of centrifugal force.

2.4. Solvent extraction of thermobitumen

Thermobitumens were extracted from solid pyrolysis residues that had been removed from the reactor after pyrolysis, by means of a Soxhlet extraction with solvent tetrahydrofuran (THF, boiling point 66 °C). In the current work the stabilised tetrahydrofuran (99% pure, Lachner, Czech Republic) was used. The tetrahydrofuran was chosen as the solvent because preliminary experiments showed that, when compared to benzene and dichloromethane, tetrahydrofuran provided the highest thermobitumen yield. The extraction process was carried out until the solvent that passed through the sample had become colourless. This took between 36 and 60 hours. After extraction the solvent was removed from the thermobitumen solution by means of a vacuum rotary evaporator at a pressure of about 4 mmHg (in a water bath at 95 °C). The collected thermobitumen was solid at room temperature. The completeness of

solvent removal was evaluated by means of thermogravimetric measurements with a heating rate of 10 °C/min up to 300 °C under an inert gas environment.

2.5. Determining the H/C ratio

The elemental composition (wt% carbon and wt% hydrogen) of the thermobitumen and oil samples was determined using an Exeter Analytical model CE440 elemental analyser. From this information the atomic H/C ratios were calculated. The oxygen content in wt%, more precisely oxygen along with smaller amounts of nitrogen and sulphur, was determined by subtracting the carbon and hydrogen contents from 100 wt%.

2.6. Determining the number average molecular weight

The number average molecular weights were determined using two different vapour pressure osmometers: first an Osmomat 070 (Gonotec GmbH, Germany), and later a Knauer K-7000 (Wissenschaftliche Gerätebau Dr Ing Herbert KNAUER GmbH, Germany). With both instruments pyridine was used as a solvent (99% pure, Sigma-Aldrich). When using the Osmomat 070 and the Knauer K-7000, measurements were carried out at temperatures of 85 °C and 75 °C, respectively. The standard deviation of number average molecular weights was less than 5%. However, for some thermobitumen samples, the standard deviation of the number average molecular weights was found to be higher, based on data measured by different devices over a one-year period. A more detailed description of the measurement and analysis methods that were used to ascertain the number average molecular weight, along with the calibration principles for the instrument, are given in an earlier article from this laboratory by Järvik and Oja [31].

2.7. Measurement of the density and refractive index of thermobitumen

The density and refractive index of the thermobitumen were measured using respectively a DMA 5000M density meter and an Abbemat HT refractometer (both Anton Paar GmbH, Austria). Because the thermobitumen samples were solid at room temperature, in order to measure their density and refractive index those samples were first dissolved in tetralin (anhydrous 99% pure, Sigma-Aldrich). For the purpose of ensuring uniform mixing, the sample solvent mixture with its known concentration levels in a closed vial was kept at a temperature of 60 °C for several hours and was then placed in an ultrasonic bath for 20 minutes to aid the dissolution process. The mass fraction of thermobitumen used fell within the range of 20–30%. Its density values (or at least provisional density values) were then calculated from the measured pre-prepared mixture density values using a defined mixing rule as shown below (Eq. (1)):

$$\rho_{th} = [\frac{1}{\rho_m X_{th}} - \frac{X_{te}}{\rho_{te} X_{th}}]^{-1}, \quad (1)$$

where ρ is density, X is the mass fraction and the subscripts *th*, *te*, and *m* stand respectively for thermobitumen, tetraline, and the mixture. The level of application for this mixing rule was checked by first measuring the density of industrial heavy oil technical fraction (from Kukersite shale oil) and then comparing it to the density value that was calculated using the mixing rule for the heavy oil that had been dissolved in tetralin (with a mass fraction of 20–30%). The application of the mixing rule provided an error margin in the heavy oil density readings less than 1%. The provisional refractive index values for the thermobitumen were calculated from the mixture information using a defined mixing rule as shown in Equation (2):

$$RI_m = Y_{th} RI_{th} + Y_{te} RI_{te}, \quad (2)$$

where *RI* is the refractive index and *Y* is the volume fraction, and subscripts are as previously defined.

2.8. Measurement of the heat capacity of thermobitumen

The specific heat capacity of thermobitumen (c_p) was measured using a Netzsch 204 HP Phoenix differential scanning calorimeter (DSC) with a nitrogen flow of 40 ml/min. For the purpose of carrying out these measurements, a sample of approximately 20 mg of thermobitumen was loaded into a pre-weighed Al capsule, and the capsule was hermetically sealed. Before carrying out the measurement process the capsule and the sample were heated to approximately 70 °C in order to melt the thermobitumen and obtain a uniform contact between the sample and the capsule. Then the sample was kept at 30 °C for 10 minutes, whereafter the specific heat capacity measurement was carried out by ramping up the temperature at 20 °C/min to as high as 200 °C. The specific heat capacity of the sample (*s*) was calculated from the previously measured sapphire standard (*st*) signal *S*, mW/mg, as follows:

$$c_p(s) = c_p(st) \frac{S(s)}{S(st)}. \quad (3)$$

The validity of the c_p measurement was confirmed by measuring the specific heat capacity of anthracene. The average deviation in the temperature range was between 40–180 °C which, when compared to the information given in the work by Goursot et al. [34], was below 5%.

3. Results and discussion

3.1. Yield of kerogen decomposition products: thermobitumen and sum of oil and water

Yields of thermobitumen and yields of volatile oil shale decomposition products – the sum of oil and water yields – which were obtained under the various pyrolysis temperature and time conditions that were included in the investigation, are summarised in Table 1 and Table 2, respectively. These yields are given on the basis of the dry organic content of the original oil shale (as the wt% of organic matter), and were calculated using the average organic content of 23.2 wt%. The changes in the isothermal yield of thermobitumen and in the total isothermal yield of thermobitumen, oil, and pyrolysis water as a function time of pyrolysis are illustrated graphically at a temperature of 340 °C in Figure 1, at 380 °C in Figure 2 and at 420 °C in Figure 3. Information from selected literature on Kukersite oil shale, for both open and closed systems, is shown for comparison in these figures. The figures also show that, in general, the thermobitumen yields that were measured in the current work were lower than those given in earlier studies on open systems for Kuklersite oil shale. The lower thermobitumen yields can be explained by the difference in the experimental procedures being used for thermobitumen preparation. In this study, a flow of inert gas was sent through the reactor to ensure the immediate removal of vaporising compounds, and care was taken to evaporate the solvent as fully as possible from the thermobitumen-solvent mixture in the vacuum rotary evaporator.

The yield profiles follow the trends that have been reported for different oil shales [11]. The yield profile for thermobitumen, the reactive intermediate product, is best illustrated at the temperature of 380 °C in Figure 2. This is the typical concentration profile for consecutive in-series irreversible reactions, during which there occurs the transformation of the parent material into an intermediate, and then the intermediate to the product. The figure shows the shape of a positive skew (skewed to the right) which, according to the most simplified reaction scheme, can be considered as having been caused by competition between the rate of formation of thermobitumen and the rate of conversion of thermobitumen into final macro-products, mostly into oil. For the full temperature-time range, the exact shape depends upon the relative strength of each competing reaction which underlies the transformation. The experiments that were carried out at a temperature of 380 °C show that the highest yield of thermobitumen was seen at a heating time of two hours. The maximum yield of thermobitumen, around 50% of organic matter at the temperature of 380 °C, is also the maximum thermobitumen yield to have been observed in this work. At 340 °C (Fig. 1), due to the relatively low temperature, after a period of around 14 hours the maximum yield of thermobitumen is reached at about 25% of organic matter (at the conclusion of the tests, as

Table 1. The yields and properties of thermobitumen from Kukersite oil shale isothermal pyrolysis at different temperatures

T, °C	Time, h	Yield,* %OM	MW, g/mol	Atomic H/C	C, wt%	H, wt%	O,** wt%	$d_{20\,°C}$, kg/m^3	$RI_{20\,°C}$	$c_{p,20\,°C}$, J/(kg·K)
340	2	8	1010	1.43	81.31	9.72	8.98	1087	1.5845	1881
	5	16	1173	1.39	79.81	9.23	10.97	1087	1.5827	1906
	8	19	1384	1.34	83.49	9.34	7.17			1808
	12	26	1320	1.3	82.98	8.97	8.05	1126	1.6297	1740
	16	25	1254					1127	1.6273	
380	0.5	22	1075	1.39	80.17	9.31	10.53	1080	1.5834	1788
	1	31	1181	1.38	82.17	9.42	8.41	1073	1.5938	1809
	2	47	1415	1.28	80.9	8.65	10.45	1125	1.6194	1693
	4	31	1316	1.2	80.91	8.08	11.02	1166	1.6583	1623
	6	22	1061	1.14	80.82	7.7	11.48	1189	1.6736	
420	0.25	33	1208	1.22	80.22	8.13	11.65	1165	1.6475	1575
	0.5	30	1104	1.02	83.19	7.03	9.79	1184	1.6724	1532
	0.75	22	857	1.04	81.75	7.05	11.21	1191	1.7004	
	1	7	717	1.07	78.75	7.01	14.26			1580

* as percent of the total organic content of oil shale, dry basis
** more precisely oxygen along with smaller amounts of nitrogen and sulphur

MW – number average molecular weight, H/C – atomic hydrogen carbon ratio, $d_{20\,°C}$ – density at 20 °C, $RI_{20\,°C}$ – refractive index at 20 °C, $c_{p,20\,°C}$ – heat capacity at 20 °C

Table 2. Total yields of oil and pyrolysis water from Kukersite oil shale isothermal pyrolysis at different temperatures, and number average molecular weight, elemental composition and H/C ratio of oil

T, °C	Time, h	Oil + water Yield, %OM***	Oil				
			MW, g/mol	C, wt%	H, wt%	O,** wt%	H/C
340	2	8	188	79.46	10.5	10.03	1.59
	5	15	196	79.86	10.34	9.8	1.55
	8	21	190	79.69	10.32	9.99	1.55
	12	25	186	79.79	10.3	9.92	1.55
	16	40					
380	0.5	14	178	79.91	10.59	9.51	1.59
	1	19	180	80.32	10.91	8.77	1.63
	2	28	180	80.62	10.7	8.69	1.59
	4	44	200	80.94	10.32	8.75	1.53
	6	56	199	81.63	10.4	7.98	1.53
420	0.25	37	198	81.5	10.32	8.18	1.52
	0.5	56*	182	81.23	10.7	8.08	1.58
	0.75	45*	172	80.99	10.66	8.37	1.58
	1	59	201	81.34	10.4	8.28	1.52

* the total yield of oil and water can only increase over time, therefore, the lower yield at 0.75 h compared to that at 0.5 h is due to the experimental error
** more precisely oxygen along with smaller amounts of nitrogen and sulphur
***as percent of the total organic content of oil shale, dry basis

the last points were measured at 12 and 16 hours). In experiments that were conducted at a temperature of 420 °C (Fig. 3), the processes described tend to occur in the shortest times. The maximum thermobitumen yield of about 35% of organic matter at 420 °C is reached at resident times corresponding to the start of the tests (the first point was measured at 15 minutes).

During the process of isothermal pyrolysis, the overall yield profile (the thermo-bitumen, oil, and water profile) increases with residence time, followed by stabilisation or a slight decrease in their yield before stabilization. An explanation of this yield trend can be found in the reference material by Miknis et al. [11]. In short, depending on the type of oil shale kerogen used, competing pyrolysis reactions (including the pathway through thermobitumen formation) resulted in different yield ratios for the final macroproducts (oil, gas, pyrolysis water, and char). The pyrolytic reactions of kerogens with high oil yields promote oil (the highest yielding product) formation, and low oil

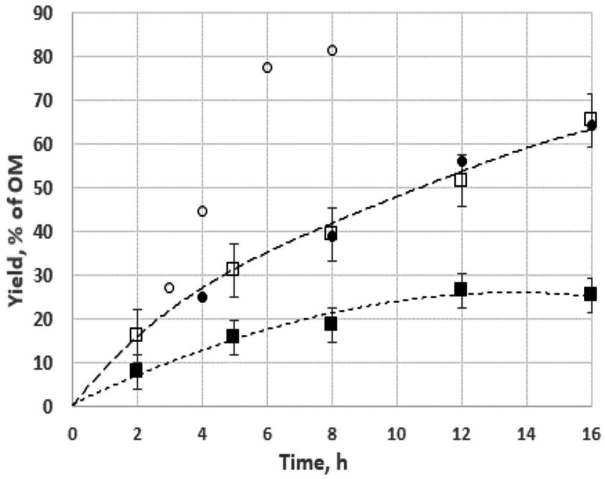

Fig. 1. The yield of thermobitumen (■) and the total yield of thermobitumen, oil, and water (□) produced during the isothermal pyrolysis of Kukersite oil shale as a function of pyrolysis time at a temperature of 340 °C. Literature-based information for Kukersite oil shale at 340 °C (○ open system [17]; ● closed system [12]) is shown for comparison.

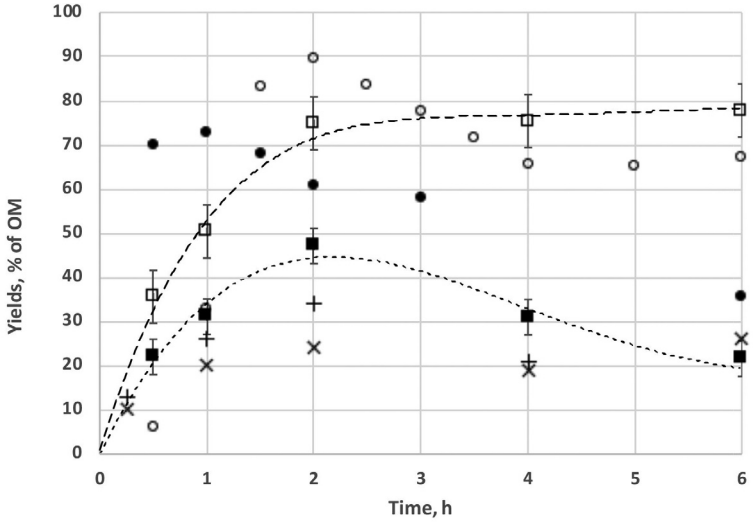

Fig. 2. The yield of thermobitumen (■) and the total yield of thermobitumen, oil, and water (□) produced during the isothermal pyrolysis of Kukersite oil shale as a function of pyrolysis time at a temperature of 380 °C. Literature-based information for Kukersite oil shale at 380 °C (○ open system [17]; ● closed system [14]), and for Green River oil shale (+ for 375 °C [11]; × for 394 °C [12]), is shown for comparison.

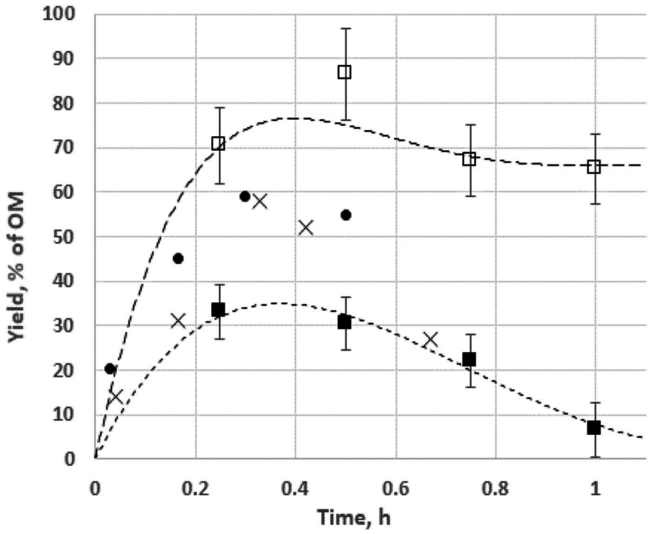

Fig. 3. The yield of thermobitumen (■) and the total yield of thermobitumen, oil, and water (□) produced during the isothermal pyrolysis of Kukersite oil shale as a function of pyrolysis time at a temperature of 420 °C. Literature-based information for Kukersite oil shale at 420 °C (● closed system [10, 15]), and for Green River oil shale at 425 °C (+) [11], is shown for comparison.

yield kerogens give more char and gas. In the case of Kukersite oil shale, it has been shown that the maximum oil yield is obtained at the point of complete decomposition of thermobitumen, which is about at 450 °C under slow heating rate conditions [16]. It can be seen from Table 2 that, at temperatures of 380 °C and 420 °C, the total yield of oil and water reached was between 56–59% of organic matter, which is close to the oil yield obtained in retorting Kukersite oil shale in a Fischer retort (which produced about 60% of organic matter [15, 30]). The proportion of pyrolysis water formed during decomposition of kerogen in the temperature range used in this work could be about 2–5 wt% of the organic content of dry oil shale [12, 15].

Figures 2 and 3 also compare thermobitumen yield information for Kukersite oil shale against that of Green River oil shale [11]. Experiments on both oil shales were carried out under conditions in which volatile pyrolytic products (oil and water) were removed from a pyrolysis system by means of an inert gas flow (one which was flowing through the material that was undergoing pyrolysis). Figures 2 and 3 indicate that thermobitumen yield curves were of similar shape. However, in Figure 2, at a temperature of about 380 °C, the yield for Green River oil shale was lower than that of Kukersite oil shale (the maximum yield was lower by about 10–15 units, being expressed as a percentage of organic matter). In Figure 3, at a temperature of about 420 °C, the yield for Green River oil shale was higher than that of Kukersite oil shale

(the maximum yield was higher by about 20–25 units, being expressed as a percentage of organic matter). This indicated different rates of formation and/or conversion of thermobitumen during the pyrolysis of these types of oil shale.

3.2. Molecular weights and atomic H/C ratios of oil accompanying thermobitumen formation

Miknis et al. [11] have shown that, for a given oil shale, molecular weights and H/C ratios for the oils released during the process of isothermal pyrolysis are essentially constant over the region of thermobitumen existence. This applies to oils associated with the formation and/or conversion of thermobitumen throughout the temperature-time history of the isothermal pyrolysis studied. The results of the current work, as presented in Table 2, show that these properties of pyrolysis oils from Kukersite oil shale also behave similarly, with the average molecular weight of oils being 188 g/mol (within about 170–200 g/mol), and the average H/C molar ratio being 1.56 (within about 1.52 and 1.63). These molecular weight values are somewhat lower and the H/C ratios are somewhat higher than those usually obtained from Kukersite oil shale pyrolysis in a Fischer retort [27, 30]. This is likely due to the lower pyrolysis temperatures obtained in the current study. When compared to the Green River oil shale oils, with an average molecular weight of 358 g/mol and an average H/C ratio of 1.71) as established by Miknis et al. [11], the respective average values of Kukersite oils in the current study were lower. The same trend could also be observed when comparing the corresponding Fischer assay oils [27, 30].

3.3. The molecular weight of thermobitumen

The number average molecular weight values for thermobitumens from Kukersite oil shale as measured in this work are tabulated in Table 1, and their pyrolysis temperature and time dependence are illustrated in Figures 4–6. Figures 4–6 suggest that the overall pattern of molecular weight change in thermobitumen under isothermal conditions over time forms a continual ‘increasing to decreasing’ dependence: the molecular weight increases, exceeds the maximum and then decreases. Therefore, at the temperature-time point at which thermobitumen is completely decomposed or vanished, its average molecular weight values should approach those of volatile oil. The Kukersite oil shale’s oil molecular weight distribution curves, which come from various pyrolysis regimes, can be found in earlier articles [31, 35, 36].

Figures 4–5 show that the molecular weight values from a previous study by Kask [12] are for the most part twice as low as those measured in the current work. However, in a few cases some similarities can be seen in the molecular weight of some of the samples. Therefore, when considering the complexity of removing solvents completely, the lower molecular weight values measured

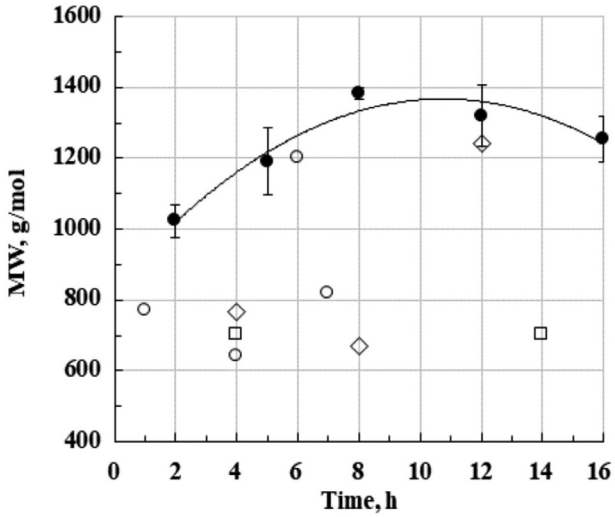

Fig. 4. Number average molecular weights (MW) for thermobitumens taken from the isothermal pyrolysis of Kukersite oil shale at 340 °C (●, this study) in comparison with earlier information (small reactor 360 ºC as ○; small reactor 340 ºC as ◊; large reactor 360 ºC as □) [12].

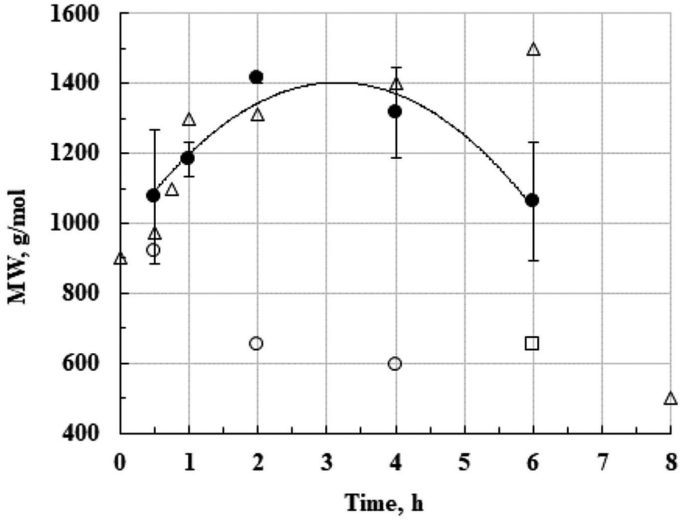

Fig. 5. Number average molecular weights (MW) for thermobitumens taken from the isothermal pyrolysis of Kukersite oil shale at 380 °C (●, this study) in comparison with earlier information at the same temperature (small reactor as ○; large reactor as □) [12], and information on thermobitumen taken from Green River oil shale and obtained at 375 °C (Δ) [11].

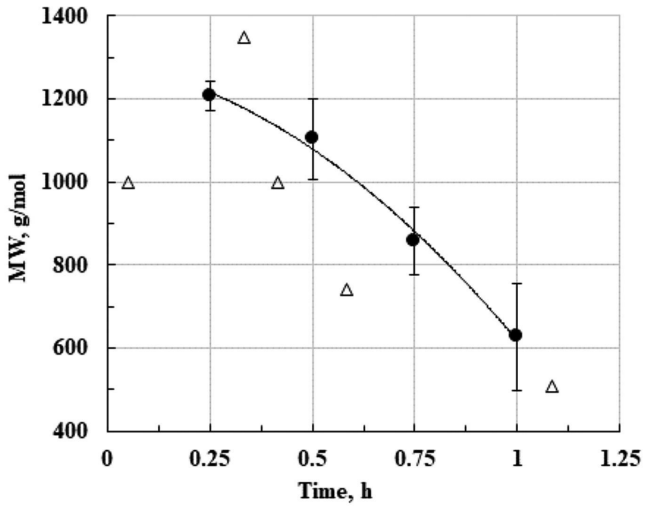

Fig. 6. Number average molecular weights (MW) for thermobitumens obtained from the pyrolysis of Kukersite oil shale at 420 °C (●, this study) in comparison with information on thermobitumen taken from Green River oil shale, obtained at 425 °C (Δ) [11].

by Kask [12], which are given here for reference purposes, could have been caused by a portion of the solvent remaining in thermobitumen. For example, if a sample of thermobitumen has a molecular weight of 1300 g/mol, then in order to have a molecular weight of 700 g/mol it must contain about 50 mol% or 5.5% by weight of benzene.

When compared to the Green River oil shale-based study by Miknis et al. [11], Figures 5–6 indicate analogous relationships between molecular weight and pyrolysis times during the isothermal processes studied. In Figure 5 it can be seen that most of the values that were obtained at different pyrolysis times match closely (with the exception of the six-hour and 380 °C point). In Figure 6 the difference in molecular weights is somewhat large (as a five degree temperature difference may be more significant at higher temperatures), but similar decreasing changes can be seen in the molecular weight of thermobitumen as a function of pyrolysis time.

3.4. The H/C ratio of thermobitumen

H/C ratio is a parameter that can be with today's capabilities determined relatively easily and quickly and with a high degree of accuracy for a collected thermobitumen sample. The carbon and hydrogen contents of Kukersite thermobitumens prepared for this work and the atomic H/C ratio calculated are given in Table 1. At temperatures of 340 °C and 380 °C the H/C ratio shows a clearly decreasing trend over time, as a result of the simultaneous

condensation and decomposition reactions and the vaporisation of the formed oil. A slight increase in the H/C ratio over a period between 30 minutes and one hour during the 420 °C experiment, as seen in Table 1, could also be an actual trend. As expressed by Aarna and Rikken [16], at every temperature the decomposition products of kerogen tend towards their most stable form, which causes the H/C ratio to decrease. Kask [12] and Miknis et al. [37] were able to show this decreasing trend respectively in pyrolysis of Kukersite oil shale and of both Green River (Colorado) and New Albany oil shales. Miknis et al. [37] also found that the total mass of aromatic carbon in the oil and solid products that were formed during pyrolysis serves to reach its maximum level at about the same time as the thermobitumen yield reaches its maximum value and then remains constant after that.

H/C ratio is also a characteristic parameter of a material that is used in different correlations for calculating other properties [38]. Therefore, from the results of the ongoing work, an easy-to-use empirical Equation (4) was derived to calculate the Kukersite oil shale thermal bitumen H/C ratio as a function of pyrolysis temperature (T) and time (t) as follows (with an absolute average deviation of 0.05 units):

$$H/C = 3.354 - 5.336 \times 10^{-3} \times T[\text{°C}] - 2.404 \times 10^{-2} \times t[h]. \quad (4)$$

A comparison with relevant measured H/C values is given in Table 3 as a relative percentage difference. Equation (4) was also used to calculate the H/C ratios for information that was taken from reference sources [11, 37], along with thermobitumens from the pyrolysis of Green River (Colorado) and New Albany oil shales. The best results were obtained for New Albany thermobitumen at temperatures of 375 °C and 400 °C, with an absolute average deviation of 0.12 units. In fact, the equation that was developed based on the information from this study on Kukersite oil shale provided more accurate results than the equation that was developed directly from pyrolysis information for New Albany thermobitumen reported by Miknis et al. [37]. For thermobitumens from Green River oil shale Equation (4) provided scattered results and H/C values that were about 0.25 units less than the actual values. Therefore the following exemplary equation was derived from the reference information [11] for Green River oil shale:

$$H/C = 2.681 - 3.122 \times 10^{-3} \times T[\text{°C}] - 1.027 \times 10^{-3} \times t[h]. \quad (5)$$

3.5. The density, refractive index and heat capacity of thermobitumen

The density, refractive index, and heat capacity of thermobitumen, all at 20 °C, are given in Table 1. The thermobitumen heat capacity at 20 °C remains in the range of 1532–1906 J/(kg·K), being respectively about 350–750 J/(kg·K) larger than the heat capacity of Kukersite oil shale kerogen. The Kukersite

kerogen (with a 91% organic content) has a heat capacity of 1150 J/(kg·K) [39]. Thermobitumen's density values at 20 °C fall between 1073 and 1191 kg/m^3. The density of Kukersite oil shale kerogen is at 1100 kg/m^3 [39]. Figure 7 shows density and heat capacity as a function of the H/C ratio of thermobitumen. The figure reveals that as the H/C ratio increases, i.e. as the aromatic levels decrease, the density decreases and the heat capacity increases. Figure 7 also shows that there is a rough linear dependence between density (and therefore refractive index) and heat capacity on the H/C ratio, and therefore the density ($d_{20°C}$), refractive index ($RI_{20°C}$), and heat capacity ($C_{p,20°C}$) can be approximately calculated. For calculations taken from the H/C ratio of thermobitumen, the following Equations (6)–(8) were derived:

$$d_{20°C}[kg/m^3] = -300.9 \times (H/C) + 1510.5, \tag{6}$$

$$RI_{20°C} = 2.0075 - 0.29901 \times (H/C), \tag{7}$$

$$c_{p,20°C}[J/kgK] = 610.9 + 871.9 \times (H/C). \tag{8}$$

The evaluation of the performance of these equations against the corresponding measured values is given in Table 3 as a relative percentage difference. The average absolute deviations between the predicted and actual values of refractive index and heat capacity are 0.01 and 41 J/(kg·K), respectively. When comparing the predictions for density from Equation (6) with the results measured in the current work, the average absolute deviation

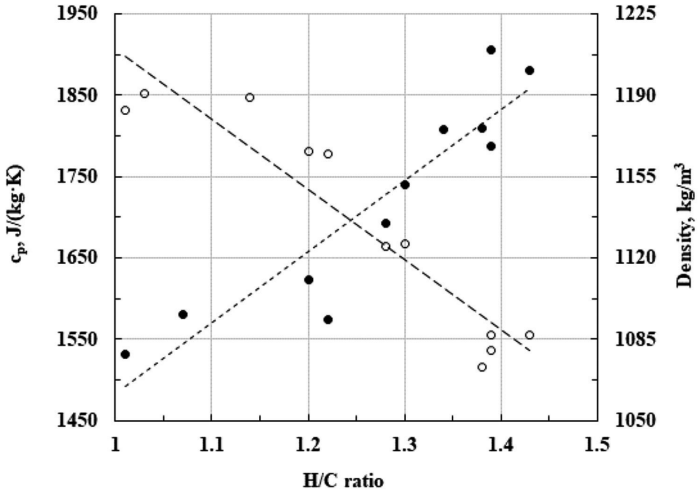

Fig. 7. Densities at 20 °C (○) and heat capacities at 20 °C (●) for thermobitumen taken from Kukersite oil shale isothermal pyrolysis as a function of the H/C ratio (information from this study).

Table 3. Relative percentage difference between the measured properties and the results calculated with easy-to-use empirical equations derived from them*

		Relative percentage difference				
T, °C	Time, h	H/C, Eq. (4), %	$d_{20\,°C}$, Eq. (6), %	$RI_{20\,°C}$, Eq. (7), %	$c_{p,20\,°C}$, Eq. (8), %	$c_{p,20\,°C}$, Eq. (10), %
340	2	–4.3	0.6	0.3	1.2	0.2
	5	–2.1	–0.5	–0.6	4.4	4.1
	8	–0.6			1.6	2.5
	12	3.7	0.6	0.7	–0.3	0.4
	16					
380	0.5	5.4	–1.1	–0.5	–1.9	–2.7
	1	5.6	–2.1	–0.1	–0.3	–0.5
	2	0.1	0.0	–0.3	–2.0	–0.8
	4	–2.5	1.4	0.6	–2.1	–1.2
	6	–3.7	1.8	0.4		
420	0.25	9.3	1.9	0.3	–6.3	–6.0
	0.5	–7.9	–1,7	–1.8	2.1	2.3
	0.75	–5.3	–0.6	0.2		
	1	–1.8			2.3	0.3

* The properties are given in the Table by temperature and time.

was about 13 kg/m^3 by using the measured H/C ratio, and 26 kg/m^3 when using the H/C ratio calculated from Equation (4). The relationship between density and H/C ratio for Kukersite thermobitumen can also be approximately calculated from a linear equation that is based on information taken from the Crude Oil Assay database [40] as:

$$d_{15°C}[kg/m^3] = 1636 - 428 \times \left(\frac{H}{C}\right). \quad (9)$$

The average absolute deviation between the measured and calculated densities was 38 kg/m^3 when using Equation (9). For heat capacity, a slightly better fit with experimental information (with an absolute average deviation of about 34 J/kg·K) can be achieved by a two-parameter equation in which the heat capacity of thermobitumen is predicted as a function of H/C ratio and MW (kg/kmol):

$$C_{p20°C}[J/kgK] = 663 + 910.2 \times (H/C) - 0.086 \times MW. \quad (10)$$

A comparison with relevant measured values is given in Table 3 as a relative percentage difference. Applying this equation means that molecular weight has been measured, which is a time-consuming measurement and is often carried out with quite high levels of uncertainty. However, analogous regression equations for calculating the refractive index ($RI_{20°C}$) or density ($d_{20°C}$) of Kukersite oil shale thermobitumen showed no useful level improvement in performance.

4. Conclusions

This paper has presented information and trends on yields and the selected physical-thermodynamic properties of thermobitumen, an intermediate product of pyrolytic decomposition, from Kukersite oil shale isothermal pyrolysis at three temperatures: 340 °C, 380 °C and 420 °C. Our literature review showed that although the yields and characteristics of thermobitumen extracted from Estonian Kukersite oil shale have been of interest for around a century, the topic still required further investigation. This study has contributed to this topic by investigating the process of thermobitumen formation under conditions in which volatile – and at room temperature condensable – pyrolytic products (oil and water) are removed from a pyrolysis system by means of an inert gas, which is flowing through the material undergoing pyrolysis. Care was also taken to remove the solvent, which was used to dissolve the thermobitumen from the pyrolysis residues, from the thermobitumen-solvent mixture as completely as possible. When compared to information that is available in the literature on earlier Kukersite oil shale tests, the yield of thermobitumen in this study was seen to be lower and the molecular weight higher.

By utilising the characteristic properties of thermobitumen, this work was able to ascertain measurements of the H/C ratio, average molecular weight, density at 20 °C, refractive index at 20 °C and heat capacity at 20 °C. The first two of these were the parameters that were commonly used to describe thermobitumen (with the H/C ratio being more commonly used as it is easily quantifiable), but no previous information was found for the latter three, whether Kukersite or any other oil shale. Therefore empirical correlations were derived to be able to calculate the last three parameters from the H/C ratio (with average absolute deviations of 13 kg/m^3, 0.01, and 34 J/kg·K, respectively). In addition, an empirical correlation was also presented in this paper to determine the H/C ratio from the temperature and time of pyrolysis.

Acknowledgements

Support for the study was provided by the National R&D program ‘‘Energy’’ under the Project AR10129 ‘‘Examination of the Thermodynamic Properties of Relevance to the Future of the Oil Shale Industry’’ (P.I. V. Oja). The authors also acknowledge earlier financial supports provided by the Estonian Ministry of Education and Research, under target financing SF0140022s10 (P.I. V. Oja), and under the Estonian Science Foundation Grants 9297, 7222 and 5632 (P.I. V. Oja). The authors are very grateful to Einart Lindaru, Ilme Rohtla, Dr. Rivo Rannaveski, Dr. Zachariah S. Baird, Dr. Natalja Savest and Dr. Jelena Hruljova for their helpful advice, and for helping with thermobitumen characterization measurements or editorial comments.

REFERENCES

1. Dyni, J. R. Geology and resources of some world oil-shale deposits. *Oil Shale*, 2003, **20**(3), 193–252.
2. Oja, V., Suuberg, E. M. Oil shale processing, chemistry and technology. In: *Encyclopedia of Sustainability Science and Technology* (Meyers, R. A., ed.). Springer, New York, 2012, 1−38.
3. Oja, V. Is it time to improve the status of oil shale science? *Oil Shale*, 2007, **24**(2), 97−99.
4. Smith, K. L., Smoot, L. D., Fletcher, T. H., Pugmire, R. J. *The Structure and Reaction Processes of Coal*. Plenum Press, New York, 1994.
5. Burnham, A. K. *Global Chemical Kinetics of Fossil Fuels: How to Model Maturation and Pyrolysis*. Springer, 2017.
6. Burnham, A. K., Braun, R. L., Coburn, T. T., Sandvik, E. I., Curry, D. J., Schmidt, B. J., Noble, R. A. An appropriate kinetic model for well-preserved algal kerogens. *Energy Fuels*, 1996, **10**(1), 49–59.
7. Savest, N., Hruljova, J., Oja, V. Characterization of thermally pretreated kukersite oil shale using the solvent-swelling technique. *Energy Fuels*, 2009, **23**(12), 5972–5977.
8. Oja, V., Yanchilin, A., Kan, T., Strezov, V. Thermo-swelling behavior of Kukersite oil shale: Commercial grade oil shale compared to its kerogen. *J. Therm. Anal. Cal.*, 2015, **119**, 1163–1169.
9. Oja, V., Elenurm, A., Rohtla, I., Tali, E., Tearo, E., Yanchilin, A. Comparison of oil shales from different deposits: oil shale pyrolysis and co-pyrolysis with ash. *Oil Shale*, 2007, **24**(2), 101–108.
10. Zaidentsal, A. L., Soone, J. H., Muoni, R. T. Yields and properties of thermal bitumen obtained from combustible shale. *Solid Fuel Chem.*, 2008, **42**, 74–79.
11. Miknis, F. P., Turner, T. F., Berdan, G. L., Conn, P. J. Formation of soluble products from thermal decomposition of Colorado and Kentucky oil shales. *Energy Fuels*, 1987,**1**(6), 477–483.

12. Kask, K. A. About bituminization of kerogen of oil shale-kukersite. Report I. *Transactions of Tallinn Polytechnic Institute*, Series A, 1955, No. 63, 51–64 (in Russian).
13. Gubergrits, M. Y. *Thermal Destruction of Shale-Kukersite*. Valgus, Tallinn, 1966 (in Russian).
14. Schulman, A. I. *Investigation of Bituminizing Process of Shale Organic Concentrate*. PhD Thesis. Leningrad, VNIINeftchim, 1968 (in Russian).
15. Lippmaa, E. Study of thermal decomposition of Estonian oil shale. *Transactions of Tallinn Polytechnic Institute*, Series A, 1958, No. 9, 39–45 (in Russian).
16. Aarna, A. Ya., Rikken, Yu. T. About the mechanism of low-temperature decomposition of kukersite oil shale. *Transactions of Tallinn Polytechnic Institute*, Series A, 1958, No. 97, 53–67 (in Russian).
17. Tiikma, L., Zaidentsal, A., Tensorer, M. Formation of thermobitumen from oil shale by low-temperature pyrolysis in an autoclave. *Oil Shale*, 2007, **24**(4), 535–546.
18. Karavayev, N. M., Wener, I. M. About thermobitum of Gdov oil shale. *Transactions of the Institute of Goryuchih Iskopayemyh, Academy of Sciences of USSR*. 1950, **2**, 285–295 (in Russian).
19. Luts, K. *Der Estländische Brennschiefer-Kukersit, seine Chemie, Technologie und Analyse*. Revaler Buchverlag G.M.B.H., Reval, 1934 (in German).
20. Aarna, A. Y. Dynamic of separation of volatile products at thermal destruction of oil shale. *Transactions of Tallinn Polytechnic Institute*, Series A, 1955, No. 63, 65–81 (in Russian).
21. Kask, K. A., Mihkelson, V. J. The chemical composition of thermobitumen of kukersite oil shale. *Transactions of Tallinn Polytechnic Institute*, Series A, 1958, No. 97. 68–84 (in Russian).
22. Broi-Karre, G., Proskuryakov, V. Investigation of low-temperature destruction of Gdov oil shale concentrate by infrared spectroscopy. *J. Appl. Chem.*, 1966, **39**(5), 1214–1216 (in Russian).
23. Aarna, A., Alev, M. Investigation of low-temperature destruction of kukersite shale by infrared spectroscopy. *Transactions of Tallinn Polytechnic Institute*, Series A, 1964, No. 210, 3–14 (in Russian).
24. Shi, J., Ma, Y., Li, S., Wu, J., Zhu, Y., Teng, J. Characteristics of Estonian oil shale kerogen and its pyrolysates with thermal bitumen as a pyrolytic intermediate. *Energy Fuels*, 2017, **31**(5), 4808–4816.
25. Lille, Ü., Pehk, T., Purre, T., Bitter, L. Examination of the structure of heavy shale oil by means of NMR-spectroscopy. *Proc. Acad. Sci. ESSR. Chem.*, 1973, **22**(1), 17–25 (in Russian with English summary).
26. Akalin, E., Kim, Y.-M., Alper, K., Oja, V., Tekin, K., Durukan, I., Siddiqui, M. Z., Karagöz, S. Co-hydrothermal liquefaction of lignocellulosic biomass with Kukersite oil shale. *Energy Fuels*, 2019, **33**(8), 7424–7435.
27. Urov, K., Sumberg, A. Characteristics of oil shales and shale-like rocks of known deposits and outcrops. *Oil Shale*, 1999, **16**(3 SPECIAL: Monograph), 1–64.
28. Kilk, K., Savest, N., Yanchilin, A., Kellogg, D. S., Oja, V. Solvent swelling

of Dictyonema oil shale: Low temperature heat-treatment caused changes in swelling extent. *J. Anal. Appl. Pyrol.*, 2010, **89**(2), 261–264.
29. Lille, Ü., Heinmaa, I., Pehk. T. Molecular model of Estonian kukersite kerogen evaluated by ^{13}C MAS NMR spectra. *Fuel*, 2003, **82**(7), 799–804.
30. Elenurm, A., Oja, V., Tali, E., Tearo, E., Yanchilin, A. Thermal processing of dictyonema argillite and kukersite oil shale: Transformation and distribution of sulfur compounds in pilot-scale Galoter process. *Oil Shale*, 2008, **25**(3), 328–334.
31. Järvik, O., Oja, V. Molecular weight distributions and average molecular weights of pyrolysis oils from oil shales: Literature data and measurements by size exclusion chromatography (SEC) and atmospheric solids analysis probe mass spectroscopy (ASAP MS) for oils from four different deposits. *Energy Fuels*, 2017, **31**(1), 328−339.
32. Aarna, A., Paluoja, V. Determination of hydroxyl groups in shale oil by the acetylation method. In: *Analytical Methods for Oil Shale and Oil Shale Products*. Tallinn, Estonia, 1961, 23–26 (in Russian).
33. Siitsman, C., Oja, V. Extension of the DSC method to measuring vapor pressures of narrow boiling range oil cuts. *Thermochim. Acta*, 2015, **622**, 31–37.
34. Goursot, P., Girdhar, H. L., Westrum Jr., E. F. Thermodynamics of polynuclear aromatic molecules. III. Heat capacities and enthalpies of fusion of anthracene. *J. Phys. Chem*., 1970, **74**(12), 2538–2541.
35. Oja, V. Examination of molecular weight distributions of primary pyrolysis oils from three different oil shales via direct pyrolysis Field Ionization Spectrometry. *Fuel*, 2015, **159**, 759−765.
36. Oja, V. Characterization of tars from Estonian Kukersite oil shale based on their volatility. *J. Anal. Appl. Pyrol.*, 2005, **74**(1–2), 55–60.
37. Miknis, F. P., Conn, P. J., Turner, T. F., Berdan, G. L. *Isothermal Decomposition of New Albany Shale From Kentucky*. Work Performed Under Cooperative Agreement DE-FC21-83FE60177, Laramie, Wyoming, 1985.
38. Riazi, M. R. *Characterization and Properties of Petroleum Fractions*. ASTM International, 2005.
39. Savest, N., Oja, V. Heat capacity of kukersite shale oil: Literature overview. *Oil Shale*, 2013, **30**(2), 184–192.
40. Speight, J. G. *Crude Oil Assay Database – Knovel*. Online version 2014. http://app.knovel.com/hotlink/toc/id:kpCOAD0005/crude-oil-assay-database/crude-oil-assay-database (accessed Feb 25, 2016).

Publication IV

S. Mozaffari, Z. S. Baird, and O. Järvik, "Sulfur in kukersite shale oil: its distribution in shale oil fractions and the effect of gaseous environment" J. Therm. Anal. Calorim., 2022, doi: 10.1007/s10973-022-11359-8.

Journal of Thermal Analysis and Calorimetry
https://doi.org/10.1007/s10973-022-11359-8

Sulfur in kukersite shale oil: its distribution in shale oil fractions and the effect of gaseous environment

Sepehr Mozaffari[1] · **Zachariah Steven Baird**[1] · **Oliver Järvik**[1]

Received: 9 December 2021 / Accepted: 2 April 2022

Abstract
In this article, data on the distribution of sulfur in Estonian kukersite shale oil obtained using pyrolysis at temperatures below 520 °C were presented. It was found that the highest concentration of sulfur is present in the fractions boiling between about 150 and 190 °C. Also, we studied the effect of N_2, N_2/steam, CO_2, and CO_2/steam environments on the distribution of sulfur in pyrolysis products and concentrations of some sulfur compounds in shale oil. The results show that thiophenic compounds comprise most of the sulfur compounds in crude kukersite shale oil. Furthermore, CO_2 increased the concentration of some of the identified sulfur compounds in the shale oil as compared to N_2. The presence of steam increased the concentration of sulfur compounds in the shale oil as compared to dry sweep gases and significantly increased the sulfur concentration in pyrolysis gas. This was also supported by the investigation of the release of H_2S and SO_2 gases during the pyrolysis of oil shale in which steam contributes to an increase in the formation of sulfurous gases. The presence of steam not only enhances the release of sulfur compounds from oil shale, but also causes it to occur at lower temperatures.

Keywords Sulfur distribution · Thiophenes · Kukersite shale oil · Gaseous environment · Pyrolysis

Introduction

Due to the increase in demand for energy resources, shale oil has drawn attention as an alternative fuel [1]. A promising approach is to utilize shale oil for producing valuable chemicals. Estonian kukersite shale oil is extensively studied and the corresponding oil shale is considered to be the most industrially utilized oil shale resource in the world [2, 3]. Vast exploitation in Estonia, which has mainly been used for electricity generation, made the country one of the least energy-dependent countries in the EU [4]. However, the increase in the price of CO_2 emissions in the European Emissions Trading System has led to a decrease in electricity production from oil shale in Estonia. In 2019 and 2020, Estonia produced 1.156 and 1.173 million tons of shale oil. However, the electricity generated from oil shale in 2020 was 1.834 TWh which is 40% less compared to 2019. It is worth noting that the total electricity production from the oil shale industry in 2020 was 2.949 TWh. This accounts for the electricity produced from oil shale and pyrolysis gas. The corresponding value in 2019 was 4.873 TWh [5]. 99% of shale oil produced in Estonia is sold to other countries and the export of chemical and phenolic products rose by 33% [5, 6].

To produce shale oil, oil shale is pyrolyzed, i.e., thermally processed at temperatures around 500 °C in the absence of oxygen [7, 8]. The solid heat carrier (SHC) method is preferred over the gaseous heat carrier method for shale oil production mainly because of the higher production rate, ability to use lower quality oil shale, and lower environmental impact [9]. In the SHC method, the shale ash produced from the combustion of solid pyrolysis residue (semi-coke) is used as the heat carrier. For the pyrolysis process, dried oil shale is mixed with hot shale ash to produce liquid and gaseous products [10]. These products are made up mainly of the elements found in kerogen (the organic matter in oil shale): carbon and hydrogen as well as organic oxygen, nitrogen, and sulfur [11]. However, inorganic compounds may also contribute. This is especially relevant in the case of sulfur compounds. Estonian oil shale contains about 1–2% of sulfur [12], which is further classified as either organic or inorganic sulfur [13]. In the molecular model proposed for the structure of Estonian kukersite kerogen, mercaptans, thiophene,

✉ Sepehr Mozaffari
Sepehr.mozaffari@taltech.ee

[1] Department of Energy Technology, Tallinn University of Technology, Ehitajate tee 5, 19086 Tallinn, Estonia

Published online: 28 April 2022

and thioether compounds are mainly present [13, 14]. Pyrite, marcasite, or small amounts of sulfates are categorized as inorganic sulfur [16]. The formation and distribution of sulfur compounds depend on covalent bond dissociation and the thermochemical characteristics of kerogen [15].

Thiols, sulfides, and thiophenes are the main sulfur compounds in kukersite shale oil [17], among which alkyl thiophenes are the most common [18]. Because of the properties that kukersite shale oil has, it finds use as a component in marine fuels. However, in order to avoid the environmental issues caused by sulfur, the International Maritime Organization (IMO) has applied strict regulations for marine fuels. The sulfur content of the marine fuels in SOx Emission Control Areas has been limited to 0.1% by mass since 2015. The global sulfur limit was also lowered to 0.5% from 2020 onward [19].

Due to the detrimental effect of sulfur on the oil shale upgrading process, the connection to environmental problems, and the strict regulations set on the sulfur content of marine fuels, information on the distribution of sulfur in different fractions of kukersite shale oil is needed. Therefore, the primary aim of this work is to analyze the distribution of sulfur in different fractions of Estonian shale oil. Also, the effect of the gaseous atmosphere used in pyrolysis (N_2, CO_2, and their mixtures with steam) on shale oil sulfur compounds was investigated. The results of this study would be beneficial to the development and improvement of sulfur removal.

Experimental

Sample preparation

Shale oil samples for studying the sulfur distribution were obtained from the Enefit Oil Plants in Narva, Estonia, which use the solid heat carrier (also known as Galoter) method [10]. The crude oil is separated at the plant into three fractions: gasoline, fuel oil (also referred to as the "middle oil fraction" in some older Galoter process based publications), and heavy oil. Two fuel oil samples and one shale gasoline sample were used. One fuel oil sample was from the newer Enefit-280 technology, and the other two samples were from the Enefit-140 technology (also called the UTT 3000 process in older publications).

The samples from the SHC process were further separated into narrow boiling range fractions by laboratory distillation. The fuel oil distillations were performed in a vacuum (around 7–70 mbar) to avoid the decomposition that can otherwise occur at higher temperatures. The distillation fractions were volume based, so each narrow fraction was taken to have roughly the same volume as the other fractions. Most of the fractions spanned distillation temperature intervals of about 5–10 °C and had average atmospheric boiling points ranging from about 80 to 420 °C. More information on how the samples were prepared, along with basic characteristic data for the samples, can be found in our earlier article [20].

In order to analyze the sulfur compounds of crude kukersite shale oil, a modified Fischer assay method was used to produce shale oil from an oil shale sample. The oil shale sample was crushed to the particle size of 500–710 μm. Then, 50 g of oil shale sample was subjected to N_2, CO_2, N_2/steam, and CO_2/steam environments for pyrolysis. The temperature program used for the Fischer assay method is as follows: heating up to 500 °C at 10 °C min^{-1}heating from 500 to 520 °C at 1 °C min^{-1}, and holding at 520 °C for 20 min. For the tests without steam, a flow rate of approximately 20 mL min^{-1} was used to inject N_2 and CO_2. For experiments using steam, water and CO_2/N_2 were injected at 0.1 mL min^{-1} and 10 mL min^{-1}, respectively. The oil yield of above-mentioned technologies, Enefit-280, Enefit-140, and Fischer assay, are about 13.2%, 11.5%, and 16.1%, respectively, on a dry oil shale basis [6, 20].

Analytical methods

Sulfur analysis

The sulfur content of the shale oil fractions was measured using a Lab-X 3500 Benchtop XRF Analyser (Oxford Instruments, Abingdon, United Kingdom), which uses the ASTM D 4294 method. The estimated standard uncertainty of the sulfur measurements was 0.0024 mass% (expanded uncertainty of 0.0043 mass% at the 95% level). The sulfur content of the oils and semi-cokes obtained using Fischer assay was measured using elemental analysis (Vario MACRO CHNS Cube, Elementar Analysensysteme GmbH, Langenselbold, Germany) as reported in our previous work [22].

TGA-MS analysis

The evolution of H_2S and SO_2 gases during pyrolysis of the oil shale sample (approximately 8 mg) was analyzed with a NETZSCH STA 449 F3 Jupiter® TG-DSC coupled with a NETZSCH QMS Aëolos® mass spectrometer. To pyrolyze the shale samples, conditions similar to those of a Fischer assay were used, such as the sweep gas flowrate and temperature profile. The relative abundance of the gases can be fragmented at different mass-to-charge ratios. On the other hand, even though m/z of 32, 33, and 34 can be used to detect the H_2S fragment, the relative abundance of H_2S at m/z 34 is considered 100%, and other mass-to-charge ratios are calculated with respect to that. Similarly, m/z 64 was used to analyze the evolution of sulfur dioxide gases as this mass-to-charge ratio refers to the relative intensity of 100% for this gas. Because the highest intensity for the evolution

H_2S and SO_2 compounds are recorded at mass-to-charge ratios (m/z) of 34 and 64, respectively, these m/z ratios were mainly used to interpret the evolution of these sulfurous gases. The tests in each carrier gas were conducted at least three time to make sure the results were reproducible. Initially, the baseline was subtracted so that the background noise was removed. Then, a cubic spline interpolation method was used to smooth the intensity data using a Python script. The smoothed peaks were normalized by dividing the intensity by the sample mass to eliminate the effect of sample mass on the peak intensity values and multiplied by a factor of 10^{12}. The standard deviation of the intensities of these runs at similar temperatures were grouped and then averaged so that the final expanded uncertainty (95% level) could be calculated. The value for the normalized intensity of the TGA measurements was computed to be 0.02.

GC–MS analysis

To analyze the sulfur compounds in shale oil samples produced in a Fischer assay, an Agilent 7890B gas chromatograph coupled to an Agilent 5975C Inert MSD mass spectrometer and Agilent Flame Photometric Detector (FPD) Plus was employed. The samples were injected using a CTC Combi/GC-PAL 80 autosampler. Injections (1 µl) were made with a split ratio of 10:1 at an injector temperature of 260 °C. Helium (0.9 mL min^{-1}, 99.9999% purity) was used as the carrier gas. The temperature program was as follows: initial temperature of 40 °C held for 5 min, then ramped up to 160 °C at 3 °C min^{-1}, and finally from 160 °C to 280 °C at a rate of 20 °C min^{-1}. The total run time was 51 min. The temperature of the FPD was set to 300 °C and the detector flow rates were 60 mL min^{-1} for both hydrogen and air (1:1). The column was a DB Petro (100 m × 250 µm × 0.5 µm). Also, the capillary to the MS had dimensions of 1 m × 250 µm × 0 µm and to the FPD + the dimensions were 5 m × 200 µm × 0 µm. Components were identified based on mass spectra compared to the National Institute of Standards and Technology (NIST) database and high purity standards. Three shale oil samples produced under each test atmosphere were used to calculate the concentration of sulfur compounds, and then an average was reported. Based on these repeat measurements, the calculated absolute standard uncertainty for the parallel runs and the estimated expanded uncertainty (95% level) for each compound was calculated separately and is presented in Table 1.

Results and discussion

Sulfur distribution

Information on the presence of sulfur compounds in different fractions of Estonian shale oil is important to understand so that essential processing for sulfur removal can be developed. According to Fig. 1, crude kukersite shale oil usually has a sulfur content between 0.3 and 1.5 mass%, which is higher than the sulfur limit of the marine fuels: 0.1%. As seen from the distribution of sulfur in shale oil, the concentration of sulfur in the gasoline fraction of shale oil increases with temperature and is greatest in the fractions boiling between about 150 and 190 °C. However, at higher temperatures, the shale oil sulfur content becomes lower and remains level at around 0.7 mass%. The experimental data for the kukersite samples measured in this study are presented in Table S1 in the supplementary material.

Table 1 Effect of sweep gases on the concentration of sulfur compounds in shale oil

Sulfur content (mg S/kg)	N_2	N_2/steam	CO_2	CO_2/steam	Expanded absolute uncertainty (95% level)
H_2S	442	1249	639	1040	56
SO_2	313	312	350	331	44
Thiophene	14	23	16	21	3
Thiophene, 2-methyl-	80	149	101	143	24
Thiophene, 3-methyl-	8	13	11	13	2
Thiophene, 2-ethyl-	50	80	63	79	10
Thiophene, 2,5-dimethyl-	31	48	39	47	6
Thiophene,2,4-dimethyl-	13	26	17	24	3
Thiophene, 2,3-dimethyl-	15	22	19	22	2
2/3/4-methylbenzenethiol	42	71	53	66	2
2-isopropylthiophene	54	77	57	80	9
Thiophene, 2-butyl-	18	23	21	25	3
Thiophene, 2-ethyl-5-propyl-	8	55	11	45	4
Benzo[c]thiophene	30	42	31	39	16

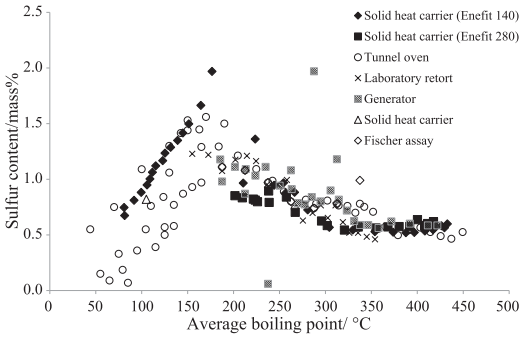

Fig. 1 The sulfur content of kukersite shale oil fractions from different retorts. Data from this study are shown as solid black points. Literature data from [23–29]

Also, earlier elemental composition data for the shale oil produced from other processing technologies can be found in the literature [18–24], and much of this data is presented in Table S2.

Past studies have determined that the sulfur compounds in kukersite shale oil are mostly alkylthiophenes and thioesters, although some mercaptans and disulfides are also present [29, 30].

The shape of the sulfur distribution is different from that normally seen with conventional petroleum. For conventional fuels, the sulfur content generally continues to increase with the average boiling point of the fraction [31, 32]. Coal liquid fractions also show a continual increase in the sulfur content [33]. Other shale oils, however, seem to have a distribution that resembles that of kukersite shale oil, as Fig. 2 shows. Even Jordanian El-Lajjun shale oil, which is known for its high sulfur content, shows a decrease in sulfur content in the heavier fractions. That is, the heavier fractions contained less sulfur.

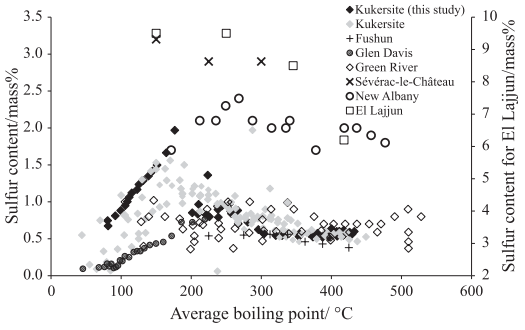

Fig. 2 Sulfur distributions of various shale oils. Note that the scale for El Lajjun shale oil has been placed on a second axis. Literature data for other shale oils from [34–42]

Identification of sulfur compounds in kukersite shale oil

To study the effect of various sweep gases on sulfur compounds, a quantitative analysis was performed to compare the presence of such compounds in the shale oil produced in different atmospheres. The chromatography analysis technique was used to identify several sulfur compounds however, due to the complexity of shale oil, it is quite difficult to detect all of them. Table 1 presents several common sulfur compounds identified using in the GC–MS-FPD, although it is worth noting that there are other sulfur compounds present that were not quantitatively identified. The detailed analysis of kukersite oil shale and corresponding shale oil used in this study can be found in the literature [4, 22].

It can be seen from the table that a large number of sulfur compounds can be found in the oil samples. As shown in the Table 1, most of the sulfur compounds in the shale oil samples are different forms of thiophenes originating from organic sulfur in kukersite oil shale (Table 2). Thiophenes are the main sulfur compounds and comprise about 80% of the sulfur. The rest of the sulfur compounds are thiols, sulfides, and disulfides [43]. The dominance of thiophene compounds can be explained by their thermal stability, which means they are not easily decomposed [44]. According to the analysis conducted on Huadian shale oil by Cui et al. [44], they reported that 87% of sulfur compounds consist of H_2S, thiophene, benzophenthiophene, and dibenzophenthiophene compounds, and also implied that the sulfur atoms are mostly present in the thiophene structures of kerogen macromolecules. The generation of H_2S which is mainly in the gaseous phase, but also dissolves in the shale oil, is partly formed through the decomposition of aliphatic and aromatic sulfur in the kerogen or conversion of mercaptans to thioethers or sulfur compounds and C=C double bonds [44]. Therefore, it can be inferred that the organic sulfur in oil shale is converted mainly into H_2S and thiophene derivatives as well as other thermostable heterocyclic compounds [43], especially at lower temperatures. The type of oil shale and the production process used will have an impact on properties of the shale oil produced. Therefore, differences in the production and distribution of sulfur compounds are not only dependent on experimental conditions, but is also associated with the covalent bond dissociation and thermochemical characteristics of kerogen during decomposition [15, 45].

As is seen from Table 1, there is a minor increase in the content of several sulfur compounds for CO_2 compared to N_2, although for other compounds the difference is too

Table 2 Forms of sulfur in the kukersite oil shale sample, mass% [4]

S_{total}	S_{pyrite}	$S_{sulfate}$	$S_{organic}$
1.72	1.1	0.13	0.49

small to be considered significant. This suggests that CO_2 could slightly increase the concentration of sulfur compounds in the shale oil. On the other hand, the addition of steam has a significant effect on the content of sulfur compounds and increases the concentration of sulfur in the oil. This indicates that the use of reactive gases (CO_2 and H_2O) promotes the release of sulfur from mineral and organic part of oil shale and transforms it into volatile sulfurous compounds, which later get incorporated into the liquid product or released as sulfurous gases. Similarly, as reported by Huang et al. [46], the release of sulfur in CO_2 environment by means of the pyrite decomposition is promoted by H_2O and this increases along with increasing H_2O concentration in the sweep gas. In a study done on coal, it was found that when CO_2 was added to dry N_2, more sulfur ended up in the liquid product rather than in the gaseous product at temperatures below 500 °C [47]. Based on the literature data the increase in sulfur compounds (Table 1) in the presence of reactive gases is mainly due to the decomposition of pyrite to pyrrhotite (FeS_x) as an intermediate step according to the following reaction [46]:

$$FeS_2 \rightarrow Fe_yS_x + \left(y + \frac{1}{2}x\right)S_2 \quad (1)$$

Also, Al-Ayed and Matouq [48, 49] investigated the sulfur content of El-Lajjun shale oil obtained in different atmospheres and concluded that steam plays an important role in increasing the shale oil sulfur content. According to the reactions suggested by them the increase in sulfurous compounds in shale oil is caused by the decomposition of pyrite and pyrrhotites in the mineral part of oil shale in the presence of steam:

$$3FeS_2 + 2H_2O \rightarrow 3FeS + 2H_2S + SO_2 \quad (2)$$

$$FeS_2 + 2H_2O + C \rightarrow FeS + H_2S + CO \quad (3)$$

$$FeS_2 + 2H_2O \rightarrow 3FeS + 2H_2 + SO_2 \quad (4)$$

$$FeS + H_2O \rightarrow FeO + H_2S \quad (5)$$

$$Fe_3O_4 + 4H_2O \rightarrow Fe_3O_4 + 4H_2S \quad (6)$$

$$Fe_3O_4 + 3H_2O \rightarrow Fe_2O_3 + 3H_2S \quad (7)$$

In the current study, a remarkable increase in concentration of H_2S in shale oil (Table 1) was noticed, while the increase in SO_2 concentration was small (within the measurement uncertainty). Therefore, for the shale oil produced under CO_2 atmosphere, a slight increase in concentration of SO_2 is expected considering the following reactions [46, 50]:

$$FeS_x + CO_2 \rightarrow Fe_3O_4 + CO + SO_2 \quad (8)$$

$$Fe_3O_4 + CO_2 \rightarrow Fe_2O_3 + CO \quad (9)$$

$$FeS_2 + 2CO_2 \rightarrow Fe_{1-x}S + 2CO + SO_2 + xFe \quad (10)$$

It should also be stated that since water vapor is a by-product in a pyrolysis process, the reactions 2–7 may take place in CO_2 environment as well, however, the effect of these reaction is not as significant simply because of lower amount of H_2O in pyrolysis atmosphere.

Analysis of sulfur in semi-coke

Prior to analyzing the concentration of sulfur in semi-coke and also, release of sulfurous gases during pyrolysis, it is beneficial to know about the forms of sulfur that are present in the shale sample. Therefore, Table 2 is provided to present the corresponding data for the sample used in the study.

According to Table 2, majority of sulfur in the oil shale sample is in the form of pyrite. In addition, the elemental analysis conducted on semi-coke derived after pyrolysis is shown in Table 3. The results indicate that the semi-cokes from the tests in CO_2 and steam atmospheres contain smaller amount of sulfur. This demonstrates that presence of steam as well as CO_2 has an impact on the release of sulfur from the oil shale sample as explained previously.

Table 4 demonstrates the distribution of sulfur in pyrolysis products under different atmospheres. The sulfur content of the oil shale sample and the produced shale oil was taken from the authors' previous work [22]. This data were then used to calculate the sulfur mass balance. Subsequently, the amount of sulfur in the pyrolysis gas was computed by difference. The data in Table 4 show that majority of sulfur will remain in semi-coke while large part of the liberated sulfur is released as non-condensable gases. The steam, however, is remarkably increasing the release of sulfur from the char in pyrolysis process. This result is similar to that reported in the literature [51].

Table 3 Ultimate analysis of derived semi-cokes from pyrolysis in different atmospheres, mass%

Pyrolysis atmosphere	N	C	H	S
N_2	0.04	13.55	0.24	1.80
CO_2	0.04	13.88	0.28	1.76
N_2/steam	0.04	13.74	0.29	1.67
CO_2/steam	0.04	13.86	0.27	1.65

Table 4 Distribution of sulfur in different pyrolysis atmospheres, mass%

Sulfur balance	Semi-coke	Shale oil	Gas
N_2	80.5	7.7	11.8
CO_2	78.4	8.2	13.4
N_2/steam	72.2	8.4	19.4
CO_2/steam	71.5	8.0	20.5

Evolution of H_2S and SO_2 gases during pyrolysis

To investigate further the evolution of SO_2 and H_2S, oil shale samples were also run in a TGA-MS to observe the effect of sweep gases on the evolution of these sulfur compounds. Using this technique, it is possible to determine the relative abundance of H_2S and SO_2 during oil shale pyrolysis.

Figures 3 and 4 depict the intensity trends for the evolution of H_2S and SO_2 gases during the pyrolysis of the oil shale sample. The intensity values were normalized based on the sample mass used. These figures compare the effect of different sweep gases on the release of sulfur compounds. Also, the expanded uncertainty (95% level) of 0.02 is presented as a dotted line in the graphs. Comparing the figures demonstrates that the generation of H_2S is generally greater than SO_2 during the pyrolysis process at low temperatures implying that H_2S accounts for most of the sulfurous gas released during pyrolysis [52]. According to literature, pyrolysis of the sample in a standard Fischer assay (under N_2) generated about 16% v/v H_2S of pyrolysis gas [4]. In one study, it was reported that the addition of steam to argon increased the yield of H_2S gas while reducing the formation of SO_2 [51]. That could be the major reason that our analysis showed that the generation of H_2S in oil was significantly higher than that of SO_2.

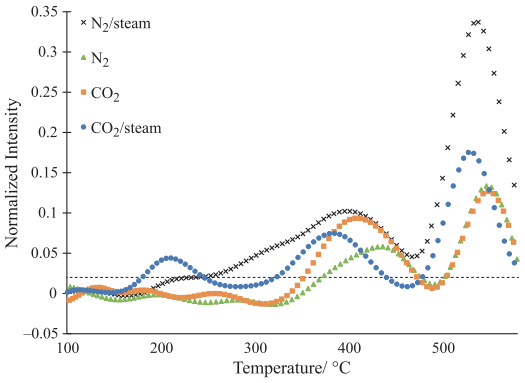

Fig. 3 Evolution of H_2S during oil shale pyrolysis (dotted line shows the measurement uncertainty, below which the results can be considered as noise)

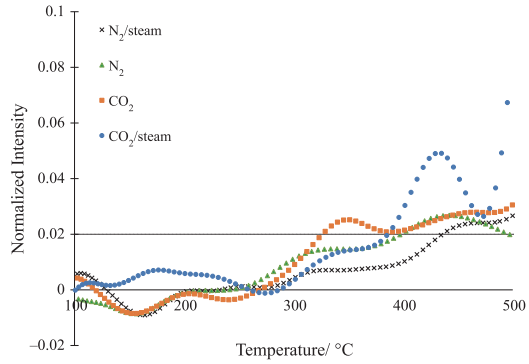

Fig. 4 Evolution trend for release of SO_2 during oil shale pyrolysis (dotted line shows the measurement uncertainty, below which the results can be considered as noise)

It is worth noting that the generation of various gases during pyrolysis would have a great effect on the release of sulfur in the process. Studying profiles of the generated gases during pyrolysis would be very beneficial to understand how the presence of pyrolysis gases plays a role in transforming sulfur from the sample and thus, the generation of sulfurous gases. Such information can be used to optimize sulfur removal processes. According to the study done by Zhou et al. [47] on pyrolysis of several coals in different atmospheres, it was found that the presence of H_2 in the pyrolysis environment noticeably intensified the evolution of H_2S gas as compared to pure N_2. Whereas the presence of CO_2 reduced the intensity of H_2S at temperatures below 500 °C. Although they found that CO_2 reduced the intensity there was only 10% of CO_2 in the gaseous environment. A decrease in H_2S intensity could be due to the presence of an insufficient amount of CO_2 gas in the environment to react with the sample. Moreover, greater formation of H_2S in an H_2 atmosphere was attributed to hydrogenation and reduction in sulfur compounds as compared to CO_2 and N_2 sweep gases [50]. In another study, it was described that the addition of CO_2 to an inert gas enhances the release of sulfur compounds such as H_2S and SO_2 during coal thermal decomposition [53]. Gu et al. also found that the release of volatile sulfur compounds such as SO_2 and thiophenes is mostly higher in CO_2 atmosphere than in N_2 because of oxidizing effect that CO_2 has during pyrolysis [50]. Sinha and Walker also compared several different gaseous environments and found that the amount of sulfur released from a coal sample increased in the following order: air, CO-steam, CO, N_2 [54].

It is seen from Fig. 3 that the formation of H_2S in a steam atmosphere exhibited a different behavior than that of dry sweep gases. Although the H_2S is formed during decomposition of both organic sulfur and pyrite [51], the suggested reactions 2–7 explain the enhancement of the formation of H_2S in the steam environment [49]. Also, it can be noticed that steam lowers the liberation temperature of sulfurous volatile compounds as well. More specifically, the intensity of peaks was at around 440 °C and 410 °C for N_2 and CO_2, respectively, and below 400 °C for the atmospheres with steam. Moreover, it can be noticed that in steam environment the H_2S starts forming at temperatures between 200 °C and 300 °C, while this for the dry sweep gases is a little above 300 °C. This indicates that the presence of steam in a pyrolysis environment causes the increase in H_2S concentration in pyrolysis gas at lower temperatures. Furthermore, it can also be derived from Fig. 3 that the formation of H_2S is lowest in both dry carrier gases, in particular N_2. This could be due to the low extent of hydrogenation/reduction reactions taking place in dry pyrolysis atmospheres [50].

In our previous work, it was shown how different gases such as H_2 evolve during oil shale pyrolysis [55]. Our earlier results indicated that during oil shale pyrolysis the concentration of H_2 in the pyrolysis environment intensifies with an increase in temperature and the generation rate was much sharper at around 400–500 °C. This could be one of the reasons that a higher H_2S intensity within this range is observed. Yan et al. [56] reported that generation of H_2S increased at a slow rate up to a temperature of 280 °C. However, after this temperature, the H_2S was formed at a higher rate and reached a maximum at 360 °C. The decomposition reaction of most of the pyrite in oil shale begins at around 280 °C and H_2S formation is dependent on the interaction of pyrite with the hydrogen donor [57]. Burnham et al. [58] described that oxidation of pyrite to form iron oxide is the main cause of H_2S increase in the steam environment. As stated previously, the intensity of the peaks for pyrolysis in CO_2/steam and N_2/steam was significantly higher than in dry sweep gases. Subsequently, a greater amount of H_2S compounds were dissolved in the corresponding shale oils.

From Fig. 4, the intensity of the SO_2 peak for all test atmospheres can be seen. It is obvious that by increasing the temperature, the generation of SO_2 increased as well. This can be explained by a higher reactivity of oxygen-bearing groups when temperature increased, which resulted in larger generation of SO_2 [59]. Also, it can be seen that the intensity of SO_2 in all environments does not generally get affected by the type of sweep gas applied at temperatures below 500 °C, which means that the steam effect is insignificant in this range. Hence, the yield of SO_2 is observed to be lower, resulting in a lower SO_2 content, accordingly. Although little SO_2 is observed to form, it can be perceived from the figure that the generation of SO_2 was initiated at around 300–350 °C. Moreover, from Fig. 4 it can be derived that until below 400 °C, the SO_2 generation is small. However, at about 400 °C, due to the higher oxidizing effect of CO_2 as compared to N_2, higher amount of SO_2 gas was formed under CO_2 and CO_2/steam atmospheres. This formation of SO_2 could originate from decomposition of aliphatic and elemental sulfur species at around 330 °C, with subsequent decomposition of aromatic and pyritic sulfur at higher temperatures leading to the larger peaks [60]. Therefore, appearance of a more intense peak could be as a result of overlapping of both decomposition peaks, and also the presence of larger amount of pyrite than organic sulfur in the shale sample (Table 2). However, it was reported in the literature that for this sample, about 60% of organic sulfur were released as pyrolysis gas [4].

The formation of SO_2 is from the reaction of oxygen-containing compounds with pyrite and unstable elemental sulfur when an inadequate amount of hydrogen is present to form H_2S. In the presence of steam, however, since more hydrogen radicals are present in the pyrolysis atmosphere, a bigger amount of H_2S is generated [51]. Moreover, when H_2O is present in pyrolysis atmosphere, because of lower molar mass of H_2O, the diffusion rate of sulfur gas is higher. Consequently, the sulfur gas escape the sample at higher rate [46]. According to the results of Wang et al. on coal pyrolysis, employing CO_2 in place of an inert gas (argon) not only increased the intensity of H_2S and SO_2 but also lowered the maximum peak temperature in the evolution of these gases as well [61]. Maaten et al. [9] investigated the release of H_2S and SO_2 gases in different oil shales with different origins under N_2 and concluded that keeping the pyrolysis temperature below 480 °C would be effective in reducing the sulfur content in the oil. However, they specified that this would not be the case for some oil shales such as Estonian oil shale because the evaporation maximum for this type of oil shale is approximately 400 °C and above this temperature the intensification lowers.

Combining analysis of the mass spectrometry results, it can be perceived from Figs. 3 and 4 that the release of sulfurous gases intensified starting at around 300–450 °C, even though for some curves it is small. The first peak could mainly take place as a result of decomposition of organic sulfur compounds—occurring at around 350 °C, and it further intensified above 400 °C as the pyrolysis of pyrite begins. As reported, pyrite decomposes at 400–500 °C [12]. This suggests that the decomposition of organic matter could increase the extent of the release of sulfurous gases. Also, comparing the effect of CO_2 and N_2 in shale oils, the difference in concentration of sulfur compounds was significant only for some of the identified compounds at low temperatures. In addition, the difference in concentrations of H_2S and SO_2 under CO_2 could be mainly as a result of the noticeable difference that was observed in the evolution of SO_2 and

H_2S gases during pyrolysis. This could confirm that CO_2 is more effective in the liberation of volatile sulfur compounds as well as sulfurous gases from oil shale due to its higher reactivity, however, at low temperature the difference seems to be small. Unlike N_2 in which the volatiles are released as a result of pyrolysis, CO_2 can increase the release of volatiles even more by reacting with the semi-coke throughout the pyrolysis, although the effect of CO_2 seems to be larger at higher heating rates and temperatures [62]. Another conclusion that can be drawn from applying steam in a pyrolysis environment is that steam increased the evolution of H_2S in contrast with SO_2. It can be deduced from the analysis that steam considerably enhances the concentration of sulfur compounds in shale oil.

Conclusions

In this study, the sulfur content in different fractions of Estonian kukersite shale oil was analyzed. Also, the effect of various sweep gases on behavior of sulfur in the oil shale pyrolysis process at temperatures below 520 °C was investigated as well. The main results are as follows:

- The analysis on the sulfur content of kukersite shale oil fractions from different retorts show that the concentration of sulfur in the fractions boiling between about 150 °C and 190 °C was the highest. In fractions with higher average boiling points, the sulfur content decreases until it becomes almost constant.
- GC–MS analysis on shale oils produced in N_2, CO_2, and their mixtures with steam demonstrated that the majority of the identified sulfur compounds in the shale oils were thiophenic compounds. Also, CO_2 increased the concentration of some of the sulfur compounds in the shale oil as compared to N_2. In addition, steam promotes the volatilization of sulfur compounds, which consequently increases the concentration of sulfur compounds in the shale oil.
- The analysis on the evolution trend of H_2S and SO_2 gases showed that steam significantly increased the release of H_2S gas, and its dissolved amount in the oil was the highest in comparison with other sulfur compounds. Also, the effect of steam on the evolution of these gases suggests that steam contributes to an increase in the formation of H_2S and SO_2.
- The elemental analysis conducted on semi-coke derived after pyrolysis indicates that the semi-cokes from the tests in CO_2 and steam atmospheres contain smaller amount of sulfur. This explains that the use of reactive gases (CO_2 and H_2O) has an impact on the release of sulfur from the oil shale sample.

Overall, sulfur analysis gives insight into how to decrease the sulfur content in oil and assist in the reduction in sulfurous gases during oil shale and coal industrial processes such as pyrolysis and gasification.

Supplementary Information The online version contains supplementary material available at https://doi.org/10.1007/s10973-022-11359-8.

Acknowledgements This research was funded by Estonian Research Council from National Programme for Addressing Socio-Economic Challenges through R&D (RITA1/01-60), which is supported by the Estonian Government and European Regional Development Fund. The authors would like to thank Silvia East for her help in measuring the sulfur and nitrogen contents of the shale oil fractions.

Author contributions All authors made substantial contribution to design of the study as well as the analysis and interpretation of the obtained results; Conceptualization was contributed by SM, OJ, Methodology was contributed by SM, OJ, ZSB, Data curation was contributed by ZSB, SM, Formal analysis and investigation were contributed by SM, OJ, ZSB, Writing—original draft preparation, was contributed by SM, Writing—review and editing, was contributed by OJ, ZSB, Supervision was contributed by OJ, ZSB.

Declarations

Conflict of interest The authors declare no conflict of interest.

References

1. Jiang Z, Zhang W, Liang C, Wang Y, Liu H, Chen X. Basic characteristics and evaluation of shale oil reservoirs. Pet Res. 2016;1(2):149–63. https://doi.org/10.1016/S2096-2495(17)30039-X.
2. Motlep R, Kirsimae K, Puura E. Mineral composition of Estonian oil shale semi-coke sediments. 8th Int Sci Conf Mod Manag Mine Prod Geol Environ Prot SGEM. 2008;2(3):309.
3. Mozaffari P, Baird ZS, Listak M, Oja V. Vapor pressures of narrow gasoline fractions of oil from industrial retorting of Kukersite oil shale. Oil Shale. 2020;37(4):288–303. https://doi.org/10.3176/oil.2020.4.03.
4. Maaten B, Järvik O, Pihl O, Konist A, Siirde A. Oil shale pyrolysis products and the fate of sulfur. Oil Shale. 2020;37(1):51–69. https://doi.org/10.3176/oil.2020.1.03.
5. "Eesti põlevkivitööstuse aastaraamat 2020 (in Estonian). 2020, [Online]. Available: http://data.vk.edu.ee/PKYB20/.
6. "Oil Shale Industry Yearbook. 2019. 2019, [Online]. Available: http://data.vk.edu.ee/pkk_aastaraamat_2019_eng/.
7. Neshumayev D, Pihu T, Siirde A, Järvik O, Konist A. Solid heat carrier oil shale retorting technology with integrated CFB technology. Oil Shale. 2019;36(2S):99–113. https://doi.org/10.3176/oil.2019.2S.02.
8. Astra H, et al. Yields and the selected physicochemical properties of thermobitumen as an intermediate product of the pyrolysis of Kukersite oil shale. Oil shale. 2021;38(4):295–316. https://doi.org/10.3176/oil.2021.4.02.
9. Maaten B, Loo L, Konist A, Pihu T, Siirde A. Investigation of the evolution of sulphur during the thermal degradation of different oil shales. J Anal Appl Pyrol. 2017;128:405–11. https://doi.org/10.1016/j.jaap.2017.09.007.

10. Golubev N. Solid heat carrier technology for oil shale retorting. Oil Shale. 2003;20(3):324–32.
11. Dijkmans T, Djokic MR, Van Geem KM, Marin GB. Comprehensive compositional analysis of sulfur and nitrogen containing compounds in shale oil using GC x GC - FID/SCD/NCD/TOF-MS. Fuel. 2015;140:398–406. https://doi.org/10.1016/j.fuel.2014.09.055.
12. Maaten B, Pikkor H, Konist A, Siirde A. Determination of the total sulphur content of oil shale by using different analytical methods. Oil Shale. 2018;35(2):144–53. https://doi.org/10.3176/oil.2018.2.04.
13. Qin H, Hao Z, Wang Q, Bai J. Sulfur release from oil shale in retort. Energy Procedia. 2012;17:1747–53. https://doi.org/10.1016/j.egypro.2012.02.307.
14. Lille Ü, Heinmaa I, Pehk T. Molecular model of Estonian kukersite kerogen evaluated by 13C MAS NMR spectra. Fuel. 2003;82(7):799–804. https://doi.org/10.1016/S0016-2361(02)00358-7.
15. Pan S, et al. Investigation of behavior of sulfur in oil fractions during oil shale pyrolysis. Energy Fuels. 2019. https://doi.org/10.1021/acs.energyfuels.9b02406.
16. Guffey FD, Barbour FA, Cummings RE. Analysis of oil shale retort production stream gases for sulfur species. Liq Fuels Technol. 1983;1(4):235–57. https://doi.org/10.1080/07377268308915324.
17. Speight J. Shale oil and gas production processes. Houston: Gulf Professional Publishing; 2019.
18. Al-Harahsheh A, Al-Otoom AY, Shawabkeh RA. Sulfur distribution in the oil fractions obtained by thermal cracking of Jordanian El-Lajjun oil Shale. Energy. 2005;30(15):2784–95. https://doi.org/10.1016/j.energy.2005.01.013.
19. Van Chu T, Ramirez J, Rainey T, Ristovski Z, Brown RJ. Global impacts of recent IMO regulations on marine fuel oil refining processes and ship emissions. Transp Res Part D Transp Environ. 2019;70:123–34. https://doi.org/10.1016/j.trd.2019.04.001.
20. Baird ZS, Järvik O, Oja V, Rannaveski R. Properties of kukersite shale oil. Oil Shale. 2021;38(4):265. https://doi.org/10.3176/oil.2021.4.01.
21. Oja V, Elenurm A, Rohtla I, Tali E, Tearo E, Yanchilin A. Comparison of oil shales from different deposits: oil shale pyrolysis and co-pyrolysis with ash. Oil Shale. 2007;24(2):101–8.
22. Mozaffari S, Järvik O, Baird ZS. Effect of N2 and CO2 on shale oil from pyrolysis of Estonian oil shale. Int J Coal Prep Util. 2021;00(00):1–15. https://doi.org/10.1080/19392699.2021.1914025.
23. Luts K. The Estonian Oil Shale Kukersite, its Chemistry, Technology and Analysis. Tartu, Estonia, 1934.
24. Hissin JO. Sulfur in shale and shale gasoline [in Russian]. Oil Shale, no. 10, 1932.
25. Klesment I, Hallik E. Comparative properties of pyrolysis oils from oil shale (Сравнительная характеристика смолполукоксования горючнх сланцев) [in Russian]. Chem Technol oil shale Prod (Химия и технология горючих сланцев и продуктов их переработки). 1963;12:169–80.
26. Yefimov V, Lille Ü, Piik E, Tuln M, Murb A. The results of thermal processing of Estonian oil shale in a small pilot gas retort (Rezul'taty termicheskoy pererabotki estonskogo slanca na malom opytnom gazogeneratore) [in Russian]. Goryuchie slancy, khimija i Technol. 1963;12:90–105.
27. Lille Ü. On the chemical composition of the 60–150 °C light fraction from a solid heat carrier retort (о химическом составе фракции 60–150 с легкой смолы установки с твердьім теплоносителем) [in Russian]. Chem Technol oil shale Prod (Химия и технология горючих сланцев и продуктов их переработки). 1963;12:127–33.
28. M. Wittlich. About the sulfur in Kukersite and its pyrolysis products (Einiges über den Schwefel im Kukersit und dessen Verschwelungsprodukten) [in German]. *Acta Comment. Univ. Dorpat.*, 1925.
29. Zelenin NI, Feinberg VS, Chernyshev KB. The chemistry and technology of shale oil. Leningrad: Chemistry Publishing House; 1968. (**in Russian**).
30. Derenne S, Largeau C, Casadevall E, Sinninghe Damsté JS, Tegelaar EW, de Leeuw JW. Characterization of Estonian Kukersite by spectroscopy and pyrolysis: Evidence for abundant alkyl phenolic moieties in an Ordovician, marine, type II/I kerogen. Org Geochem. 1990;16(4–6):873–88. https://doi.org/10.1016/0146-6380(90)90124-I.
31. Riazi MR. Characterization and properties of petroleum fractions. 1st ed. Pennsylvania: ASTM International; 2005.
32. Baird ZS, Rang H, Oja V. Desulfurization, denitrogenation and deoxygenation of shale oil. Oil Shale. 2021;38(2):137–54. https://doi.org/10.3176/oil.2021.2.03.
33. Gray JA, Brady CJ, Cunnlngham R, James R, Wllson GM. Thermophysical properties of coal liquids 1. Selected physical, chemical, and thermodynamic properties of narrow boillng range coal liquids. Ind Eng Chem Process Des Dev. 1983;22(3):410–24.
34. Mapstone GE. Some properties of crude shale oil and naphtha. Oil Shale and Cannel Coal. 1951;2:662–72.
35. Cady WE, Seelig HS. Composition of shale oil. Ind Eng Chem. 1952;44(11):2636–41.
36. Lovell PF. Production of Utah shale oils by the Paraho DH and Union 'B' retorting processes. In: *Eleventh Oil Shale Symposium Proceedings*, 1978, pp. 184–192.
37. Hill GR, Dougan P. The characteristics of a in situ shale low temperature oil. 1967.
38. Miknis, FP. Characterization of DOE reference oil shale: Tipton member, Green River formation oil shale from Wyoming. 1988.
39. Qian J, Liang Y. Oil shale: petroleum alternative. Beijing: China Petrochemical Press; 2010.
40. Marecaux PP. Essais de valorisatsion integrale des huiles de schiste de Severac. Oil Shale and Cannel Coal. 1951;2:673–89.
41. Miknis FP, Robertson RE. Characterization of DOE reference oil shales: Mahogany zone, Parachute Creek member, Green River formation oil shale, and Clegg Creek member, New Albany shale. Western Research Inst., Laramie, WY (USA); 1987.
42. Bunger JW. Shale oil value enhancement research. Salt Lake City, 2007.
43. Fainberg V, Garbar A, Hetsroni G. Secondary pyrolysis of the products of the thermal destruction of high-sulfur oil shale. Energy Fuels. 1997;11(4):915–9. https://doi.org/10.1021/ef9601733.
44. Cui D, et al. Compositional analysis of heteroatom compounds in Huadian shale oil using various analytical techniques. Energy Fuels. 2019;33(2):946–56. https://doi.org/10.1021/acs.energyfuels.8b03889.
45. Mozaffari P, Järvik O, Baird ZS. Vapor pressures of phenolic compounds found in pyrolysis oil. J Chem Eng Data. 2020. https://doi.org/10.1021/acs.jced.0c00675.
46. Huang F, Zhang L, Yi B, Xia Z, Zheng C. Effect of H2O on pyrite transformation behavior during oxy-fuel combustion. Fuel Process Technol. 2015;131:458–65. https://doi.org/10.1016/j.fuproc.2014.12.027.
47. Zhou Q, Hu H, Liu Q, Zhu S, Zhao R. Effect of atmosphere on evolution of sulfur-containing gases during coal pyrolysis. Energy Fuels. 2005;19(3):892–7. https://doi.org/10.1021/ef049773p.
48. Al-Ayed OS, Matouq M. Influence of pyrolysis environment on liquid product and sulfur of oil shale. Energy Sour Part A Recover Util Environ Eff. 2009;31(8):679–86. https://doi.org/10.1080/15567030701752529.

49. Al-Ayed OS, Matouq M. Factors affecting sulfur reactions in high sulfur oil shale pyrolysis. J Energy Resour Technol Trans ASME. 2009;131(1):0125011–4. https://doi.org/10.1115/1.3068338.
50. Gu Y, Yperman J, Vandewijngaarden J, Reggers G, Carleer R. Organic and inorganic sulphur compounds releases from high-pyrite coal pyrolysis in H2, N2 and CO2: test case Chinese LZ coal. Fuel. 2017;202:494–502. https://doi.org/10.1016/j.fuel.2017.04.068.
51. Wang M, Du Q, Li Y, Xu J, Gao J, Wang H. Effect of steam on the transformation of sulfur during demineralized coal pyrolysis. J Anal Appl Pyrol. 2019;140:161–9. https://doi.org/10.1016/j.jaap.2019.03.011.
52. Qin H, Zheng Z, Wang Q, Sun B, Bai J. H2S evolution during oil shale pyrolysis. In: Asia-Pacific Power Energy Eng Conf APPEEC, pp. 2–5, 2010, https://doi.org/10.1109/APPEEC.2010.5448345.
53. Yang N, Guo H, Liu F, Zhang H, Hu Y, Hu R. Effects of atmospheres on sulfur release and its transformation behavior during coal thermolysis. Fuel. 2018;215:446–53. https://doi.org/10.1016/j.fuel.2017.11.099.
54. Sinha RK, Walker PL. Desulphurization of coals and chars by treatment in various atmospheres between 400 and 600 °C. Fuel. 1972;51(4):329–31. https://doi.org/10.1016/0016-2361(72)90012-9.
55. Mozaffari S, Järvik O, Baird ZS. Composition of gas from pyrolysis of Estonian oil shale with various sweep gases. Oil Shale. 2021;38(3):215–27. https://doi.org/10.3176/oil.2021.3.03.
56. Yan Q, Peng P, Yu C, Liu J. The role of sulfur in the pyrolysis of kerogen. Chin Sci Bull. 2004;49:10–8. https://doi.org/10.1007/BF02890448.
57. Fadeff SK, Burnham AK, Richardson JH. Organic and pyritic sulfur determination in oil shale. No. 1983.
58. Burnham GJ, Bey AK, Koskinas NK. Hydrogen sulfide evolution from colorado oil shale. ACS Symp Ser. 1981. https://doi.org/10.1021/bk-1981-0163.ch005.
59. Li L, et al. Release of sulfur and nitrogen during co-pyrolysis of coal and biomass under inert atmosphere. ACS Omega. 2020;5(46):30001–10. https://doi.org/10.1021/acsomega.0c04372.
60. Frigge L, Elserafi G, Ströhle J, Epple B. Sulfur and chlorine gas species formation during coal pyrolysis in nitrogen and carbon dioxide atmosphere. Energy Fuels. 2016;30(9):7713–20. https://doi.org/10.1021/acs.energyfuels.6b01080.
61. Wang X, Guo H, Liu F, Hu R, Wang M. Effects of CO2 on sulfur removal and its release behavior during coal pyrolysis. Fuel. 2016;165:484–9. https://doi.org/10.1016/j.fuel.2015.10.047.
62. Zhao S, Sun Y, Lü X, Li Q. Kinetics and thermodynamics evaluation of carbon dioxide enhanced oil shale pyrolysis. Sci Rep. 2021;11(1):1–14. https://doi.org/10.1038/s41598-020-80205-4.

Curriculum vitae

Personal data

Name:	Sepehr Mozaffari
Date of birth:	08.09.1992
Place of birth:	Tehran
Citizenship:	Iranian

Contact data

E-mail:	Sepehr.mozaffari@taltech.ee

Education

2017–2022	Tallinn University of Technology – PhD
2014–2015	University of Aberdeen, Petroleum Engineering – MSC
2010–2014	University of Indonesia, Chemical Engineering – BSC
2007–2010	Iran High School

Language competence

Persian	Native
English	Fluent

Professional employment

01.09.2017–…	Tallinn University of Technology, School of Engineering, Department of Energy Technology, early stage researcher

Completed projects

LEP18004	“Heavy oil research (1.01.2018−31.12.2018)”, Vahur Oja, Tallinn University of Technology, School of Engineering, Department of Energy Technology.
LEP18071	“Innovative Gasification, Pyrolysis, and Combustion Technologies for Oil Shale (3.09.2018−2.09.2021)”, Andres Siirde, Tallinn University of Technology, School of Engineering, Department of Energy Technology.
LEIEE22013	“Study on production of oil from plastic waste and organic waste (2.02.2022−15.07.2022)”, Oliver Järvik, Tallinn University of Technology, School of Engineering, Department of Energy Technology.

Projects in progress

LEIEE22021	“Find more cost-effective solutions to use CO_2 captured from Enefit-280 plants as a raw material (1.03.2022−1.11.2022)”, Oliver Järvik, Tallinn University of Technology, School of Engineering, Department of Energy Technology.

Elulookirjeldus

Isikuandmed

Nimi:	Sepehr Mozaffari
Sünniaeg:	08.09.1992
Sünnikoht:	Teheran
Kodakondsus:	Iraani

Kontaktandmed

E-post:	Sepehr.mozaffari@taltech.ee

Hariduskäik

2017–2022	Tallinna Tehnikaülikool – PhD
2014–2015	University of Aberdeen, Petroleum Engineering – MSC
2010–2014	University of Indonesia, Chemical Engineering – BSC
2007–2010	Iran High School

Keelteoskus

Pärsia keel	Emakeel
Inglise keel	Kõrgtase

Teenistuskäik

01.09.2017–…	Tallinna Tehnikaülikool, Inseneriteaduskond, Energiatehnoloogia instituut, doktorant-nooremteadur

Lõppenud projektid

LEP18004	“Raskeõli laboriuuring (1.01.2018−31.12.2018)”, Vahur Oja, Tallinna Tehnikaülikool, Inseneriteaduskond, Energiatehnoloogia instituut.
LEP18071	“Innovatiivsed põlevkivi gaasistamise, pürolüüsi ja põletamise tehnoloogiad (3.09.2018−2.09.2021)”, Andres Siirde, Tallinna Tehnikaülikool, Inseneriteaduskond, Energiatehnoloogia instituut.
LEIEE22013	“Plastjäätmetest ja orgaanikat sisaldavatest jäätmetest õli tootmine (2.02.2022−15.07.2022)”, Oliver Järvik, Tallinna Tehnikaülikool, Inseneriteaduskond, Energiatehnoloogia instituut.

Jooksvad projektid

LEIEE22021	“Lahendused Enefit-280 tehastest kinni püütava CO_2 kui tooraine kasutamiseks (1.03.2022−1.11.2022)”, Oliver Järvik, Tallinna Tehnikaülikool, Inseneriteaduskond, Energiatehnoloogia instituut.

ISSN 2585-6901 (PDF)
ISBN 978-9949-83-908-7 (PDF)